Expression and Function of the Potassium Channels of the Human Heart

PhD Thesis

Balázs Ördög, MSc

Szeged

2009

Expression and Function of the Potassium Channels of the Human Heart

PhD Thesis

Balázs Ördög, MSc

Supervisors:
Professor János Szabad habil., PhD, DSc
Professor Zsolt Boldogkői habil., PhD, DSc

Department of Medical Biology
Faculty of Medicine, University of Szeged

Szeged

2009

Publications related to the thesis

I. Ördög B, Brutyó E, Puskás LG, Papp JG, Varró A, Szabad J, Boldogkői Z.
Gene expression profiling of human cardiac potassium and sodium channels.
International Journal of Cardiology; 2006; 111: 386–393.
IF: 2.234

II. Prorok J, Kovács PP, Kristóf AA, Nagy N, Tombácz D, Tóth JS, Ördög B, Jost N, Virág L, Papp JG, Varró A, Tóth A, Boldogkői Z.
Herpesvirus-mediated delivery of a genetically encoded fluorescent Ca(2+) sensor to canine cardiomyocytes.
Journal of Biomedicine and Biotechnology; 2009; 2009:361795.
IF: 2.563

III. Ördög Balázs és Szabad János.
Miért dobog a szívünk?
Természet Világa; 2006; 137: 103-108.

Cumulative impact factor: 4.797

Contents

Aim of the study

The spatial and temporal regulation of muscle contraction in the heart is based on region-specific action potential configurations. The action potential, which is the change of membrane potential in time, is the result of the subtly balanced and concerted action of the underlying ion currents driven by transmembrane ion channels. Under pathophysiological conditions, changes in ion currents result in abnormal action potential waveforms which may provide an arrhythmogenic substrate and lead to life threatening arrhythmias or sudden cardiac death. Ion channels - the main objectives of our study - are protein complexes formed by pore-forming and regulatory ion channel subunits. The pore-forming subunits serve as pathways for ions through the cell membrane, while the regulatory subunits are substantial modifiers of ion channel function. The ion channel function depends primarily on the subunit composition of the ion channel complex. The ion currents have been thoroughly characterized by electrophysiological and pharmacological methods, however, little is known about the subunit composition of the ion channel complexes. Revealing the subunit composition of the ion channels and determining the subunit-specific function of individual ion channel subunits would help us not only to understand better how the heart is functioning both under normal and pathophysiological conditions, but with the gene therapy on the horizon, it would also open avenues for novel therapeutic approaches. The aim of the present study is the development of an experimental system to characterize the specific function of individual ion channel subunits in heart muscle cells *ex vivo* and potentially *in vivo*. The first project described here was designed to quantitatively measure the expression level of a comprehensive set of ion channel subunit-coding genes, with particular emphasis on potassium channel genes, in two regions of the normal human heart by the real time PCR technique. Based on the gene expression data we aim to conclude which ion channel subunits are expressed in the human myocardium and which of them could have physiological importance. In the second project we explore possibilities to utilize *Pseudorabies virus* as a general vehicle for delivering genetic material into heart muscle cells *ex vivo*. In our third project we apply lentivirus delivered artificial microRNAs to study the function of potassium channel subunits in cardiomyocytes. We particularly focus on MiRP2, a novel member of the KCNE gene family, of which a possible function has been proposed based on *in vitro* data, but has not been confirmed *ex vivo* or *in vivo*. We show direct evidence for the regulatory role of MiRP2 in the transient outward potassium channels in cardiomyocytes.

Introduction

Resting potential

Every living cell is surrounded by the cell membrane. The cell membrane is composed of a lipid bilayer and various protein molecules. The lipid bilayer is not permeable for charged and large molecules and is thus an excellent insulator. Some of the protein molecules embedded in the cell membrane form pores across the lipid bilayer. The two most important types of pore-forming membrane proteins are the ion channels and the ion pumps. Ion channels facilitate the passive diffusion of ions across the cell membrane. Ions move through ion channels according to their concentration and electric gradients without energy consumption. Most types of the ion channels possess selectivity for certain types of ions and thus there are potassium-, chloride- and sodium-selective ion channels. Ion pumps, by using ATP stored energy, transport ions against their electrochemical gradients.

In cardiomyocytes, the cytoplasmic surface of the membrane is more negative than the outer membrane surface and hence a transmembrane potential can be recorded. In resting cardiomycoytes the membrane potential ranges from -50 to -95mV, depending on the cardiac cell type. The basis of membrane potential is the differential distribution of several inorganic ions, mostly K^+, Na^+, Ca^{2+}, Cl^- and proteins carrying negative charge, on the two sides of the cell membrane (Figure 1). The cell membrane is impermeable for protein anions, of which concentration is constantly higher in the intracellular space than outside the cell. The differential distribution of inorganic ions is generated and maintained by the ion pumps. The most important ion pump is the Na^+/K^+ pump.

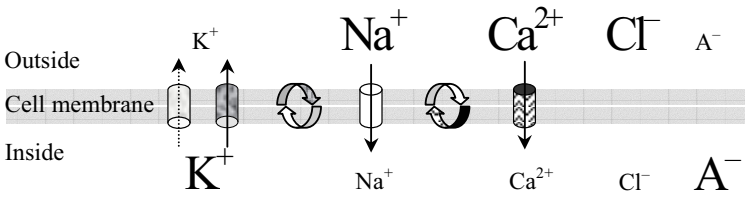

Figure 1. Differential distribution of cations and anions on two sides of the cell membrane. The figure indicates the most important ion channel types and ion pumps that are involved in the generation and maintenance of the resting potential. A^- represents negatively charged proteins. The size of the letters refers to the different ion concentrations. The dotted arrow shows K^+ movement through the non-voltage-gated channels, solid arrows indicate the voltage-gated channel types. The direction of arrows corresponds to the direction of ion movement through open channels. The ❍ symbols stand for Na^+/K^+ and a Na^+/Ca^{2+} ion pumps.

The Na^+/K^+ pump transports three K^+ ions from the extracellular space to the cytoplasm and two Na^+ ions at the same time in the opposite direction. Due to the never-ending activity of the Na^+/K^+ pump the cytoplasm is poor in Na^+ and rich in K^+, while the extracellular space is rich in Na^+ and poor in K^+ (Figure 1).

The resting membrane potential can be modeled by the Nernst and the Goldman-Hodgkin-Katz (GHK) equations (Figure 2 and 3). The Nernst equation gives the equilibrium potential for a given ion, a potential at which the ionic flux is zero. The equilibrium potential for a given ion depends solely on its concentration on the two sides of the membrane and on temperature (Figure 2). The membrane of resting cardiomyocytes is permeable mostly for K^+ only, while membrane permeability for other ions is relatively low. Therefore the resting membrane potential is very close to the equilibrium potential of K^+. When concentrations and relative permeabilities of other ions are taken into account, the membrane potential is calculated by the GHK equation (Figure 3).

$$E_{eq,K^+} = \frac{RT}{zF} \ln \frac{[K^+]_o}{[K^+]_i}$$

Figure 2. The Nernst equation. $E_{eq,K+}$ is the equilibrium potential for K^+ ion in Volts, R is the universal gas constant, T is the absolute temperature, z is the number of elementary charges of the ion in question and F is the Faraday constant, $[K^+]_o$ is the extracellular concentration of K^+ and $[K^+]_i$ is the K^+ concentration in the cytoplasm.

$$E_m = \frac{RT}{F} \ln \left(\frac{P_{Na^+}[Na^+]_o + P_{K^+}[K^+]_o + P_{Cl^-}[Cl^-]_i}{P_{Na^+}[Na^+]_i + P_{K^+}[K^+]_i + P_{Cl^-}[Cl^-]_o} \right)$$

Figure 3. The Goldman-Hodgkin-Katz equation. E_m is the membrane potential, R, T and F are as in Figure 3, P_X is membrane permeability for ion X and $[X]_i$ and $[X]_o$ are the cytoplasmic and extracellular concentrations of X ion, respectively.

Action potential

Excitable cells like heart muscle cells respond to proper stimulus by characteristic changes in membrane potential. This change in the membrane potential is termed action potential.

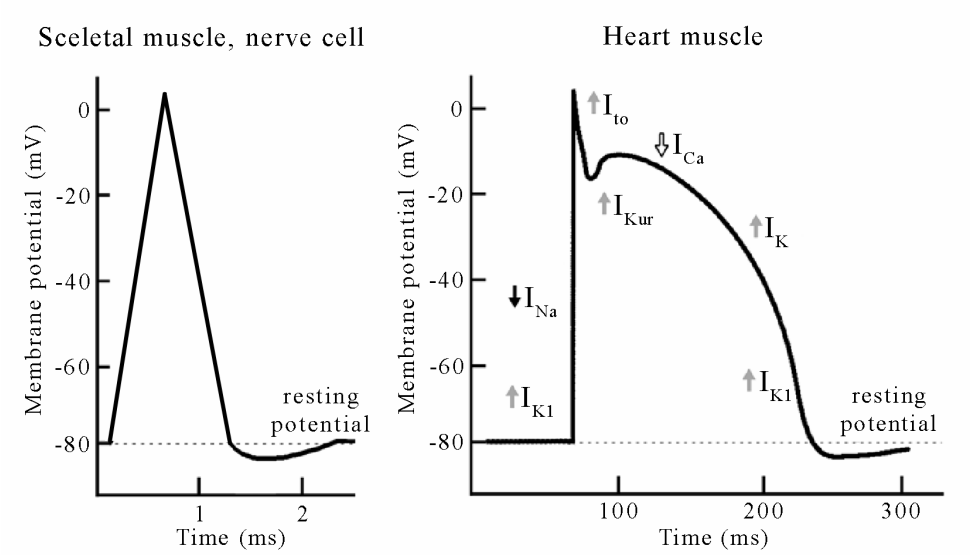

Figure 4. Action potential in nerve, skeletal and heart muscle cells. Note the different time scales of the two diagrams. Cardiac action potential is the result of the concerted action of the various ion channel types. While the K^+ channels lead to outward (↑) currents (I_{K1}, I_{to}, I_{Kur} and I_K), the Na^+ and the Ca^{2+} channels facilitate inward (↓) flow of Na^+ and Ca^{2+} ions, respectively (I_{Na} and I_{Ca}).

The basis of the action potential is a sequential change in membrane permeability for certain types of ions. During cardiac action potential the membrane permeability changes due to the activity of voltage-gated ion channels. The voltage-gated Na^+ and the Ca^{2+} selective channels drive inward Na^+ and Ca^{2+} currents, while the K^+ selective channels drive outward K^+ currents.

In the cardiac action potential 5 phases are generally distinguished (Figure 4) (70). Phase zero is the rapid depolarization or 'upstroke' of the membrane potential. In phase zero Na^+ channels open (I_{Na}, Figure 4) in response to a depolarizing stimulus large enough to reach a threshold. The Na^+ influx lasts only a few milliseconds and as the intracellular Na^+ concentration increases, the driving force for the Na^+ decreases. There is no more Na^+ influx when the membrane potential reaches the equilibrium potential for Na^+ and the Na^+ channels are functionally inactivated. In phase one the membrane potential rapidly and transiently returns near to 0 mV partly due to the inactivation of the Na^+ channels and to the opening of the so-called transient outward K^+ channels (I_{to}, Figure 4). The magnitude of the transient outward K^+ current determines the height and duration of the forthcoming phase of the action potential, the so-called plateau phase (phase two). During the plateau phase there is a dynamic

balance between Ca^{2+} influx (I_{Ca}, Figure 4) driven by voltage-gated Ca^{2+} channels and K^+ efflux, hence the membrane potential is almost stable or only slightly decreases. In phase three the Ca^{2+} influx decreases because of the inactivation of the Ca^{2+} channels while an outward current increases mainly because of the activation of the so-called delayed rectifier K^+ channels (I_K, Figure 4) and the membrane potential returns to more negative ranges. In phase four beside I_K the so-called inward rectifier K^+ channels are involved (I_{K1}, Figure 4). The differential distribution of ions that are typical for the resting membrane are rearranged mainly by the action of the Na^+/K^+ pump and the Na^+/Ca^+ exchanger. The Na^+/Ca^+ exchanger is an antiporter that facilitates the transport of Ca^{2+} ions out from the cytoplasm with the help of the Na^+ concentration gradient.

Excitation contraction coupling in the heart

The direct trigger for muscle contraction is the release of Ca^{2+} from the sarcoplasmic reticulum (SR) (21). The Ca^{2+} release is induced by Ca^{2+} ions and is manifested by the voltage-gated Ca^{2+} channels during phase 1 and phase 2 of the action potential. The phenomenon is called the Ca^{2+} induced Ca^{2+} release. The heart muscle cells, like the striated muscle cells are enmeshed by invaginations of the sarcolemma (Figure 5). These invaginations are the transversal tubules (t-tubules). At certain places the membrane of the t-tubules and the membrane of the SR are very close to each other. They are so close that the voltage-gated Ca^{2+} channels of the cell membrane and the Ca^{2+} channels of the SR, the so-called ryanodine receptors are placed in direct vicinity of each other. The ryanodine receptor is basically a Ca^{2+} sensitive Ca^{2+} channel. It opens whenever the cytoplasmic Ca^{2+} concentration is elevated. Thus in the phase one and two of the action potential the Ca^{2+} ions that flow through the voltage-gated Ca^{2+} channels of the sarcolemma and arrive to the cytoplasmic surface of the ryanodine receptors induce opening of the ryanodine receptor. The Ca^{2+} needed for muscle contraction is then released from the Ca^{2+} store through the open ryanodine receptors. When the task of the cardiomyocytes is completed and their microfilaments should be released the Ca^{2+} ions are removed from the cytoplasm mostly by the Ca^{2+} pumps built into the membrane of the SR (Figure 5). However, in most mammalian ventricular myocytes the SR Ca^{2+} pumps account for about 60-70% of the Ca^{2+} uptake and the rest 30-40% is removed by the sarcolemmal Na^+/Ca^{2+} exchanger molecules and by the sarcolemmal Ca^{2+} pumps.

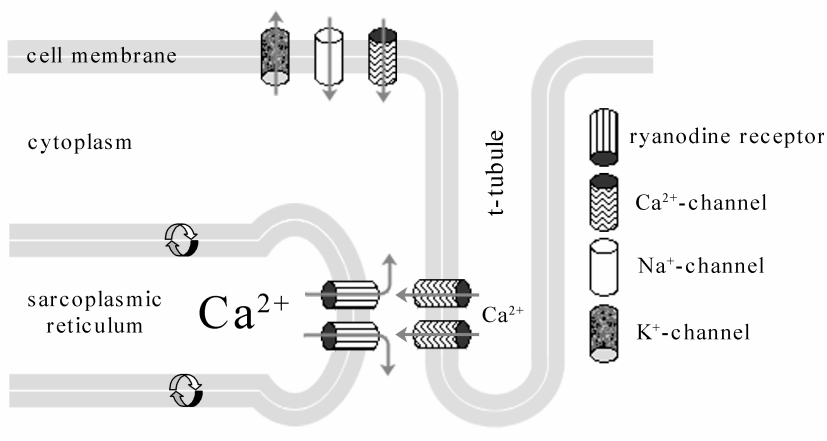

Figure 5. Distribution of ion channels in the sarcolemma, in the t-tubule membrane and in the membrane of the sarcoplasmic reticulum. The ↻ symbols stand for Ca^{2+} pumps of the sarcoplasmic reticulum.

In both the skeletal and in heart muscles, the action potentials regulate the duration and strength of muscle contraction. In the skeletal muscles the duration of the action potential is shorter than the duration of the shortening of muscle filaments. Thus additional action potentials may take place while muscle filaments are still shortened and a continuous contraction can be maintained. In the heart, a continuous contraction would completely abolish pump function and it never happens under normal conditions. Cardiac action potential takes longer time than contraction does, so heart muscle filaments relax before the action potential is completed. A new action potential can be initialized only when the myofilaments are relaxing, which thus ensures the rhythmical function of the heart.

The heartbeat

The proper pump function of the heart depends on regular generation of action potentials and the well-organized conduction of the stimulus through electrically coupled cells by gap junctions or through the specific excitation conduction system of the heart (Figure 6). While contraction of the skeletal muscles is induced by action potentials generated in the nervous system, the heart does not need external stimulus for contraction and beating. There is a specialized portion of the heart positioned in the wall of the right atrium, called the sinoatrial node (SAN) that controls heart beats (Figure 6). The modified heart muscle cells of the SAN perform only weak contractions. However they possess the ability to generate action potentials and regulate contractions in the entire heart. This function of the SAN is known of pacemaker activity. Hence there is no stimulus conduction system in the atria, action potential

generated in the SAN spreads through the muscle cells of the left and right atrium and induces contraction. The atria and the ventricles are electrically insulated by a fibrous connective tissue. The so-called atrio-ventricular node (AVN), placed between the atria and ventricles, is the only path through which action potentials can reach the ventricles.

The SAN is the primary pacemaker of the heart, however, in the absence of SAN function, or when conduction is blocked, cells of the AVN, or cells in the Purkinje fiber are also able to generate action potentials. However, without the primary pacemaker function the heart rate drastically slows down. The action potential suffers a few milliseconds delay after reaching the AVN and before traveling further towards the ventricles. The short delay allows the blood to be pumped out from the atria while the ventricles are still in diastole. For an effective pump function muscle cells of both ventricles have to be excited at almost the same time. For this purpose the action potential is driven from the AVN through the specific excitation conduction system of the heart. The excitation conduction system is composed of the His bundles, the Tawara branches and the Purkinje fibers and contains modified heart muscle cells that were "designed" to conduct excitation (Figure 6). The His bundles and the Tawara branches are placed in the septum while Purkinje fibers enmesh the walls of both ventricles. The His bundles and the Tawara branches lead action potential effectively from the AVN to the network of Purkinje fibers where the excitation spreads toward the muscle cells of the wall of the ventricles and triggers contraction.

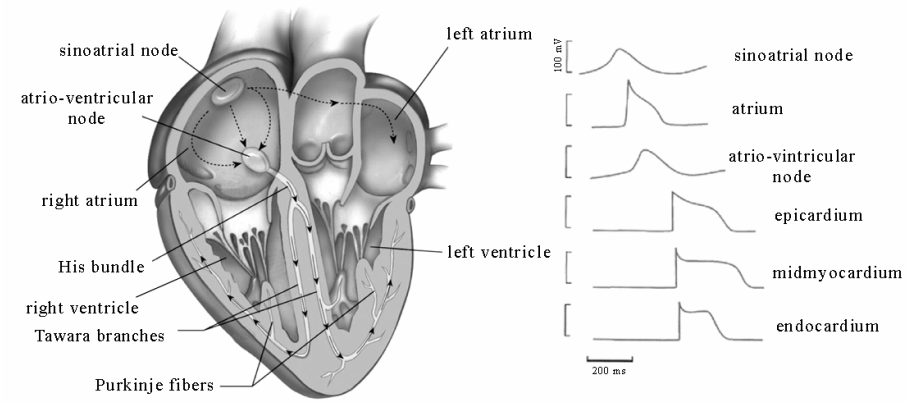

Figure 6. The pacemaker and the excitation conduction system of the heart. Schematic diagrams of specific action potential waveforms in the different regions of the heart are shown on the right panel.

Structure-function relationships of the cardiac ion channels

The central role of ions in the excitability of nerve and muscle has been first described by Sidney Ringer and Walther Nernst in the 1880s. A decade later Julius Bernstein correctly proposed that excitable cells are surrounded by a membrane selectively permeable to certain ions. However, experimental evidences for the existence of ion channels appeared only in the early 1980s when Erwin Neher and Bert Sakmann developed the patch-clamp technique (62). Analysis of ion channels at the molecular scale began in 1984 when the Na^+ channel gene of the electric eel was cloned (46). The molecular techniques made the analysis of the biophysical properties of ion currents and ion channels possible. The most prominent step in understanding the structure of ion channels was achieved by Roderick MacKinnon and his colleagues who determined the structure of the bacterial *KcsA* K^+ channel (18). It appears that despite the enormous functional heterogeneity of the different ion channel types they are built up from the same or similar structural units. Therefore, findings achieved from the studies made on the bacterial *KcsA* channel may be applied to most of the ion channels of higher animals including humans.

Every known ion channel is composed of two basic structural elements, the transmembrane α-helices and the so-called pore domain (Figure 7). While transmembrane helixes mostly serve as a 'scaffold' of the ion channel, the pore domain determines the shape of the pore in the ion channel and contribute to basic properties of the channel like selectivity and conductivity. The most simple ion channels are the inwardly rectifying K^+ channels (31) that resemble to the bacterial *KcsA* channel (Figure 7). One functional inwardly rectifying K^+ channel is composed of four subunits. The subunits are structurally identical, even though they may be products of different genes. One subunit of an inwardly rectifying K^+ channel consists of two transmembrane α-helixes and one pore domain between the two helixes. The cardiac voltage-gated K^+ channels are also tetramers (64). One subunit of a voltage-gated K^+ channel consists of six transmembrane helixes and one pore domain between the two most C-terminal helixes. The cardiac Na^+ and Ca^{2+} channels are composed of a single polypeptide chain, however, these huge proteins consist of four domains. One of their domains corresponds to one subunit of the voltage-gated K^+ channels (Figure 7). The last class of the cardiac ion channels discovered is the so-called two pore domain K^+ channels (Figure 7). The two pore domain channels are dimers composed of two structurally identical subunits (36).

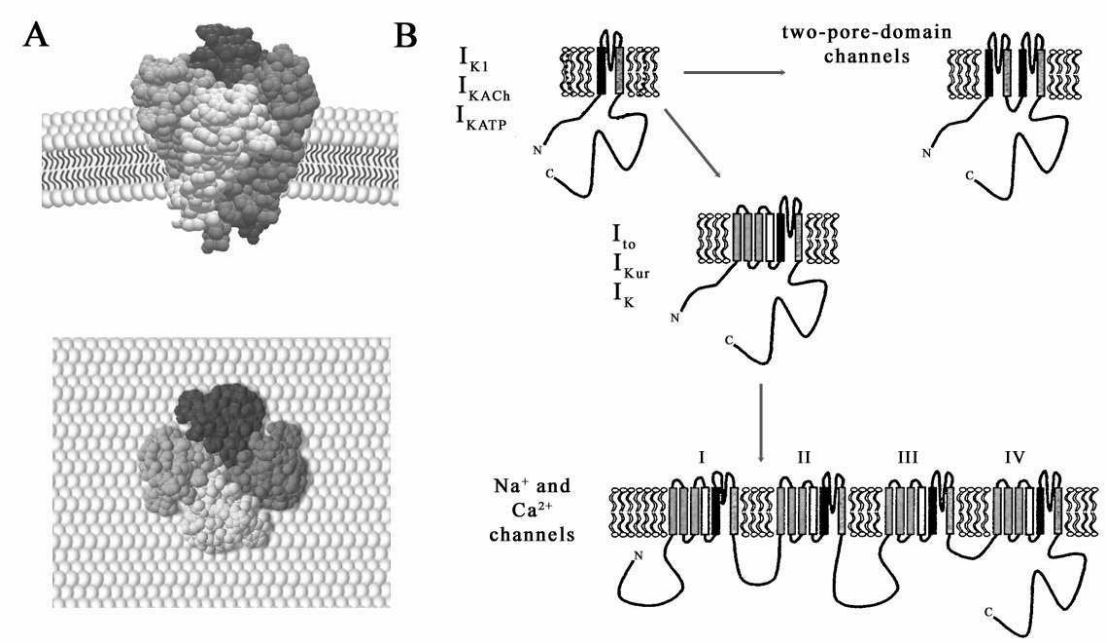

Figure 7. Three dimensional structure of the bacterial KcsA channel (A). Tertiary structure of different cardiac ion channel types (B).

One subunit contains two domains and the structure of each domain is identical with the structure of an inwardly rectifying K^+ channel-forming subunit. There is a schematic illustration of the structure of an inwardly rectifying K^+ channel in Figure 8. It is the narrow bottleneck-shaped portion of the pore of the channel that is probably the most important with respect to channel function. The narrow bottleneck-shaped portion of the pore is often called the selectivity filter of the channel, hence the ion selectivity of the channel depends on the dimensions of the bottleneck. The selectivity filter is composed of amino acids of the four pore domains belonging to the four subunits that form the channel. It is 1.2 nm long and 0.28 nm in diameter. Clearly, it is too narrow for a hydrated K^+ ion. Removing the primary hydration shell of the K^+ ion would cost lots of energy. However, ion channels do not consume energy for ion transport. How are the K^+ ions able to pass through the ion channels without using energy? The answer becomes clear when one looks at the high-resolution structure of a K^+ channel. The inner surface of the selectivity filter is covered by carbonyl oxygen atoms that carry partial negative charges and are positioned exactly at the same distance as the distance in between the water molecules in the primary hydration shell of the K^+ ion. Hence, K^+ ions moving through the selective filter can easily interact with the carbonyl oxygen atoms instead of the water molecules. The carbonyl oxygen atoms provide a preferred environment for the K^+ ions and thus the K^+ ions can flow through the channel without using energy. It has been shown that two K^+ ions bind into the selectivity filter at the

same time. Binding of a third K^+ ion is associated with a concerted K^+ ion exit at the other side of the pore giving rise thus to efficient K^+ ion conductance. Other types of ions that differ in size from the K^+ ions can not interact with these oxygen atoms and can not get across the channel.

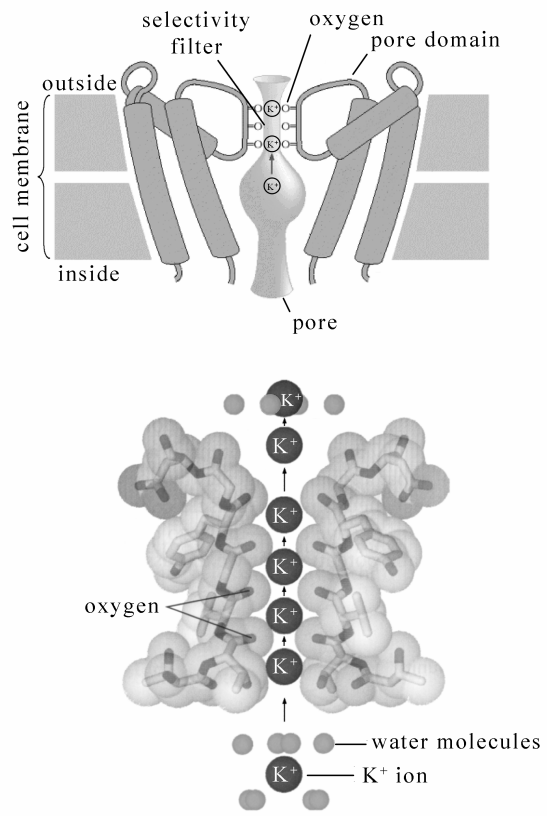

Figure 8. Upper panel: schematic illustration of the cross section of the bacterial KcsA channel. Lower panel: ion selectivity depends on dimensions of the selectivity filter.

Effective ion conductance is the basic function that an ion channel accomplishes. However, in case of voltage-gated channels – like cardiac Na^+, Ca^{2+}, transient outward and delayed rectifying K^+ channels – another important task is needed to be done. The latter types of channels are voltage-gated implying that they change their behavior depending on the actual value of the membrane potential. In general, cardiac voltage-gated ion channels open with depolarization, are inactivated in the depolarized membrane and they have to recover from this inactivated state before they are able to open again. It has been hypothesized, following the cloning the first Na^+ channel gene, that the fourth transmembrane helix of each subunit of the voltage-gated K^+ channels or the corresponding transmembrane segments of the Na^+ and Ca^{2+} channels serve as the voltage sensor of the channel (Figure 7 and 9). There are positively

charged amino acids (arginine or lysine) in the voltage sensor transmembrane helixes in every 3rd position. This set of charged amino acids is present in the fourth transmembrane helixes of every known voltage-gated ion channels. The above assumption is further supported by the following observation. When the charged amino acids of the putative voltage sensor were changed to cysteines the opening or closing of the channel was drastically altered (23, 81). It is very likely that the voltage sensor helix moves toward the inner or the outer surface of the membrane depending on the actual membrane potential (Figure 9). Movement of the voltage sensor may induce conformation changes in the entire channel complex resulting in changes in the channel conductance. However, the exact nature of the voltage-dependent conformation rearrangements has not yet been revealed.

Many voltage-gated ion channels like the Na^+, the Ca^{2+} and the transient outward K^+ channels display inactivation, that is, an entry into a non-conducting state during depolarization. Two major mechanisms of inactivation are proposed, namely N- and C-type inactivation (Figure 9). In the N-type inactivation the N-terminus of the channel subunit binds to the cytoplasmic entry site of the pore physically occluding the channel (3). In the C-type inactivation, despite what the terminology suggests, rearrangement of amino acid side chains in or near the pore are involved, similarly to the closing of the shutter on a camera (29).

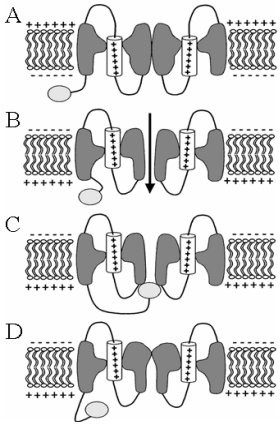

Figure 9. Conformation transitions in voltage-gated ion channels. **A:** resting state; **B:** open state in the depolarized membrane; **C:** N-type inactivation; **D:** C-type inactivation.

Molecular bases of cardiac ion currents

Revealing molecular features of the cardiac ionic currents is like building a bridge between electrophysiology and molecular biology. The majority of the conclusions are drawn in the light of expression levels of the ion channel subunit coding genes in the heart muscle and

through comparing the electrophysiological properties of the currents produced by cloned and heterologously expressed ion channel subunits to native cardiac currents. Isolating mutations in ion channels genes with known effect in ion channel related diseases may also provide useful information.

Interestingly, in case of the inward currents the molecular bases of the ionic currents are well founded. The voltage gated Na^+ channel gene family counts 11 members named as *SCN1A* to *SCN11A*. Each member shows similar structure with four six transmembrane helix-containing domains (Figure 7). Most of the gene family members are expressed in the central nervous system, while in the heart only the fifth isoform is present (4) (*SCN5A*, Table 1). It is the cardiac variant of voltage gated Na^+ channels that is responsible for the depolarization events in most of the cardiac tissue types.

Table 1. Molecular features of cardiac ion currents

Current	Pore forming subunit genes		Auxiliary subunit genes	
	Kv name	KCN name	Kv name	KCN name
I_{NA}	$Na_v1.5$	*SCN5A*	β1	*SCN1B*
			β2	*SCN2B*
I_{Ca} T-type	$Ca_v3.2$	*CACNA1H*		
L-type	$Ca_v1.2$	*CACNA1C*	β1	*CACNAB1*
			β2	*CACNAB2*
			α2δ	*CACNA2D1*
I_{to}	Kv1.4	*KCNA4*	KChIP2	*KCNIP2*
	Kv4.3	*KCND3*		
I_{Kur}	Kv1.5	*KCNA5*	Kvβ1	*KCNAB1*
			Kvβ2	*KCNAB2*
I_K (slow)	KvLQT1	*KCNQ1*	Mink	*KCNE1*
I_K (rapid)	HERG	*KCNH2*	Mink	*KCNE1*
			MiRP1	*KCNE2*
Pacemaker current	-	*HCN2*		
	-	*HCN4*		
I_{K1}	Kir2.1	*KCNJ2*		
	Kir2.2	*KCNJ12*		
$I_{K\text{-}ATP}$	Kir6.1	*KCNJ8*	SUR2	*ABCC9*
	Kir6.2	*KCNJ11*		
$I_{K\text{-}Ach}$	Kir3.1	*KCNJ3*		
	Kir3.4	*KCNJ5*		

The other important inward current is the Ca^{2+} influx conduced by sarcolemmal voltage-gated Ca^{2+} channels (I_{Ca}, Figure 4). I_{Ca} is produced by two different types of voltage-gated Ca^{2+} channels that are distinguished by their electrophysiological properties (71). The so-called T-type Ca^{2+} channels activate in the relatively hyperpolarized membrane and inactivate very fast. T-type Ca^{2+} channels are thought to contribute to pacemaker activity in the SAN and in the AVN. The second type of cardiac voltage gated Ca^{2+} channels is the L-type Ca^{2+}

channels. It plays a role in maintaining the characteristic long lasting plateau phase of the cardiac action potential and in excitation conduction coupling. Both the T-type and the L-type channels are encoded by the *CACNA1* gene family. The *CACNA1* gene family contains 10 members called *CACNA1A* to *CACNA1S*. T-type and L-type channels are encoded by the *CACNA1H* and *CACNA1C* genes, respectively (Table 1).

Contrary to the inward currents, determining the molecular features of the cardiac outward, mainly K^+ currents is much more challenging. The K^+ channels show the largest functional and structural diversity among the ion channels. According to their function, the K^+ channels may be classified as I_{to}, I_{Kur}, I_K and I_{K1} channels (Figure 4). On the other hand, there are approximately one hundred K^+ channel coding subunit genes in the human genome (15) and it appears that at least half of them are expressed in the heart. Furthermore, there are strong evidences showing that different K^+ channel subunits may co-assemble in channel complexes, further increasing the possible functional heterogeneity. Moreover, there are auxiliary subunits that may join to various channel complexes modulating channel function. The co-assembly of channel subunits and the existence of the auxiliary subunits in the heart muscle raise the number of theoretical combinations to almost infinite.

According to the Gene Nomenclature Committee of the Human Genome Organization most of the K^+ channel subunit coding genes belong to the *KCN* gene family. However, there is an alternative and widely used nomenclature. According to the latter, the six transmembrane domain subunits are denoted as KvN.N ('v' for voltage gated) and the two transmembrane domain subunits as KirN.N ('ir' for inwardly rectifying) where 'N'-s stand for numbers showing the number of the subfamily and the number of the member in the subfamily, respectively.

The known molecular bases of cardiac ion currents (45) are summarized in Table 1 including two K^+ channel types that have not been mentioned previously: the $I_{K\text{-}ATP}$ and the $I_{K\text{-}Ach}$ channels. Both of them conduct repolarizing K^+ currents and are built up by two transmembrane domain subunits (Figure 7). In the ventricles $I_{K\text{-}ATP}$ channels are located in the cell membrane, in the inner membrane of the mitochondria, as well as in the nuclear envelope (83). They provide a link between cellular metabolism and the electrical activity of the heart muscle cells since they are inhibited by ATP and opened by nucleotide diphosphates. Opening of $I_{K\text{-}ATP}$ channels is an important cellular response under hypoxic conditions and results in shortening of action potential durations and minimizing K^+ efflux. They are most likely involved in ischemic preconditioning of the heart. Mitochondrial $I_{K\text{-}ATP}$ channels are thought to help in maintaining the mitochondrial matrix volume in high-work states of the heart. $I_{K\text{-}Ach}$

channels are primarily present in the pacemaker regions of the heart (31). They are gated by a G protein-coupled mechanism mediated by muscarinic acetylcholine receptor. Acetylcholine is released on the axon termini of nervus vagus and mediates parasymphatic effects. Following the activation of the acetylcholine receptors, the opening of the $I_{K\text{-}Ach}$ channels results in a decrease of the pacemaker potential and slows down the heartbeat rate.

Channel disorders

Because heartbeat depends on the proper streaming of ions through the cell membrane during the heart cycle, disorders of ion channels play key roles in cardiac diseases. Ion channel diseases may result in disturbances of normal heart rhythm. When heart beats are too slow (bradycardia), or are so rapid that the heart can not be filled up with blood properly (tachycardia), circulatory collapse or heart failure may occur.

Ventricular tachycardia and ventricular fibrillation are the most serious and frequent consequences of many cardiac ion channel disorders. The mechanism of ventricular fibrillation is unclear, however, abnormal repolarization that results in elongated action potential duration is likely to play a role. The archetypical repolarization disease is called the long-QT syndrome since the elongated action potential appears as an expanded QT interval in the ECG. An elongated QT interval does not necessary result in abnormal heart rhythm; however, patients affected by long-QT syndrome are predisposed to ventricular tachyarrhythmias that may lead to sudden heart failure and death (61).

There are inherited and acquired types of long-QT syndrome. The heritable form is caused by mutations in ion channel genes and is inherited as autosomal dominant or autosomal recessive mutations (14). The more frequent dominant form is caused by gain of function mutations in the Na^+ channel genes or by loss of function mutations in one of the four I_K channel subunit coding genes (Table 2). The gain of function mutant Na^+ channels fail to become inactivated and thus drive an excess inward current during the plateau phase of the action potential, which leads to disruption in the balance between inward and outward currents resulting in delayed repolarization and prolonged action potential duration. In contrast, the long-QT causing K^+ channel mutant alleles are of dominant negative types that decrease I_{Kr} or I_{Ks}. The weaker repolarizing currents expand the action potential. The dominant negative effect of the above mutations may be explained by the fact that I_K channels are assembled from four subunits (Figure 7). Incorporation of a dominant negative mutant subunit changes the structure of the channel complex in a way that it results in a decreased ion conductance.

In addition to the dominant ones recessive mutations have also been reported to cause QT interval elongation. In patients homozygous for the far less frequent long-QT causing recessive alleles the slow component of I_K (I_{Ks}, Table 1 and 2) is absent. Such patients also suffer from congenital deafness due to lack of endolymph in the inner ear. Studies motivated by such individuals led to the recognition that I_{Ks} may be necessary for the endolymph production in the inner ear.

Several of the long-QT patients possess no clinical syndromes and go undetected. They are predisposed not only to eventual ventricular arrhythmias but also to effects of a number of extracardial medications including antibiotics, antidepressants or appetite suppressants. Many of these medicines have been shown to elongate QT interval by selectively blocking I_{Kr} channels (43). It is very likely that there is a repolarization reserve built in the large variability in the K^+ channels that is able to compensate the effects of some long-QT causing mutations. However, chemical block of repolarizing channels together with the effect of mutations may lead to the depletion of the repolarization reserve and to unexpected sudden cardiac death because of serious arrhythmias (60).

Table 2. Genes affected by mutations that cause inherited long QT syndrome. The autosomal dominant and the autosomal recessive forms are often called Romano-Ward and Jervell-Lange-Nielsen syndrome, respectively.

Gene	Current
Autosomal dominant (Romano-Ward)	
KvLQT1 (*KCNQ1*)	I_{Ks}
HERG (*KCNH2*)	I_{Kr}
SCN5A	I_{Na}
minK (*KCNE1*)	I_{Ks}
MiRP1 (*KCNE2*)	I_{Kr}
Autosomal recessive (Jervell-Lange-Nielsen)	
KvLQT1 (*KCNQ1*)	I_{Ks}
minK (*KCNE1*)	I_{Ks}

Studies on heritable forms of long-QT syndrome provided important insights into the pathophysiology of a far more frequent cardiac disease: heart failure (39). Heart failure represents the common consequence of many pathological processes like atherosclerosis, hypertension or viral infections. Regardless of the initiating factors the common phenotype is a dilated, poorly contracting heart. The affected patients suffer from decreased ability to exercise and shortness of breath. It has been shown that in heart failure the repolarizing K^+

currents are downregulated, which results in prolonged action potentials (7). Longer action potentials are adaptive in short term, because a longer plateau phase means more time available for excitation-contraction coupling which may compensate the inadequate pump function of the heart. However, longer action potential durations are maladaptive in long term since – similarly to the long-QT syndrome – they increase the risk of fatal ventricular arrhythmias.

In addition to the extension of the QT interval, shorter action potentials may also result in abnormalities in the heart rhythm through a slightly different mechanism. Certain mutations result in faster than normal inactivation of the Na^+ channels. This Na^+ channel dysfunction results in insufficient depolarization that may appear in the form of shortened action potentials. However, action potential shortening is most dramatic in those regions where the phase 1 transient K^+ current (I_{to}, Figure 4) is more prominent than in the adjacent regions, like in the epicardial layer of the ventricular wall compared to the inner layers (Figure 6). Due to the shorter action potentials in the epicardium the inner layers may re-excite the prematurely repolarized epicardial cells leading to idiopathic ventricular fibrillation, another frequent cause of unexpected sudden cardiac death (12).

Viral gene transfer into cardiomyocytes

The conventional ways of introducing genes into cells, such as calcium phosphate transfections and liposome- or lipofectamine-mediated methods, work poorly in primary cultures of adult cardiomyocytes and are of little value when genes need to be introduced into a large number of cardiac cells. Viral vectors, however, can be used to achieve this goal. In the past decades, several different viral gene transfer systems have been developed and most of them have been tested in cardiomyocytes. Type 5 adenoviruses work well in cardiomyocytes, but they are challenging to produce, and moreover, their immunogenicity prevents their use in long-term *in vivo* experiments (25). The adeno-associated virus is suitable for *in vivo* myocardial gene transduction because of its low or absent immunogenic potential (25), but its use for *in vitro* studies is limited by the low gene expression achieved in cardiomyocytes (73). According to our knowledge, the herpes viruses have not been suggested to use for gene transfer into cardiomyocytes. However, given the fact that herpes viruses are known to efficiently infect post-mitotic cells and considering our promising preliminary results on successful infections with a herpes virus into cardiomyocytes, the potential of herpes viruses for cardiac gene transfer *in vitro* and potentially *in vivo* is undeniable. In our second project the main objective was the development of an efficient herpes-virus-based-vector and the assessment of its capabilities in delivering genes into

ventricular cardiomyocytes. We chose to use the Pseudorabies virus, of which molecular biology is one of the best known ones among herpeviruses. In addition, in our third project, encouraged by recent reports on successful infections of cardiomycoytes by lentivirus vectors, we applied a lentivirus-based system to deliver artificial microRNAs to induce RNA interference thereby in atrial cardiomyocytes.

The Pseudorabies virus

Pseudorabies virus (PRV) is present and affects many aspects of our life. PRV is the causative agent of Aujeszky's disease in swine. Causing destructive disease and economic losses worldwide, PRV is of primary importance for those who are concerned about disease control in swine agriculture. PRV has served as a model organism for the study of molecular biology of herpesviruses. The virus is also being used as a tracer of neuronal pathways, making use of its remarkable ability to infect synaptically connected neurons (reviewed in 19).

Based on its broad host range, its rapid rate replication to produce new virus particles in a matter of hours accompanied by strong cytophatic effects and based on its ability to establish life-long infections in the sensory ganglia, PRV is classified into the Alphaherpesvirinae subfamily and into the Varicellovirus genus of herpesviruses. Like all herpesviruses, the PRV virion has a double stranded DNA genome enclosed in an icosahedral capsid. The capsid is surrounded by tegument proteins which are organized into two layers, one which interacts with the capsid and one which interacts with the envelope. The envelope, the outmost layer of the PRV virion is a lipid bilayer infused with transmembrane proteins. The life cycle of a herpesvirus consists of two main stages. While the *lytic cycle* has strong cytotoxic effects and results in the generation of new virions, in *latency*, the virus resides in rest in the nucleus of the host cell throughout the lifetime of the infected cell or until the virus returns into the lytic cycle in the course of a reactivation process. During the virion entry, the envelope fuses with the cell membrane and the capsid, together with the tegument proteins, is released into the cytoplasm. The tegument proteins interact with the protein synthesis machinery of the host cell immediately after entering the cell. The capsid is transported along the microtubules to the nucleus. Upon arrival to the nucleus, the only immediate early protein of PRV (*IE180,* Figure 10) is transcribed by RNA polymerase II and a transcriptional cascade begins. The IE180 protein is a transcriptional transactivator, it initiates transcription of early genes. Some early genes, such as *EP0* (Figure 10), act as transactivators and others are involved in the replication of viral DNA. Viral DNA is replicated by a rolling-circle mechanism. The onset of viral DNA replication signals the production of late proteins, including capsid proteins. The capsid is assembled in the nucleus and the virus genome is packed into the capsid. The fully

assembled capsid buds out of the nucleus into the cytoplasm, where it associates with tegument and envelope proteins. The virion gains its final envelope by budding into the trans-Golgi apparatus and finally, the mature virion is transported to the cell surface within a sorting vesicle. In latency, however, only a small portion of the virus genome is transcribed, resulting in the so-called latency associated transcripts (LATs, LLT and LRT, Figure 10). LATs are transcribed from the opposite strand of the *IE180* and *EP0* genes and are thought to negatively regulate their expression (56).

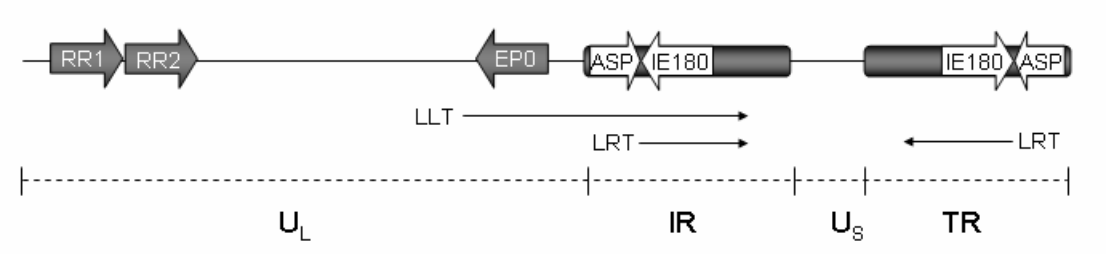

Figure 10. Schematic illustration of the PRV genome. RR1 and RR2 are open reading frames for the large and small subunits of ribonucleotide reductase. EP0 encodes early protein 0. ASP shows location and orientation of the latency associated antisens promoter, which mediates expression of LRT. IE180 encodes the immediate early protein 180. LLT and LRT stand for large latency associated transcript and latency related transcript, respectively. The scale bar in the bottom shows the main structural landmarks of the PR genome (U_L: long unique, IR: internal repeat, U_S: short unique, TR: terminal repeat).

Lentivirus vectors

Lentiviruses are classified into the *Lentivirnae* genus of retroviruses. Retroviruses are dependent on the host cell undergoing mitosis for the integration of the viral DNA with the host genomic DNA. Unlike other retroviruses, lentiviruses can enter the nucleus even without mitosis. This unique ability of lentiviruses among retroviruses makes them an ideal choice for delivering genetic material into growth-arrested cell types, such as cardiomyocytes. In the past decade, lentivirus-based gene transfer vectors have been developed from feline, simian, equine and human lentiviruses (80). Based on our massive and increasing knowledge on the molecular biology of the human lentivirus Human immunodeficiency virus type 1 (HIV-1), HIV-derived lentivirus vectors have evolved to be superior over vectors developed from viruses of other species.

HIV-1 is the etiologic agent of the acquired immunodeficiency syndrome (AIDS), a condition in which the immune system begins to fail leading to increased susceptibility for life-threatening opportunistic infections. HIV-1 primarily infects leukocytes such as helper T cells (specifically CD4 positive T cells), macrophages and dendritic cells. HIV-1 infection leads to low levels of CD4+ T cells through three main mechanisms: direct viral killing of

infected cells, increased rates of apoptosis in infected cells and killing of infected CD4+ T cells by CD8+ cytotoxic T cells that recognize infected cells. When CD4+ T cell numbers decline below a critical level, cell-mediated immunity is lost, and the body becomes progressively more susceptible to opportunistic infections.

The HIV-1 virion carries two copies of the single-stranded RNA genome, packed in a truncated cone-shaped nucleocapsid. Together with the RNA genome, several different enzymes, such as reverse transcriptase, protease, ribonuclease and intagrase are packed in the nucleocapsid. The nucleocapsid is surrounded by the matrix, which is composed of the viral matrix protein and which ensures the integrity of the nucleocapsid. The matrix, in turn, is surrounded by the envelope, a phospholipid bilayer, in which the hexameric envelop glycoprotein complexes are embedded. The envelop complexes, which can interact with the CD4 glycoprotein and with one of the co-receptors (usually CXCR4 or CCR5 chemokin receptors) on the surface of the leukocytes, are responsible for the tropism of the virus.

The HIV genome is extremely compact and has complicated structures. HIV has three structural and six accessory genes encoding altogether 19 proteins. During the production of viral proteins, the primary RNA transcript is multiply spliced, the spliced mRNAs are alternatively translated by the differential usage of overlapping reading frames and the primary protein precursors are further processed by proteolitic enzymes. The three structural genes encode viral proteins. *Gag* encodes matrix, capsid and nucleocapsid proteins, *pol* encodes three proteins that have enzymatic activities (reverse transcriptase, protease and integrase) and *env* carries information for the production of the two subunits of the envelope protein complex. The six accessory genes are regulatory genes that control expression of viral proteins (*tat* and *rev*) or interact with host cell processes (*nef*, *vif*, *vpr*, and *vpu*) determining virulence, pathogenicity of the virus (77).

During the development of modern HIV-based lentivectors, measures have been made to ensure biosafety and broad host range of the vector and the long-term expression of the transgene that is to be delivered into the target cells. Accessory genes which are not required for the generation of the vector or for a successful transduction, such as *nef*, *vif*, *vpr* and *vpu*, have been deleted from the HIV genome (Figure 11 A). The remaining genome has been split into three parts and has been engineered to be carried by three bacterial plasmids, which are often called packaging plasmids, allowing easy manipulation and production. One plasmid carries structural genes (*gag* and *pol*) and genes that transactivate either viral protein production or the transcription of the virus RNA genome during vector production (*rev* and *tat*). Another plasmid carries the gene encoding the envelope protein. In most of the cases,

instead of the *env* gene of HIV, pseudotyped lentivirus vectors are produced by using the envelope protein G of the Vesicular stomatitis virus (VSV-G). Pseudotyping by the VSV-G protein has two main advantages. Firstly, it confers the broad host range of VSV to the lentivirus vector. Secondly, the VSV-G pseudotyped lentivirus vector can withstand the shearing forces that are generated during ultracentrifugation, allowing the production and purification of high-titer virus stocks. The third plasmid, the so-called vector plasmid, in addition to the transgene, carries essential structural landmarks of the HIV genome, such as the packaging signal and the long terminal repeats (LTRs). The packaging signal is indispensable in the assembly of the virus capsid during production of new virions. LTRs have multiple functions. They govern replication of the virus genome by transcription, initiate reverse transcription during transduction and play a role when the virus genome is inserted into the genome of the host cell. Self-inactivating lentivectors have been developed by introducing a deletion in the 3` LTR, resulting in the loss of promoter function (SIN-LTR, Figure 11 B). During the vector production, the intact 5`LTR promotes transcription of the vector genome. When the vector genome is reverse transcribed in the host cell, however, the 5` LTR is replaced by the SIN-LTR which is no longer able to initiate transcription of the virus genome. Hence, the vector that is incorporated into the genome of the infected cell remains silent, only the transgene remains transcriptionally active. In the case of the so-called advanced generation of the lentivectors, two cis-acting elements, the so-called central polypurine tract (cPPT) of the HIV *pol* gene and a posttranscriptional regulatory element of the Woodchuck hepatitis virus (WPRE) have been added to the vector. These additions have been shown to enhance transduction efficiencies under various conditions (11).

Lentivectors are generated by introducing a mixture of the three packaging plasmids into the producer cells by calcium-phosphate or liposome mediated transfection. Most commonly Hek 293 cells are used for this purpose. Newly formed virus particles are harvested from the culture medium in the following 24-48h after transfection. Under these conditions, all essential structural proteins are provided *in trans* in the producer cells. However, only RNA molecules that are transcribed from the vector plasmid carrying the packaging signal are packed into the newly formed virions. Therefore, no viral protein-coding genes are introduced by the vector into the target cells during transduction, which greatly enhances biosafety by minimizing chances for the formation of replication-competent vectors (Figure 11 B).

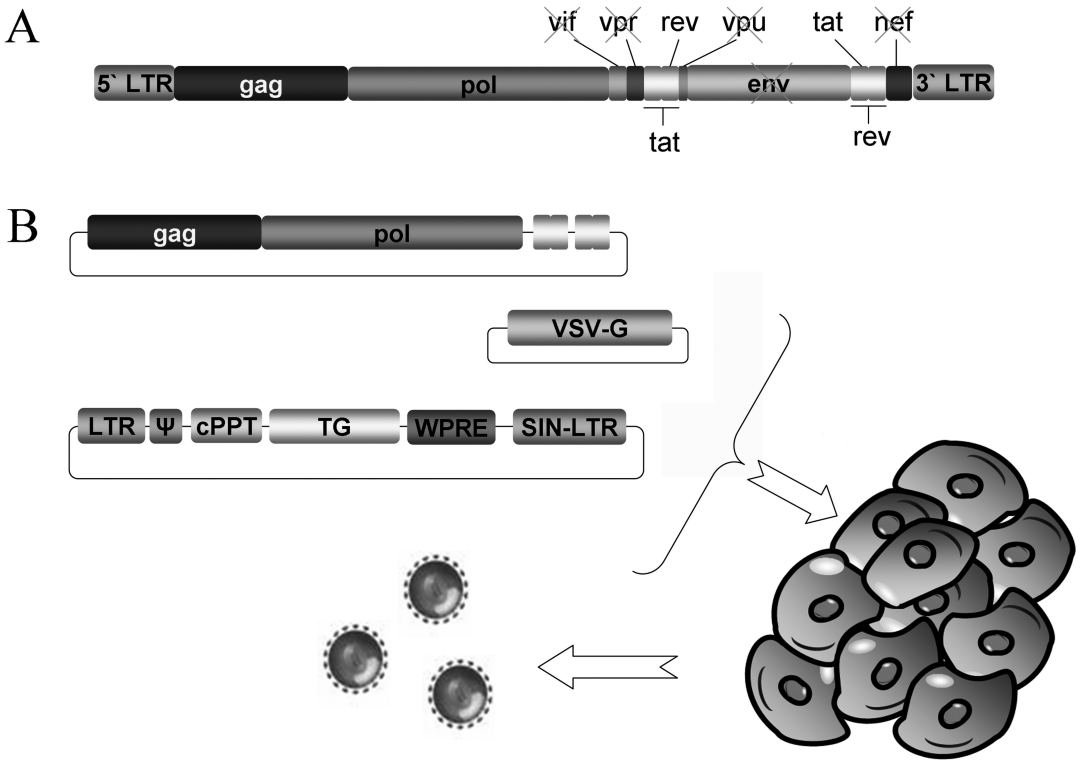

Figure 11. A: Genetic map of the HIV-1 genome. In the multiply attenuated lentiviral vectors five genes which contribute to the virulence and pathogenicity of HIV-1 are deleted. **B**: Working schema of lentivirus vector production. The packaging plasmids are co-transfected into Hek293 cells. Lentivirus particles are harvested from the supernatant of the culture medium.

RNA interference

RNA interference (RNAi) is a biological response to double-stranded RNA and is highly conserved in many organisms from yeast to human. RNAi mediates resistance to both endogenous parasitic and exogenous pathogenic nucleic acids, and regulates the expression of protein-coding genes. RNAi has become a powerful research tool for probing gene function by manipulating gene expression experimentally, and it has promising potential in biotechnology and medicine as well.

The two types of RNA molecules that play central role in the RNAi pathway are small interfering RNA (siRNA) and microRNA (miRNA) (28). siRNAs are 21-25 nucleotide long double-stranded RNAs (dsRNAs) with 3' dinucleotide overhangs and complete complementarity between the two strands. siRNAs are produced from relatively long dsRNAs through the action of the RNase III enzyme Dicer (Figure 12). Dicer recognizes dsRNA

substrates from many different sources. Viruses, transposons, experimentally introduced dsRNAs or endogenously expressed dsRNAs generated by bi-directional transcription are ultimately processed by Dicer. siRNAs operate in large ribonucleoprotein complexes termed RNA induced silencing complex (RISC). During RISC assembly, the double-stranded siRNA is unwound to incorporate only a single-stranded RNA molecule in the final active complex. Once assembled, siRNA-RISC recognizes and cleaves mRNAs complementary to the incorporated single-stranded siRNA.

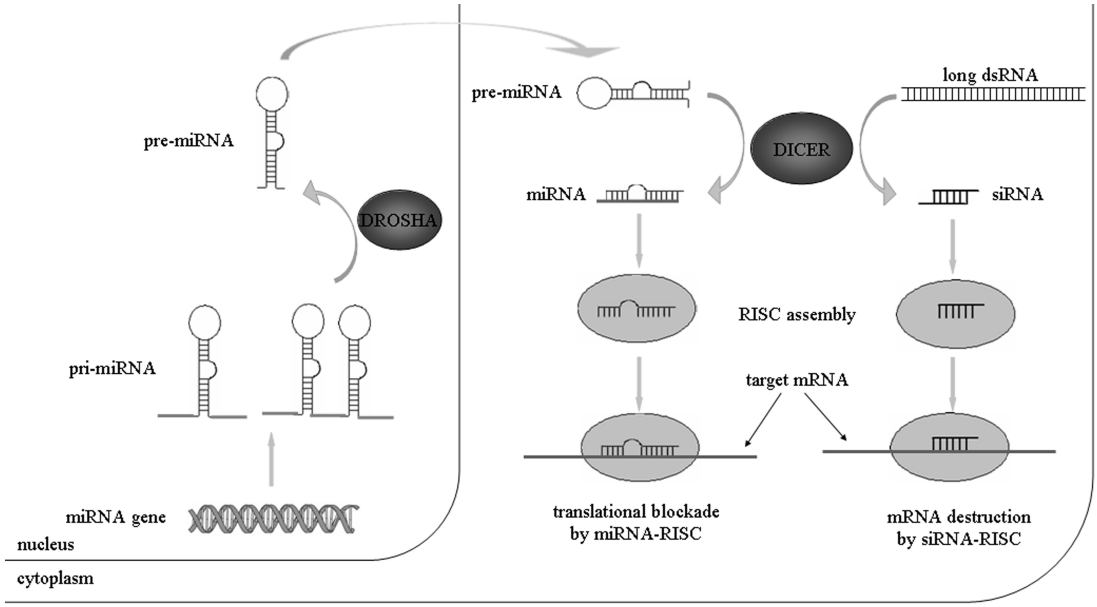

Figure 12. The RNAi pathway.

miRNAs, however, are derived from larger precursors that form characteristic imperfect stem-loop hairpin structures (pri-miRNA, Figure 12). Some miRNA genes are located in introns and some of them are clustered in polycistronic transcripts encoding two or more different miRNAs. The mature miRNA is released from the primary transcript through a stepwise processing by two RNase III enzymes: Drosha, which acts in the nucleus and Dicer, which acts in the cypolasm. One strand of the mature miRNA, the so-called guide strand, similarly to the siRNAs, is incorporated into the RISC complex. The miRNA-RISC complex binds to the complementary mRNAs. miRNAs usually have binding sites in the 3`UTR of the target mRNAs and function as translational repressors.

RNAi can be induced experimentally by several different ways. RNAi triggered by long dsRNA has been successfully used in *Caenorhabditis elegans* or in *Drosophila melanogaster*. Long dsRNA, however, is toxic for mammalian cells, possibly due to the activation of antiviral responses. In these cell types siRNAs, which are generated by *in vitro* DICER

cleavage or which are synthesized *in vitro*, can be used. Optionally, siRNAs could be genetically encoded in the form of a small hairpin RNA (shRNA). shRNAs have similar stem-loop structure to a pre-miRNA, but unlike miRNAs, they are fully complementary to their target mRNA. shRNAs are expressed from RNA polymerase III promoters, such as U6 or H1. The shRNA technology has recently been further improved by the development of miRNA-based shRNAs, the so-called shRNAmirs (72). shRNAmirs utilize the complete RNAi pathway by expressing a full-length pri-miRNA, in which the miRNA sequence has been replaced by the sequence of an siRNA complementary to the selected target mRNA (Figure 13 A). shRNAmirs can be expressed from RNA polymerase II promoters. Therefore, in addition to the greater knock-down efficiency, the shRNAmir system offers higher compatibility to the most frequently used vector systems, including those that allow regulated expression of the transgenes. shRNAmirs can also be used in combination with viral gene delivery systems. The genetic map of a lentivirus vector overexpressing a shRNAmir gene is shown in Figure 13 B.

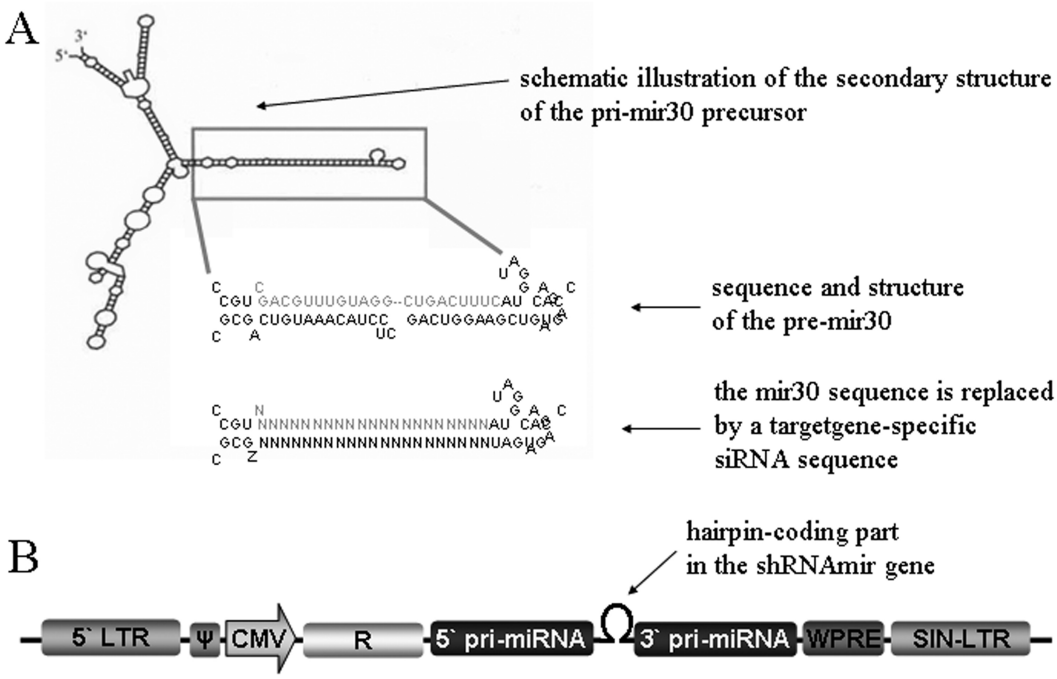

Figure 13. A: Schematic illustration of the general concept of shRNAmirs. In upper left the predicted structure of the mir30 precursor is shown. In shRNAmirs, the mir30-coding hairpin is replaced by a target gene-specific siRNA. **B**: Genetic map of shRNAmir expressing lentivectors. The shRNAmir is encoded in the 3`UTR of a reporter gene (R).

Materials and Methods

Tissue samples

Human heart tissue samples (approximately 100–150 mg for each sample) were isolated from 19 undiseased human donor hearts. The hearts were isolated from organ donor patients (Appendix) through pulmonary and aortic valve transplantation surgery. Before the explantation of the hearts, the patients did not receive any medication. Before preparation, the hearts were perfused with cardioplegic solution and were kept cool (4–6^{o}C) for 6–8 h. Cross sections of the ventricle and atrial walls were excised and frozen in liquid nitrogen. The protocol conforms to the principles outlined in the Declaration of World Medical Association proclaimed in Helsinki (Cardiovascular Research 1997; 35: 2–4) and was approved by the Ethical Review Board of University of Szeged (No.51–57/1997 OEj.).

Atrial cardiomyocyte and cardiac fibroblast isolation

Canine atrial cardiomyocytes and cardiac fibroblasts were isolated by previously described methods (82). All animal care procedures followed NIH guidelines and were approved by the Animal Research Ethics Committee of the Montreal Heart Institute. Adult mongrel dogs (20-30 kg) were anesthetized with morphine (2 mg/kg s.c.) and α-chloralose (120 mg/kg i.v.) and mechanically ventilated. The heart was removed after intra-atrial injection of heparin (10,000 U), immersed in 2 mmol/L Ca^{2+}-containing Tyrode's solution. The left coronary artery was cannulated and left-atrial tissue was perfused with Tyrode's solution (37°C, 100% O2), then with Ca^{2+}-free Tyrode's solution (~5 minutes), followed by ~40-minute perfusion with the same solution containing collagenase (~0.4 mg/mL, CLSII, Worthington) and 0.1% bovine serum albumin (BSA, Sigma). Tissue was minced and the cells were kept in medium-199. Cardiomyocytes were pelleted by centrifugation at 500 rpm (1 min) and cardiac fibroblasts were harvested from the supernatant. Cardiomyocytes were plated on laminin precoated coverslips in M199 medium (Invitrogen). Cardiac fibroblasts were plated in T25 tissue culture flasks in DMEM medium (Invitrogen), supplemented with 10% fetal calf serum (FCS, Gibco).

Ventricular cardiomyocyte isolation

All experiments were conducted in compliance with the NIH guidelines and were approved by the review board of the Committee on Animal Research of the Albert Szent-Györgyi Medical University. The modified protocol for cell isolation was based on established procedures described earlier in details (75). Canine ventricular myocytes were enzymatically

dissociated as follows. A portion of the left ventricular wall containing an arterial branch large enough to cannulate was perfused in a modified Langendorff apparatus with solutions in the following sequence:(1) normal Tyrode's solution (10 minutes), (2) Ca^{2+}-free Tyrode solution (10 minutes), and (3) Ca^{2+}-free Tyrode solution containing collagenase (type I, 0.66mg/mL) and bovine serum albumin (fraction V, fatty acid free, 2mg/mL) (15 minutes). Protease (type XIV, 0.12mg/mL) was added to the final perfusate while a further 15–30 minutes long digestion was allowed. Freshly dissociated cardiomyocytes were pelleted at 50g and resuspended in sterile solution five times. Ca^{2+} concentration was increased step-wise to 1mM. After the last centrifugation cardiomyocytes were resuspended in M199 medium (Sigma), supplemented with 5mM creatine, 2mM L-carnitine, 5mM taurine and100 units/mL insulin. Cells were plated on laminin precoated coverslips.

Whole-cell patch clamp

Whole-cell patch-clamp technique (voltage-clamp mode) was applied for characterizing macroscopic I_{to} parameters in control and transduced atrial cardiomyocytes. All experiments were performed at 36±0.5ºC. Borosilicate-glass electrodes had tip resistances between 1.5 and 3.0 MΩ when filled. Cell capacitance and series resistance were compensated by ~80% to 90% to minimize the capacitive surge on the voltage recording. Leakage compensation was not used. Cell capacitances were not different between experimental groups. The standard Tyrode solution contained (in mmol/L) NaCl 136, KCl 5.4, $MgCl_2$ 1, $CaCl_2$ 1, NaH_2PO_4 0.33, HEPES 5 and dextrose 10 (pH 7.35 with NaOH). The high-K^+ storage solution contained (in mmol/L) KCl 20, KH_2PO_4 10, dextrose 10, mannitol 40, L-glutamic acid 70, β-OH-butyric acid 10, taurine 20, EGTA 10 and 0.1% BSA (pH 7.3 with KOH). The standard pipette solution contained (in mmol/L) K-aspartate 110, KCl 20, $MgCl_2$ 1, MgATP 5, GTP 0.1, HEPES 10, Na-phosphocreatine 5, EGTA 5 with pH adjusted to 7.3 with KOH. Atropine (1-μmol/L), $CdCl_2$ (200-μmol/L) and tetraethylammonium chloride (10mmol/L) were added to the external solutions to eliminate muscarinic K^+-currents, to block I_{Ca} and I_{Kur}, respectively. I_{Na} contamination was avoided by using a holding potential at -50 mV.

Generation of recombinant PRV strains

Different PRV strains were propagated on subconfluent monolayer of porcine kidney (PK-15) cells. PK-15 cells were grown in DMEM (Sigma) supplemented with 5% FCS (Gibco). PRV was harvested from the supernatant of PK-15 cells infected by the virus at 1 m. o. i. 24 hours post-infection.

Recombinant PRV strains were generated in PK-15 cells by site-directed insertional mutagenesis. PK-15 cells were co-transfected with the purified DNA of the parent virus and a targeting plasmid. The targeting plasmid, in general, carries a reporter gene flanked by viral sequences. The viral sequences flanking the reporter gene are homologous to the genomic region where the reporter gene is to be introduced. The homologous sequences in the targeting plasmid and the viral genome allow double homologous recombination, which results in a recombinant virus genome. By careful targeting plasmid design a deletion can be introduced at the same time, compensating for the possible negative effects of an enlarged genome size on virus propagation.

The construction of the basic targeting plasmids has been described previously. The targeting plasmid for the ribonucleotide reductase (RR) gene carries a genomic fragment of PRV overlapping the open reading frames of the large (RR1) and the small (RR2) subunits of the RR enzyme (9). A deletion, including 1789 bp of the RR1 and 7 bp of the RR2 open reading frames was generated in this plasmid. The *EP0* gene targeting plasmid carries a PRV genomic fragment homologous to the *EP0* gene and a deletion affecting 1390 bps overlapping with the *EP0* open reading frame (8). The third targeting plasmid used in this study carries a viral genomic fragment homologous to the latency associated putative antisense promoter (ASP) (10). An EcoRI site was inserted into the TATA box of ASP, abolishing promoter function of ASP and allowing subcloning of reporter genes (lacZ, gfp, cameleon or troponeon).

Generation of shRNAmir expressing lentivectors

shRNAmir oligo sequences for the canine KCNE3 mRNA were designed by the web-based ‘shRNA retriever’ tool available on the homepage of Ravi Sachidanandam`s laboratory (http://katahdin.cshl.org/, Cold Spring Harbor Laboratory, NY, USA). During the entire procedure for cloning shRNAmirs, previously published protocols have been followed (50). Synthetic single-stranded shRNAmir oligonucleotides were PCR amplified and cloned directly in a modified version of pGIPZ lentivirus vector plasmid (Openbiosystems), in which the EcoRI site at position 5394 has been removed by partial EcoRI digestion, Klenow fill-in of 3` overhanging DNA ends and re-circularization.

Protocols for the generation of lentiviruses and the lentivirus packaging plasmids (psPAX2 and pMD2.G) were obtained from Didier Trono`s laboratory (http://tronolab.epfl.ch/, Ecole Polytechnique Federale de Lausanne, Lausanne, Switzerland). The vector and packaging plasmids were amplified in *E. coli* DH5α and purified by Nucleobond anion exchange columns (Macherey-Nagel) following the manufacturer’s instructions. The Hek293T/17 cell

line used for lentivirus production was obtained from ATCC (Manassas, VA, USA) and were grown in DMEM (Invitrogen) supplemented with 10% FCS. Lentiviruses were produced as it is briefly summarized below. A subconfluent monolayer of Hek293T/17 cells was transfected with a plasmid mixture containing the pGIPZ-shRNAmir vector, the psPAX2 and pMD2.G packaging plasmids in a 2:2:1 weight ratio, respectively, by the calcium-phosphate precipitation method. 12-14 hours after transfection, the culture medium was replaced by fresh DMEM supplemented with 10% FCS. The conditioned medium was harvested 36-48 hours post-transfection. The harvested medium was clarified from cell debris by filtration using a 0.45μm pore size syringe-attachable filter. For cardiac fibroblast infections, the filtered medium containing virus particles was either kept at +4^{o}C for short term or kept frozen in aliquots at -80^{o}C for long term use. For cardiomyocyte infections virus particles were precipitated by ultracentrifugation, re-dissolved in sterile PBS supplemented with 10% BSA and stored at -80^{o}C in aliquots.

Gene expression profiling in human cardiac tissue samples

Crude total RNA extracts from fresh or frozen tissues were obtained by following a protocol described by Gauthier et al (22). RNA samples were further purified by using Nucleospin RNA II kit (Macherey-Nagel), as recommended by the manufacturer. The concentration of total RNA samples was determined by UV-photometry.

Reverse transcription (RT) was performed by using Superscript II RNase H^{-} Reverse Transcriptase (Invitrogen). Each RT reaction mixture contained 5 μg total RNA, 200 U reverse transcriptase and 100 pmol $dT_{(15)}$ oligonucleotide at a final volume of 20 μl. Nine micro liters of the diluted RT products (corresponding to 56.25 ng total RNA equivalent) were used for each real-time RT-PCR assay. RNA samples were tested for the presence of genomic DNA contamination by running no-RT control reactions. Gene-specific primers were designed using the Primer Express software (Applied Biosystems) according to the software guidelines. Where splice variants were known, primers were designed in the invariable regions of mRNA splice alternatives. For primer sequences, see the online supplementary data in ref. 48). SYBR-Green PCR assays were performed on a Rotor-Gene 3000 (Corbett Research) real-time PCR platform. For each 20 μl reaction, 9 μl cDNA solution, 10 μl Absolute QPCR SYBR Green Mix (ABgene), 0.5 μl forward primer (10 μM) and 0.5 μl reverse primer (10 μM) were mixed together. To assess primer dimer formation, blank controls containing water as template were used for every primer pairs in each experiment. PCR parameters were as follows: 95^{o}C, 15 min for heat activation of DNA polymerase, followed by 94^{o}C, 25 s (denaturation), 61^{o}C, 25 s (annealing) and 72^{o}C, 15 s (synthesis) for

50 cycles. After each run a melting point analysis was performed by measuring fluorescence intensity in a temperature interval ranging from 55 to 93^{o}C. Samples showing abnormal melting point characteristics were excluded from analysis.

In a typical experiment expression levels of eight ion channel genes were analyzed along with β-actin as internal control. We calculated the relative copy numbers by normalizing each ion channel-coding mRNAs to β-actin using the 'Comparative Quantitation' module of the Rotor-Gene software (version 6.0, Corbett Research).

Based on the results of initial experiments we assumed that β-actin is stably expressed in both regions of the human heart analyzed in this study. To validate this hypothesis we compared the expression level of β-actin in the two regions of the heart. We constructed an external standard curve from a dilution series of a synthesized β-actin template. *CP* values of β-actin from ventricular and from atrial cDNAs were compared to the standard curve. We found that β-actin was 1.7-times more abundant in the left ventricle than in the left atrium. Hence, for a reliable comparison of gene expression levels in the ventricle with those in the atrium, we corrected the atrium related data by dividing the mean of the relative copy number of each mRNA by 1.7. Statistical analyses were performed using Student's t-test and significance was set at $P < 0.05$.

Validating MiRP2 knock-down in cardiac fibroblasts

Isolated canine atrial fibroblasts were plated in T-75 culture flasks in DMEM (Invitrogen) supplemented with 10% FCS. 5-7 days later, when the cells reached 60-70% confluency the fibroblasts were re-plated in 12-well culture plates at a density of 10^5 cells per well. After 3-5 hours allowing attachment of the cells, fibroblasts were transduced with shRNAmir-expressing lentivirus vectors at 10-30 m. o .i. 3 days later the culture medium was removed and the cells were lysed by adding 500 µl Trizol reagent (Invitrogen) per well. Total RNA samples were purified from the lysates by following the manufacturer's protocols supplied with the Trizol reagent.

First-strand cDNA samples were generated from 0.5 µg total RNA by the High Capacity cDNA Reverse Transcription Kit (Applied Biosystems) according to the manufacturer's instructions. SYBR-Green real time PCR reactions were performed on an MxPro 3000 platform (Stratagene), using SYBR Green PCR Master Mix (Applied Biosystems). Real time PCR data was analyzed by the Relative Expression Software Tool (REST) (54).

Statistics

In the gene expression profiling experiment, group means were compared by Student`s t-test. In other real time PCR experiments statistical analysis was done by the Pair Wise Fixed Reallocation Randomization Test implemented in REST software (54). Electrophysiological data was statistically analyzed by one-way ANOVA with Bonferroni`s post-hoc test where applicable, by SPSS 13.0 for Windows software. Significance level was set as $P<0.05$ in all experiments.

Results

Expression pattern of K^+-channel genes in the human heart

We designed PCR primer pairs for 31 ion channel genes. The well-known cardiac ion channels were selected at the first place, of which function in the heart has already been described. In addition, putative cardiac ion channel genes were also included in the study. The complete list of genes studied and the corresponding currents are shown in Table 3.

Table 3. List of the studied ion channel subunit genes. The currents to which the ion channel subunits presumably contribute in the human heart are presented in the 3rd and 6th columns.

Gene symbol	Alias	Function	Gene symbol	Alias	Function
Voltage gated K^+ channel subunits			Inward rectifier K^+ channel subunits		
KCNA2	Kv1.2	I_{Kur}	*KCNJ2*	Kir2.1	I_{K1}
KCNA4	Kv1.4	I_{to}	*KCNJ12*	Kir2.2	I_{K1}
KCNA5	Kv1.5	I_{Kur}	*KCNJ4*	Kir2.3	I_{K1}
KCNA7	Kv1.7	I_{to}	*KCNJ14*	Kir2.4	I_{K1}
KCNB1	Kv2.1	I_{Kur}	*KCNJ5*	Kir3.4	$I_{K\text{-}Ach}$
KCNC1	Kv3.1	I_{Kur}	*KCNJ8*	Kir6.1	$I_{K\text{-}ATP}$
KCNC3	Kv3.3	I_{to}	*KCNJ11*	Kir6.2	$I_{K\text{-}ATP}$
KCNC4	Kv3.4	I_{to}			
KCND1	Kv4.1	I_{to}	Auxiliary K^+ channel subunits		
KCND3	Kv4.3	I_{to}	*KCNAB1*	Kvβ1	I_{Kur}
KCNF1	Kv5.1	silent	*KCNAB2*	Kvβ2	I_{Kur}
KCNS3	Kv9.3	silent	*KCNE1*	minK	I_{Ks}
KCNH2	hERG	I_{Kr}	*KCNE2*	MIRP1	I_{Kr}
KCNQ1	KvLQT1	I_{Ks}	*KCNE3*	MIRP2	I_{Kr}
			KCNIP2	KChIP2	I_{to}
Two pore domain K^+ channel subunit			*KCNIP3*	CSEN	
KCNK1	TWIK1	I_{K1}	*ABCC8*	SUR1	$I_{K\text{-}ATP}$
			ABCC9	SUR2	$I_{K\text{-}ATP}$

The I_{to}-related K^+ channel subunits

We studied the mRNA levels of six putative I_{to}-related voltage gated K^+ channel subunits in the human left ventricle and left atrium. The comparative expression levels of the corresponding genes are as follows; ventricle: Kv1.7 > Kv4.3 > Kv3.4 >* Kv1.4 >* Kv4.1 >* Kv3.3; atrium: Kv1.7 > Kv4.3 > Kv3.4 > Kv4.1 > Kv1.4 >* Kv3.3 (Figure 14 A). The significant differences are labeled with an * (here and in the rest of the 'Expression pattern of K^+-channel genes in the human heart' section). The Kv3.3 and Kv4.1 transcripts are at least ten times more abundant in the atrium as compared to the ventricle, while expression levels of Kv1.4, Kv1.7, Kv3.4 and Kv4.3 are similar in the two regions of the heart. Surprisingly, the expression level of Kv1.7 and Kv3.4 were high and fell into the same range as that of Kv4.3 both in the ventricle and the atrium (48).

The I_{Kur}-related channel subunits

Four K^+ channel subunits have been identified thus far that produce currents in heterologous expression systems similar to the human I_{Kur}: Kv1.2, Kv1.5, Kv2.1, Kv3.1 (44). We found that the expression levels of these genes is Kv1.5 >* Kv2.1 >* Kv1.2 > Kv3.1 in the atrium and Kv2.1 > Kv1.5 >* Kv1.2 > Kv3.1 in the ventricle (Figure 14 B). Kv1.5 transcripts are approximately 30-fold more abundant in the atrium than in the ventricle. We found that Kv3.1 was 5-fold more abundant in the atrium than in the ventricle, while there was no significant difference between the expression levels of Kv1.2 and Kv2.1 in the two regions of the heart (48).

The I_{Kr}- and I_{Ks}-related subunits

I_{Kr} and I_{Ks} are the rapidly and slowly activating components of I_K. hERG subunits form those channels that are responsible for I_{Kr}, while I_{Ks} channels built up by KvLQT1 subunits (13). It has turned out by comparing abundances of the pore-forming subunits of the two I_K components that hERG mRNA was significantly more abundant ($P < 0.05$) than KvLQT1 transcripts were in the ventricle, while the two genes were expressed at approximately the same level in the atrium. Both hERG and KvLQT1 are expressed at a higher level than their possible interacting auxiliary subunits, both in the ventricle and atrium (Figure 14 C) (48).

Modulatory 'silent' subunits of the K^+ channels

We measured the expression level of two so-called 'silent' voltage gated K^+ channel subunits: Kv5.1 and Kv9.3. The Kv9.3 message appears to be more abundant than that of Kv5.1 in both the ventricle (is approximately 100 times more abundant) and in the atrium (is almost 10

times more abundant) (Figure 14 B). Both silent subunits are expressed at a significantly higher ($P<0.05$) level in the atrium compared to the ventricle. In addition, in the atrium Kv9.3 expression level is slightly higher ($P<0.05$) than that of its interacting partner Kv2.1 (48).

Auxiliary subunits of the voltage gated K^+ channels

Kvβ subunits are cytosolic proteins and have been shown to co-assemble with members of the Kv1 subfamily (24). We designed primer pairs to amplify the cDNAs that correspond to the Kvβ1- and the Kvβ2-coding mRNAs. One primer pair recognizes all three known variants of Kvβ1 mRNA and the other amplifies both of the two known Kvβ2 variants. We detected both Kvβ-coding mRNAs in both of the left ventricles and atriums. Kvβ1 was more abundant ($P<0.05$) than Kvβ2 in the atrium, while there was no significant difference between the expression levels of the two genes in the ventricle (Figure 14 D). Furthermore, both Kvβ subunits seem to be upregulated in the atrium as compared to the ventricle ($P<0.05$) (48).

KCNE gene family consist of genes that encode membrane proteins (termed mink-related peptides; MiRPs) with one transmembrane domain interacting with Kv, KCNQ and ERG channels in heterologous expression systems (41). Until today, five members of the *KCNE* gene family have been described (38). We analyzed the expression level of three members of the *KCNE* gene family and established the following expression pattern in the atrium: KCNE1 >*KCNE3 >* KCNE2 (Figure 14 C) and confirmed results of Lundquist et al. (38). However, in contrast to the data published by Lundquist et al. (38) we did not detect significant differences in the abundances of the above transcripts in the ventricle (48).

The I_{KI}- related inward rectifiers

We analyzed the four known Kir2 subunits contributing to I_{K1} and measured similar expression patterns both in the ventricle (Kir2.3>* Kir2.2>Kir2.4>Kir2.1) and atrium (Kir2.3>Kir2.2>* Kir2.4>*Kir2.1; Figure 14 E). With the exception of Kir2.2, which is almost 8-fold more abundant in the atrium than in the ventricle, all genes show the same expression levels in the two heart regions (48).

TWIK1 is a representative member of the so-called two-pore-domain K^+ channel family and is thought to play a role in the formation of I_{K1}. It has turned out that abundance of the TWIK1-coding transcript is significantly higher (approximately 5-fold; $P < 0.05$) in the atrium than in the ventricle. Furthermore, comparing the expression level of TWIK1 to that of the other subunits contributing to I_{K1} we learnt that the TWIK1-coding mRNA is most abundant in the atrium and the second most abundant in the ventricle (Figure 14 E) (48).

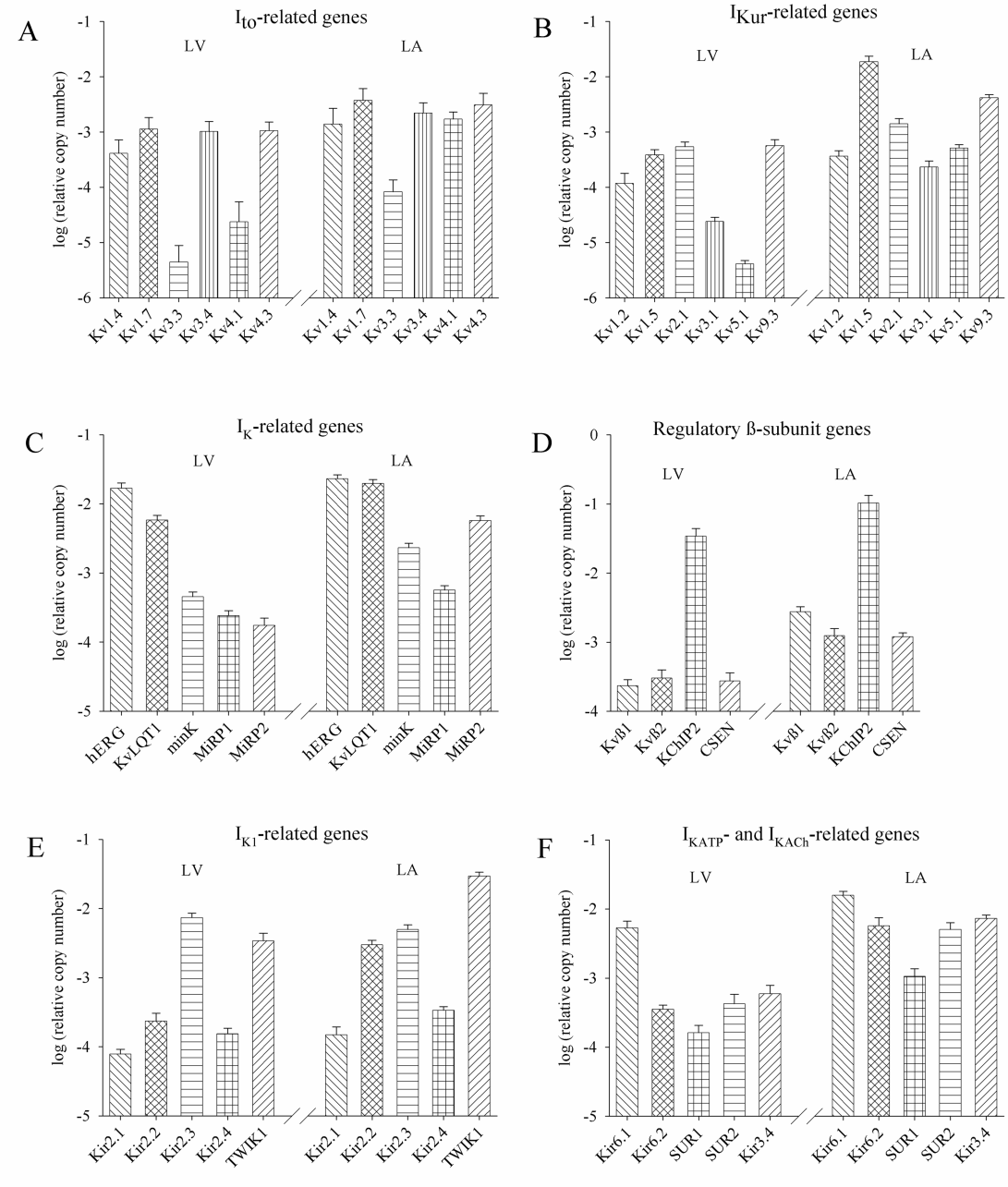

Figure 14. Relative expression level of the different ion channel subunit coding genes in the human heart as determined by real-time quantitative RT-PCR. The mRNA levels were quantified in tissue samples collected from the left ventricle (LV) and left atrium (LA). Data were normalized to the expression level of cytoplasmic β-actin and is presented as mean ± SEM.

The $I_{K\text{-}ATP}$ channel subunits

We measured the expression level of two pore-forming subunits of I_{KATP} channels, Kir6.1 and Kir6.2. In $I_{K\text{-}ATP}$ channels the Kir6.1 and the Kir6.2 subunits are associated with sulfonylurea

receptor subunits (SUR) depending on the tissue type. There are four human SUR isoforms: SUR1 and three splicing variants of SUR2 (SUR2A, SUR2B and SUR2A-delta-14). We designed one primer pair for SUR1 and another one that recognizes all of the three variants of SUR2. The expression pattern of the genes mentioned above is very similar in the two studied regions of the human heart: Kir6.1 is significantly the most abundant ($P < 0.05$), Kir6.2 and SUR2 are less abundant and expressed at the same level compared to each other ($P < 0.05$), while SUR1 shows the lowest ($P < 0.05$) expression level (Figure 14 F). However, each of the four genes is expressed at a significantly higher level ($P < 0.05$) in the atrium as compared to the ventricle (48).

Herpes-virus mediated gene transfer into cardiomyocytes

Non-viral gene delivery methods perform well in most of the immortalized cell lines, however, they have limited efficiency in primary cells like post-mitotic cardiomyocytes. We explored the applicability of the *Pseudorabies virus* as a gene delivery vector in isolated adult cardiomyocytes (57). We constructed triple-attenuated viruses that carry either the Cameleon or the Troponeon fluorescent marker genes. Deletions were generated in the *RR1*, *RR2* and *EP0* genes of the wild-type Kaplan strain of PRV (Figure 15 A) in two subsequent steps, resulting in the Δ*RR1, RR2, EP0* genotype virus. As a third step of the vector construction, reporter gene cassettes were inserted into the inverted repeat region of the virus genome (Figure 15 A). Either the Cameleon or the Troponeon Ca^{2+}-sensor reporter genes were used, resulting in the Δ*RR1, RR2, EP0, +Cam* or in the Δ*RR1 ,RR2, EP0, +Tropo* genotypes, respectively. Virus vectors of both aforementioned genotypes were used to infect isolated canine ventricular cardiomyocytes. The efficacy of the infections was high in both cases, reaching a virtual 100% efficiency, according to visual observations made by epifluorescent microscopy (Figure 15 B). There was no detectable increase in cell mortality in the virus infected group of cells compared to uninfected control cells (57). Moreover, the Troponeon reporter gene, delivered by the PRV vector into canine cardiomyocytes, as assessed by FRET-analysis in contracting cardiomyocytes, has been shown to be functional (Figure 15 C) (57).

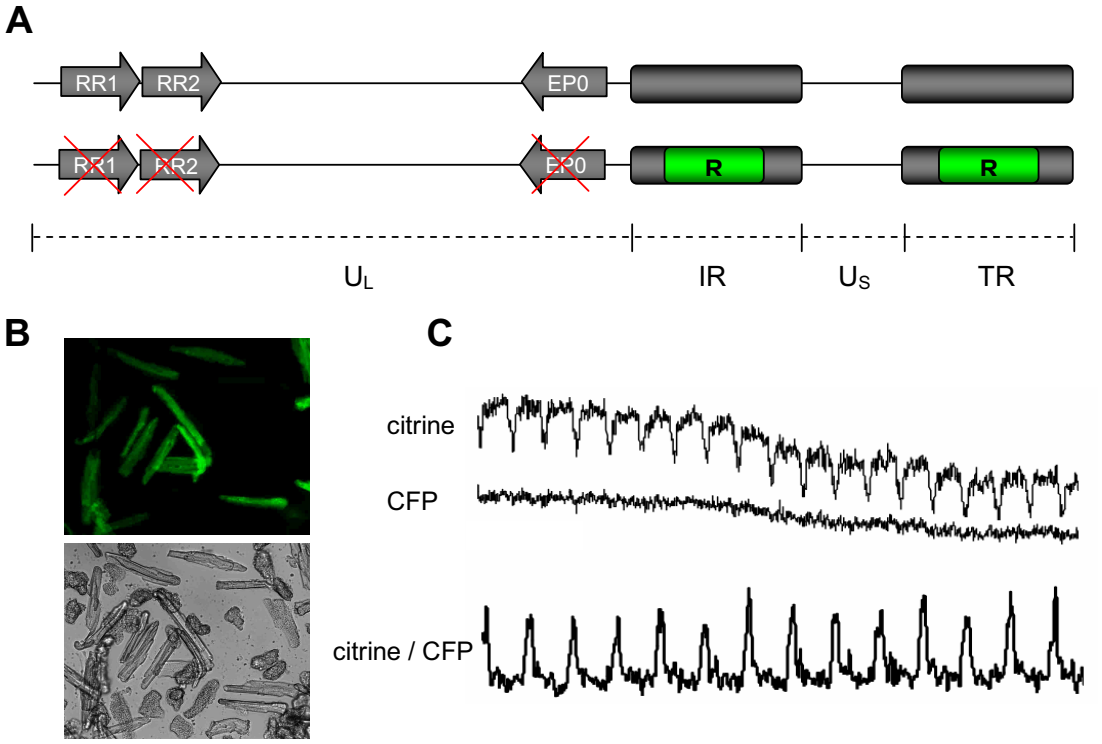

Figure 15. PRV is a potent gene delivery vector in isolated cardiomyocytes. **A:** Schematic representation of the genomic organization of the wild type Kaplan strain (upper bar) and that of the triple-attenuated vector strain (lower bar) of PRV. The triple-attenuated vector strain carries deletions in RR1, RR2 and EP0 genes and two copies of the Cameleon or Troponeon reporter genes (R). The scale bar in the bottom denote the four major genomic regions (UL: long unique, US: short unique, IR: internal repeat, TR: terminal repeat) of PRV. **B:** Photomicrographs show isolated canine ventricular cardiomyocytes 48 hours after infection by the Δ*RR1, RR2, EP0, +Cam* PRV vector carrying the Cameleon reporter gene. **C:** Fluorescence emission traces recorded from contracting cardiomyocytes that were previously transfected by the Δ*RR1, RR2, RP0, +Tropo* PRV vector expressing the Troponeon reporter gene. The recurrent peaks of the calculated citrine / CFP emission ratio indicate Ca^{2+} content increase in the cytoplasm during contractions. Fluorescence emission traces were taken from reference (57).

Role of the MiRP2 regulatory subunit in I_{to} channels

Validating MiRP2 mRNA knock-down in canine atrial fibroblasts

By gene expression profiling of ion channel genes in the human myocardium, among other interesting results we found that MiRP2 is abundantly expressed in both studied regions, particularly in the left atrium of the human heart. To assess possible role of MiRP2 in atrial cardiomyocytes, we created shRNAmir-expressing lentivirus vectors by which we aimed to generate functional MiRP2 knock-out cardiomyocytes by inducing RNAi targeted to the MiRP2 mRNA.

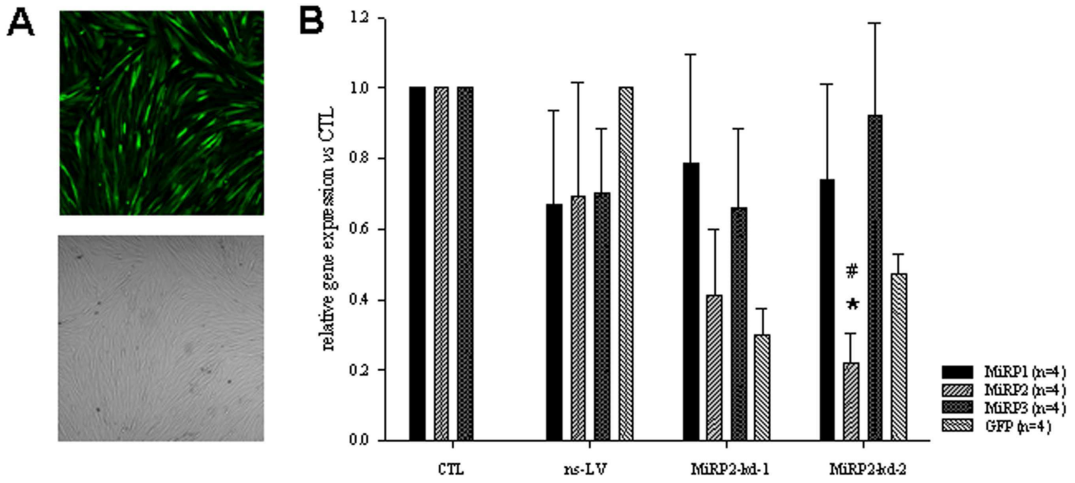

Figure 16. A: Photomicrograph examples show canine atrial fibroblasts infected by lentivirus vector at 10 m. o. i. **B:** Real time PCR results show efficient knock-down of the targeted MirRP2 mRNA in canine atrial fibroblasts. CTL: uninfected control, ns-LV: non-silencing lentivirus vector, MiRP-kd-1 and 2: lentivirus vectors expressing MiRP2-specific shRNAmirs. MiRP gene expression levels were normalized to CTL. To control virus load, gene expression level of the GFP was quantified and compared to that of the ns-LV group. Data is presented as mean ± standard error of measurement, # shows significant difference *vs* CTL ($P<0.05$) and * shows significant difference *vs* ns-LV ($P<0.05$).

To validate knock-down efficiency of the MiRP2 mRNA we used primary cultures of canine atrial fibroblasts as a model system. Real time PCR results showed an 80% knock-down *vs* uninfected control group and about 40% knock-down efficiency *vs* control group infected by a non-silencing lentivirus vector by one of our MiRP2-targeting lentivirus vectors (MiRP2-kd-2, Figure 16). mRNAs of the other two members of the KCNE gene family investigated (MiRP1 and MiRP3) were not affected.

Effect of MiRP2 knock-down on macroscopic I_{to} parameters

To evaluate possible role of MiRP2 in I_{to} channels, we functionally knocked down MiRP2 in isolated canine atrial cardiomyocytes by using our pre-validated lentivirus vector targeting MiRP2 (MiRP2-kd-2, Figure 17).

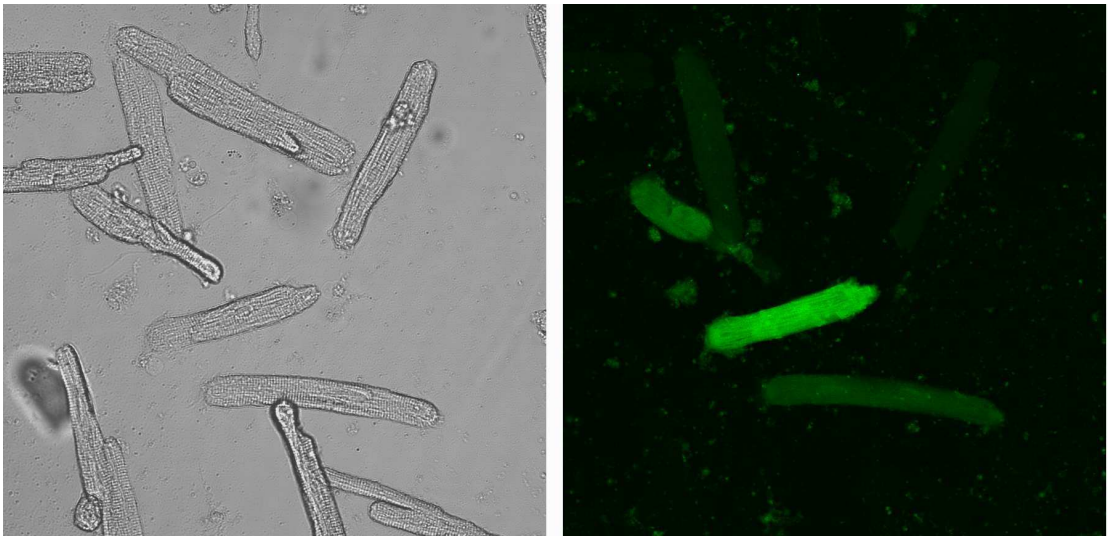

Figure 17. Photomicrograph examples show canine atrial cardiomyocytes infected by the MiRP2-targeting lentivirus vector. Images were taken 72 hours after infection.

I_{to} was characterized by the whole-cell voltage clamp method in freshly isolated cells (Fresh), in cultured cells with no virus added (CTL group) and in cultured cells that were infected by either a control lentivirus vector expressing GFP only (empty LV), a control lentivirus vector expressing a non-silencing shRNAmir (ns LV) or the MiRP2-targeting lentivirus vector (MiRP2-kd-2) 72 hours after infection. The summary of our results is shown in Table 4.

Table 4. Effect of MiRP2 knock-down on macroscopic I_{to} parameters in canine atrial cardiomyocytes. Data is presented as mean ± SEM. +, $, # and * represent significant difference *vs* Fresh, CTL, empty LV and ns LV, respectively.

	Current density (pA/pF, +50mV)	n	Activation TtP (ms , +50mV)	n	SS-act. $V_{0.5}$ (mV)	n	SS-inact. $V_{0.5}$ (mV)	n
Fresh	7.5 ± 1.1	8	4.8 ± 0.5	8	9.0 ± 1.1	6	-30.8 ± 2.4	8
CTL	11.4 ± 0.9	12	5.7 ± 0.2	12	3.2 ± 1.8	7	-25.4 ± 1.2	9
empty LV	14.0 ± 1.1 $^{+}$	9	5.0 ± 0.2	8	6.3 ± 2.9	4	-29.3 ± 1.7	6
ns LV	12.0 ± 1.1	6	5.8 ± 0.3	6	8.8 ± 2.2	6	-25.6 ± 1.9	6
MiRP2-kd-2	15.1 ± 1.6 $^{+}$	7	5.5 ± 0.4	5	4.9 ± 0.6	4	-20.9 ± 0.7 $^{+}$	4
	τ fast (ms, +50mV)		τ slow (ms, +50mV)		$A_{fast}/(A_{fast}+A_{slow})$ (%, +50mV)			n
Fresh	5 ± 0.7		24.5 ± 5.8		51.8 ± 4.2			11
CTL	10.4 ± 1.7 $^{+}$		44.3 ± 3.6		28.1 ± 3.7 $^{+}$			11
empty LV	9.8 ± 1.5		44.8 ± 5.3		35.8 ± 5.6			9
ns LV	8.9 ± 1.2		35.2 ± 4.9		32.5 ± 7.0			6
MiRP2-kd-2	18.2 ± 1.6 $^{+\$\#*}$		100.0 ± 24.1 $^{+\$\#*}$		28.0 ± 5.3 $^{+}$			6

Current-voltage relations

Current-voltage relations of I_{to} were elucidated by voltage steps from a holding potential at -50 mV to -40 to +50 mV. When measured at +50 mV, I_{to} densities were significantly increased in two of the virus-infected groups (14.0 ± 1.1, n=9, empty LV and 15.1 ± 1.6, n=7, MiRP-kd-2) compared to Fresh (7.5 ± 1.1, n=8) (Table 4), but MiRP2 knock-down had no significant effect compared to CTL or to the ns LV group (Figure 18).

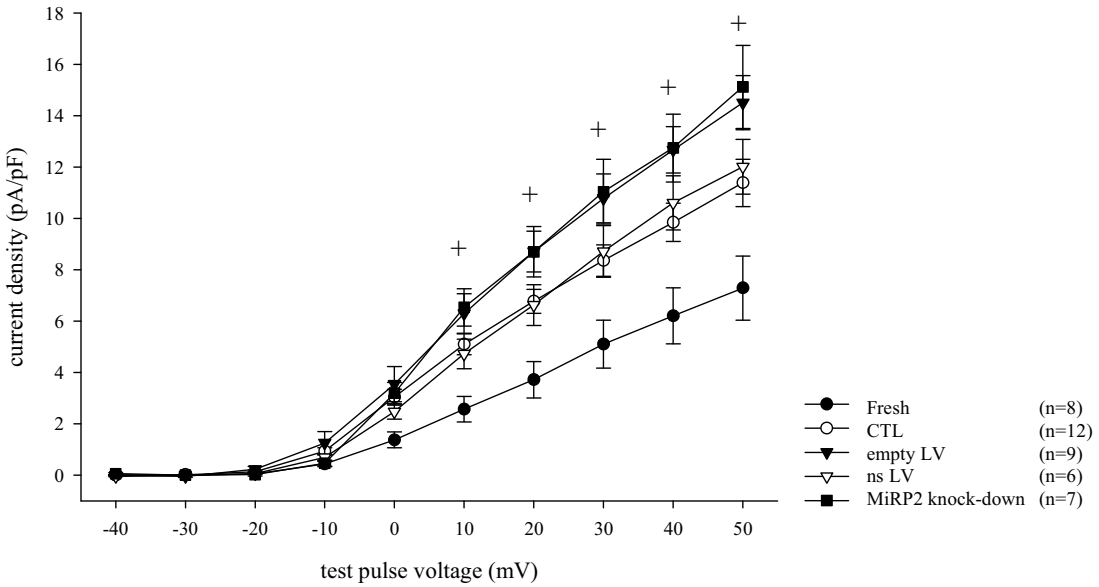

Figure 18. Current-voltage relations. Data is presented as mean ± SEM. Statistics is shown for the MiRP2 knock-down group only. + represents P<0.05 vs Fresh.

Voltage-dependence of activation and inactivation

The steady-state activation values were calculated from current-voltage relations. Reversal potentials were measured for each cell and were corrected by the liquid junction potential (-10 mV). Half-maximal activation voltage was not significantly different between the experimental groups (Table 4, Figure 19). Steady-state inactivation of I_{to} was evaluated by using a standard prepulse-test pulse voltage clamp protocol. The I_{to} amplitude was determined and plotted as a function of prepulse voltage. Half-maximal inactivation voltage in MiRP2 knock-down group was significantly less negative than in the Fresh group (-20.9 ± 0.7, n=4 *vs* -30.8 ± 2.4, n=8), but ANOVA did not detect significant differences between MiRP2-kd-2 and ns LV or empty LV groups (Table 4, Figure 19).

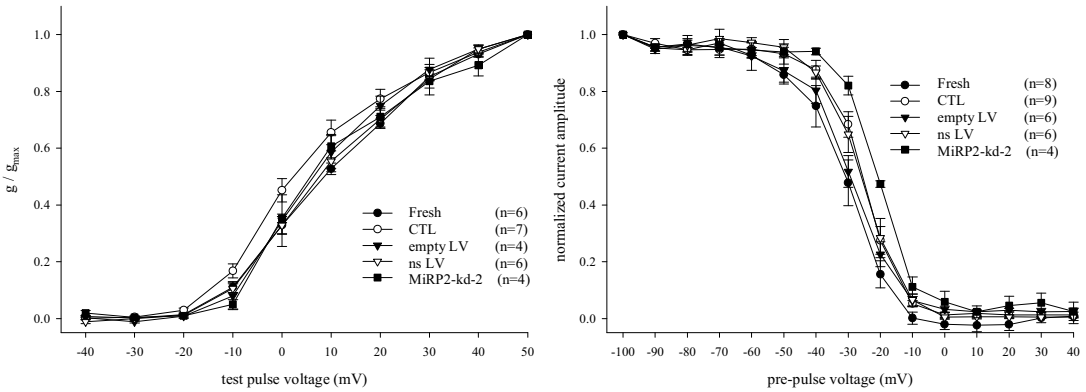

Figure 19. Steady-state gating of I_{to}. Left panel: activation voltage dependence. Right panel: voltage dependence of inactivation.

Time course of activation and inactivation

We also analyzed the effect of MiRP2 knock-down on activation and inactivation kinetics of I_{to}. Time course of activation was evaluated by measuring time to peak current (TtP). MiRP2 knock-down had no effect on activation kinetics (Table 4, Figure 20 A). Time course of inactivation was elucidated by fitting biexponential function ($f(t) = A_{slow}\, e^{-t/\tau slow} + A_{fast}\, e^{-t/\tau fast}$) to individual current traces. Time constant of the fast component of inactivation (τ_{fast}) was significantly increased in the MiRP2 knock-down group (18.2 ± 1.6, n = 6) compared to the ns LV group (8.9 ± 1.2, n = 6) at +50 mV test pulse (Table 4, Figure 20 B). Similarly, time constant of the slow inactivation component (τ_{slow}) increased significantly in MiRP2 knock-down group (100.0 ± 24.1, n = 6) *vs* ns LV group (35.2 ± 4.9, n = 6) (Table 4, Figure 20 D). Relative contribution of the fast inactivation component to total I_{to} inactivation was analyzed by comparing the amplitude of the fast inactivation component (A_{fast}) to the total amplitude ($A_{fast} + A_{slow}$). The fast component contributes significantly less to total I_{to} inactivation in the CTL group (28.1 ± 3.7, n=11) *vs* Fresh (51.8 ± 4.2, n = 11), but MiRP2 knock-down had no significant effect compared to CTL, empty LV or ns LV groups (Table 4, Figure 20 C).

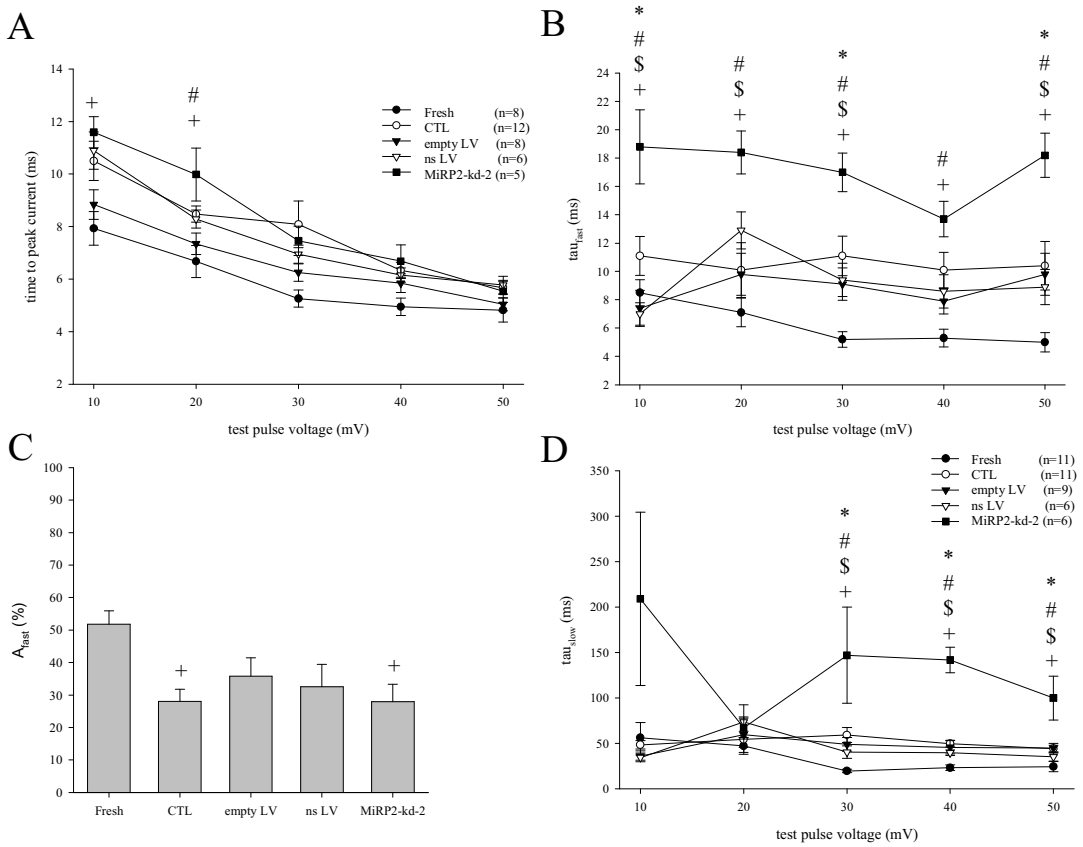

Figure 20. A: Time to peak (TtP). **B:** Time constant of the fast inactivation component (τ_{fast}). **C:** Relative contribution of the fast inactivation component (A_{fast}) to inactivation. **D:** Time constant of the slow inactivation component (τ_{slow}). Data is presented as mean ± SEM. +, $, # and * represent significant difference *vs* Fresh, CTL, empty LV and ns LV, respectively. Figure legend for panel B and D is shown in panel D.

Discussion

Expression pattern of K^+-channel genes in the human heart

In 2006 we reported among the first ones the gene expression level of a comprehensive set of ion channel genes in the undiseased human myocardium (48). We aimed to confirm and analyze the expression and relative abundance of mRNAs of the well-known ion channel genes, which may help us to extrapolate findings obtained in model organisms to the human heart. In addition, based on the notion that many more ion channel genes exist than ion currents we know, we extended the focus of this study on novel cardiac ion channel gene candidates. We carefully collected data available in the literature and selected new genes to include in the study if one of the two following criteria was met: i) the expression of the cardiac ion channel gene candidate has been shown in cardiac tissues of model organisms but not in the human heart, ii) an interaction between the cardiac ion channel candidate and a

well-known cardiac ion channel has been shown by co-expression studies or by means of biochemical techniques detecting protein-protein interactions. We reported the high expression level of novel cardiac ion channel gene candidates, of which possible role in the heart has not been considered previously. Therefore, our gene expression profiling data may serve as a basis for the design of studies aiming to reveal new ion channel gene functions in the human heart. We discuss our most important findings below.

The I_{to}-related K^+ channel subunits

I_{to} is generally considered to have two components, one based on Kv4.2/Kv4.3 alpha subunits showing rapid recovery from inactivation, and one that recovers slowly from inactivation and is based on Kv1.4 (53). We analyzed the expression level of six putative I_{to}-related K^+ channel genes: Kv1.4 (55), Kv1.7 (32), Kv3.3 (79), Kv3.4 (68), Kv4.1 (51) and Kv4.3 (69). These ion channels produce currents with fast activation and rapid inactivation kinetics in heterologous expression systems, therefore they are possible candidates for physiologically important I_{to} subunits. Nevertheless, the literature is bountiful regarding their expression in the human heart. Kv1.4 has not yet been detected in human heart by Western blot analysis (78). Furthermore, the same study showed no effect of antisense oligonucleotides targeted against the Kv1.4 transcripts on human atrial I_{to} (78). In contrast, in more recent studies it has been shown that Kv1.4 is expressed in the human atrium (6) and ventricle (74). Expression of Kv1.7 has also been described in the human heart (5), but its function has not yet been elucidated. There is no data in the literature on the expression of the Kv3.3 and Kv3.4 genes in the human heart. Kv3.3 and Kv3.4 transcripts have not been detected in rat heart (47), however, the presence of Kv3.4 protein has been shown by immunohistochemical studies and western blots both in canine Purkinje fibers and canine ventricular muscle (26). The Kv4.1 and Kv4.3 coding mRNAs have also been shown to be expressed in human heart (30). We detected all of the six putative I_{to} channel coding mRNAs in the human heart (48), including Kv3.3 and Kv3.4, which have not been described in human cardiac tissues previously. Furthermore, we have shown that expression levels of Kv1.7 and Kv3.4 are high and fell into the same range as that of Kv4.3 both in the ventricle and in the atrium (48).

In heterologous expression systems the current produced by Kv1.7 or Kv4.3 is insensitive for TEA (32), while Kv3.4 current is blocked by TEA (68). In the dog, ventricular I_{to} is not sensitive for TEA, while in Purkinje fibers a prominent block of I_{to} by TEA was reported (27). Kv3.4 protein is more abundant in canine Purkinje fibers than in ventricular muscle and Kv3.4 was suggested as a candidate responsible for the larger TEA-sensitive I_{to} component in Purkinje fibers (26). On the other hand, we found relatively high expression level of Kv3.4 in

the ventricle where I_{to} is not blocked by TEA. It thus remains to be determined whether Kv3.4 plays a role in the formation of ventricular I_{to} and whether the TEA sensitivity of Purkinje cell I_{to} is due to the presence of Kv3.4 or possibly due to associated accessory subunits.

The I_{Kur}-related channel subunits

I_{Kur} is driven by Kv1.5 (20) and is a substantial current in atrial cells, but appears to be absent in the ventricle. Accordingly we found that Kv1.5 transcripts are much more abundant in the atrium than in the ventricle (48). Kv2.1 generates currents sharing characteristic features with Kv1.5 and I_{Kur} in heterologous expression systems (44). Interestingly, we found significant expression levels of the Kv1.5- and the Kv2.1-coding genes in the human ventricular samples (48). This observation suggests a possible functional role of the subunits in the human ventricle. Since I_{Kur} has not been observed in the human ventricle, it is frequently considered as the possible target of atrium-specific antiarrhythmic drugs (65, 76). Atrium-specific blocking of I_{Kur} channels may help in chemical treatment of atrial fibrillation avoiding elongated action potential durations in the ventricles, which would increase the risk of ventricular arrhythmias. However, the presence of I_{Kur}-related ion channel subunits in the human ventricle indicates a possible limitation of the applicability of I_{Kur} blockers in treatment of atrial fibrillation without imposing proarrhytmic risk on the ventricle.

Modulatory 'silent' alpha-subunits of K^+ channels

The members of Kv5 – Kv11 subfamilies are electrically silent in homotetrameric configuration, however, they show all structural characteristics of voltage gated K^+ channels (49). They co-assemble with other voltage gated K^+ channel subunits and modulate the function of the heteromeric ion channel complex. Both silent subunits studied here (Kv5.1 and Kv9.3) are thought to alter the kinetic parameters of currents produced by Kv2.1 (34, 52, 63). Kv2.1 and Kv9.3 have been shown to co-assemble in heteromeric channels in a 3 : 1 stoichiometry (33). Evidences showing interaction between the two studied silent subunits and Kv2.1 indicate that these regulatory silent subunits may be involved in the formation of the I_{Kur} channels. According to our knowledge we reported the expression of Kv5.1 and Kv9.3 modulatory alpha-subunits in the human heart. Our data shows a higher expression level of both Kv5.1 and the Kv9.3 in the atrium compared to the ventricle (48), which finding is consistent with the known uneven distribution of I_{Kur} densities in these two regions of the heart. Confirming the possible function of Kv5.1 and Kv9.3 in the heart may help to refine our present view on the nature and number of possible interactions between ion channel subunits.

Auxiliary subunits of the K^+ channels

We measured the expression level of three members of the *KCNE* gene family. There is strong evidence showing that I_{Kr} is produced by hERG/MiRP1 (*KCNE2*)/mink (KCNE1) channels (2, 42) and I_{Ks} is generated by KvLQT1/minK (*KCNE1*) channels (66). We, among the very first ones, reported relatively high expression of a recently described member of the KCNE gene family MiRP2 (*KCNE3*) in the human heart (48). This abundant MiRP2 expression encouraged us to perform further experiments to clarify MiRP2 function by the means of RNAi technology. Our findings and the possible role of MiRP2 in the myocardium is discussed later in the `Role of MiRP2 regulatory subunit in Ito channels` section.

Herpes-virus mediated gene transfer into cardiomyocytes

Pseudorbaies virus (PRV) is best known for its ability to spread through synapses between nerve cells in the central nervous system. PRV has been used for delivering genetic material to neurons and for labeling neuronal circuits (56). According to our knowledge, PRV has not been used as a gene delivery tool in cardiomyocytes. PRV is able to infect and maintain life-long infections in post-mitotic neurons and our pilot experiments showed that under experimental conditions PRV infects cardiomyocytes as well. However, previous studies showed that the wild-type virus has cytopathic effects, which hampers its applicability as a gene transfer vector of experimental or therapeutic use (8). In general, a potent viral gene transfer vector has no or reasonably low toxic and other side-effects, allows long-term transgene expression and retains its capability to replicate under certain conditions. We developed a multiply attenuated PRV strain by the step-wise introduction of mutations into the wild-type PRV genome to meet the aforementioned requirements. Specific mutations were selected based on previously published data available in the literature.

The large (RR1) and small (RR2) subunits of ribonucletoide reductase enzyme (RR) is encoded by two separate ORFs in the PRV genome (Figure 10 and Figure 15 A) (56). RR is involved in nucleotide metabolism, it catalyzes the reduction of ribonucleotides into deoxiribonucleotides, the substrates for DNA synthesis. In a previous study it has been shown that PRV strains carrying mutation in RR1 are severely attenuated in post-mitotic or growth arrested cells, but are able to replicate in dividing cultured cells (16). We deleted a 1.8 Kb portion of the PRV genome affecting both the RR1 and RR2 ORFs, thereby generating an RR deficient virus. The RR deficient virus retains its replication capacity in cultured cells where deoxiribonucleotides produced by cellular enzymes are available, while its virulence and therefore its cytotoxicity is much lower in post-mitotic cells, such as cardiomyocytes.

The *EP0* gene of PRV is transcribed with early kinetics and encodes a transcriptional transactivator protein, regulating gene expression from several viral promoters (Figure 10 and Figure 15 A) (56). *EP0* is dispensable for viral growth and therefore *EP0* deficient virus vectors can be multiplied in cultured cells, however, viral titers and plaque sizes are reduced compared to the wild-type virus. On the other hand, *EP0* negative PRV mutants are attenuated *in vivo* (8). These properties of *EP0* make the Δ*EP0* mutation an ideal selection for the development of a low-virulence gene transfer vector.

During viral gene transfer, in addition to avoiding cytotoxic effects, the relatively long-term transgene expression should be preferably maintained. While many PRV genes, such as genes encoding viral structural proteins, are only expressed during the lytic infection, latency associated transcripts (LATs) – although in different sizes – can be detected during the lytic cycle and latency as well. Therefore, LAT promoters and downstream regions represent transcriptionally active landmarks of the PRV genome. As an insertion site of transgenes we selected a downstream area of a putative LAT promoter (ASP, Figure 10) (10), which is located in the inverted repeats and hence it is present in two copies in the PRV genome. The ASP region, therefore, ensures abundant transgene expression levels due to the double copy number of transgenes regardless of the virus life cycle stage.

With the Δ*RR1*, *RR2*, *EP0* PRV strain we were able to introduce transgenes into adult isolated cardiomyocytes. The transduced cells showed no obvious cytopathic effects. In addition, we have shown that the delivered activity markers remained fully functional. Our modified PRV strain represents a viable option for gene transfer vectors in cardiovascular research.

Role of MiRP2 regulatory subunit in I_{to} channels

MiRP2 has been first described as the interacting partner of KvLQT1 in a heterologous expression system. MiRP2/KCNQ1 channels have been shown to form a constitutively open ion channel and their role in intestinal chloride secretion has been suggested (67). Accordingly, ectopic expression of MiRP2 in guinea pig ventricles abbreviated QT interval, possibly due to MiRP2-KCNQ1 interactions which led to an increased I_{Ks} density (40). In skeletal muscle MiRP2 has been shown to interact with Kv3.4 and a MiRP2 mutation has been shown to co-associate with periodic paralysis (1). More recently, an interaction between MiRP2 and a typical I_{to} channel Kv4.3 has been shown in a co-expression study (37). Moreover, a loss-of-function MiRP2 mutation associated with Brugada syndrome affecting Kv4.3 current density and kinetics has been identified (17). MiRP2 seems to decrease densities and slow inactivation kinetics of Kv4.3 currents, without affecting steady-state

gating parameters and the overall effect is a decreased $I_{Kv4.3}$ magnitude (17). There are multiple evidences showing that the main regulatory subunit modulating Kv4.3 channel function in the heart is KChIP2 (reviewed in 53). Interestingly, when Kv4.3 was expressed in the presence of both KChIP2 and MiRP2 in a triple co-expression system, MiRP2 did not affect current densities, but decreased time constants of both activation and inactivation and shifted half-maximal inactivation voltage to more negative potentials (58). Therefore it seems that the modulatory function of MiRP2 on Kv4.3 current depends on the presence of other auxiliary subunits, such as KChIP2. MiRP2 decreases current magnitude when Kv4.3 is expressed alone, while MiRP2 has no effect on current density but accelerates activation and inactivation and shifts steady-state inactivation curves of Kv4.3/KChIP2 channels to more negative potentials.

Since KChIP2 has been suggested to be an obligatory subunit of native I_{to} (35), it is reasonable to assume that both KChIP2 and MiRP2 play a role in the formation of native I_{to} channels. Our findings strongly support the latter hypothesis. With a lentivirus-based vector system we delivered artificial microRNAs into canine atrial cardiomyocytes to knock-down MiRP2 expression. MiRP2 knock-down had no effect on current density, but significantly slowed down inactivation kinetics of I_{to}, which is consistent with the published data on Kv4.3/KChIP2/MiRP2 channels. In our experiments, MiRP2 did not affect the steady-state inactivation parameters, however, with the existing number of cases (n=4) in that experiment we cannot draw reliable conclusions in this regard.

The strength of our experimental system is that we were able to show data on the regulatory role of MiRP2 in I_{to} channels of cardiomyocytes *in situ* by the first time and our data is consistent with predictions made in *in vitro* experimental systems. Among the weaknesses we should mention that there seems to be a remodeling process taking place in cultured cardiomyocytes, which results in changes in cellular electrophysiology. Several currents that can be recorded in freshly isolated cells, such as I_{Ks} and I_{K1}, go nearly undetectable in cultured cells (data not shown). Kinetic and steady-state gating parameters of I_{to} are mainly unaffected during culture, however, current densities are significantly higher in cultured cells compared to freshly isolated ones and the contribution of the fast inactivation component to I_{to} inactivation is less prominent in cultured *vs* fresh cells. These latter differences strongly suggest remodeling in the expression level of one or more I_{to} channel subunits during culturing. The better understanding of the remodeling process in cultured cardiomyocytes would help us not only to better interpret the MiRP2 knock-down data, but also to better recognize the possible limitations and applicability of our experimental system in general.

Summary

Ion channels are one of the key determinants of heart function and are of primary importance in the pathophysiology of heart rhythm disorders. Moreover, they show an extreme functional diversity as well. In this work we aimed to lay the fundamentals for new approaches to study the function of individual ion channel subunits.

We studied the gene expression level of a large selection of known and putative cardiac ion channel genes in the human heart. Our work – showing up a cross-section of an important part of the human cardiac transcriptome – provides a substantial insight into the molecular basis of ionic currents in the human heart muscle. As a functional genomics approach, our study raises many intriguing questions about the function of specific ion channel subunits and may serve as the foundation for forthcoming functional studies.

Despite the recent enormous advances in the field of the development of virus-based gene transfer methods it seems that the ultimate vector for cardiac gene delivery that fulfills the versatile needs of experimental work and also meets the special requirements of gene therapy has not been found yet. Here we report the development of a gene transfer vector based on the *Pseudorabies virus*. Our multiply attenuated virus vector efficiently transduces isolated adult cardiomyocytes and represents a viable alternative for the existing viral gene delivery methods in cardiovascular research.

We report among the first ones the expression of a novel auxiliary ion channel subunit MiRP2 in the human heart. Based on data obtained in co-expression studies, MiRP2 has been suggested to play a regulatory role in I_{to} channels. To assess the possible function of MiRP2 in heart muscle cells we combined viral gene transfer with the RNA interference technology. We show that MiRP2 accelerates the time course of inactivation of I_{to} channels in atrial cardiomyocytes.

Our experimental system will help us to unveil subunit-specific functions and multiple interactions that are anticipated among ion channel subunits and will help us to set ground for therapeutic strategies as we press forward in the field of gene therapy of cardiac arrhythmias.

References

1) Abbott GW, Butler MH, Bendahhou S, Dalakas MC, Ptacek LJ, Goldstein SA. MiRP2 forms potassium channels in skeletal muscle with Kv3.4 and is associated with periodic paralysis. Cell 2001; 104(2):217-31.
2) Abbott GW, Sesti F, Splawski I, Buck ME, Lehmann MH, Timothy KW, Keating MT, Goldstein SA. MiRP1 forms IKr potassium channels with HERG and is associated with cardiac arrhythmia. Cell 1999; 97: 175–87.
3) Armstrong CM, Bezanilla F. Inactivation of the sodium channel. II. Gating current experiments. J Gen Physiol. 1977; 70(5): 567–90.
4) Balser JR. The cardiac sodium channel: gating function and molecular pharmacology. J Mol Cell Cardiol. 2001; 33(4): 599–613.
5) Bardien-Kruger S, Wulff H, Arieff Z, Brink P, Chandy KG, Corfield V. Characterisation of the human voltage-gated potassium channel gene, KCNA7, a candidate gene for inherited cardiac disorders, and its exclusion as cause of progressive familial heart block I (PFHBI). Eur J Hum Genet. 2002; 10(1): 36–43.
6) Bertaso F, Sharpe CC, Hendry BM, James AF. Expression of voltage-gated K+ channels in human atrium. Basic Res Cardiol. 2002; 97(6): 424–33.
7) Beuckelmann DJ, Näbauer M, Erdmann E. Alterations of K+ currents in isolated human ventricular myocytes from patients with terminal heart failure. Circ Res. 1993; 73(2): 379–85.
8) Boldogkoi Z, Braun A and Fodor I. Replication and virulence of early protein 0 and long latency transcript deficient mutants of the Aujeszky's disease (pseudorabies) virus. Microbes Infect 2000; 2(11):1321–1328.
9) Boldogkoi Z, Braun A, Antal J and Fodor I. A restriction cleavage and transfection system for introducing foreign DNA sequences into the genome of a herpesvirus. Res Virol 1998; 149(2):87–97.
10) Boldogkoi Z, Erdelyi F and Fodor I. A putative latency promoter/enhancer (P(LAT2)) region of pseudorabies virus contains a virulence determinant. J Gen Virol 2000; 81(2):415–420.
11) Bonci D, Cittadini A, Latronico MV, Borello U, Aycock JK, Drusco A, Innocenzi A, Follenzi A, Lavitrano M, Monti MG, Ross J Jr, Naldini L, Peschle C, Cossu G, Condorelli G. 'Advanced' generation lentiviruses as efficient vectors for cardiomyocyte gene transduction in vitro and in vivo. Gene Ther 2003; 10(8):630-6.
12) Chen Q, Kirsch GE, Zhang D, Brugada R, Brugada J, Brugada P, Potenza D, Moya A, Borggrefe M, Breithardt G, Ortiz-Lopez R, Wang Z, Antzelevitch C, O'Brien RE, Schulze-Bahr E, Keating MT, Towbin JA, Wang Q. Genetic basis and molecular mechanism for idiopathic ventricular fibrillation. Nature. 1998; 392(6673): 293–6.
13) Cheng JH, Kodama I. Two components of delayed rectifier K+ current in heart: molecular basis, functional diversity, and contribution to repolarization. Acta Pharmacol Sin. 2004; 25(2): 137–45.
14) Chiang CE, Roden DM. The long QT syndromes: genetic basis and clinical implications. J Am Coll Cardiol. 2000; 36(1): 1–12.
15) Coetzee WA, Amarillo Y, Chiu J, Chow A, Lau D, McCormack T, Moreno H, Nadal MS, Ozaita A, Pountney D, Saganich M, Vega-Saenz de Miera E, Rudy B. Molecular diversity of K+ channels. Ann N Y Acad Sci. 1999; 868: 233–85.
16) de Wind N, Berns A, Gielkens A, Kimman T. Ribonucleotide reductase-deficient mutants of pseudorabies virus are avirulent for pigs and induce partial protective immunity. J Gen Virol 1993;74 (Pt 3):351-9.

17) Delpón E, Cordeiro JM, Núñez L, Thomsen PE, Guerchicoff A, Pollevick GD, Wu Y, Kanters JK, Larsen CT, Hofman-Bang J, Burashnikov E, Christiansen M, Antzelevitch C. Functional effects of KCNE3 mutation and its role in the development of Brugada syndrome. Circ Arrhythm Electrophysiol 2008; 1(3):209-18.
18) Doyle DA, Morais Cabral J, Pfuetzner RA, Kuo A, Gulbis JM, Cohen SL, Chait BT, MacKinnon R. The structure of the potassium channel: molecular basis of K^+ conduction and selectivity. Science. 1998; 280(5360): 69–77.
19) Ekstrand MI, Enquist LW, Pomeranz LE. The alpha-herpesviruses: molecular pathfinders in nervous system circuits. Trends Mol Med 2008;14(3):134-40.
20) Feng J, Wible B, Li GR, Wang Z, Nattel S. Antisense oligodeoxynucleotides directed against Kv1.5 mRNA specifically inhibit ultrarapid delayed rectifier K+ current in cultured adult human atrial myocytes. Circ Res 1997; 80: 572–9.
21) Ferrier GR, Howlett SE. Cardiac excitation-contraction coupling: role of membrane potential in regulation of contraction. Am J Physiol Heart Circ Physiol. 2001; 280(5): H1928–44.
22) Gauthier ER, Madison SD, Michel RN. Rapid RNA isolation without the use of commercial kits: application to small tissue samples. Pflugers Arch 1997; 433: 664–8.
23) Goldstein SA. A structural vignette common to voltage sensors and conduction pores: canaliculi. Neuron. 1996; 16(4): 717–22.
24) Gulbis JM, Zhou M, Mann S, MacKinnon R. Structure of the cytoplasmic beta subunit-T1 assembly of voltage-dependent K+ channels. Science. 2000; 289(5476): 123–7.
25) Hajjar RJ, del Monte F, Matsui T, Rosenzweig A. Prospects for gene therapy for heart failure. Circ Res 2000; 86(6):616-21.
26) Han W, Bao W, Wang Z, Nattel S. Comparison of ion-channel subunit expression in canine cardiac Purkinje fibers and ventricular muscle. Circ Res. 2002; 91: 790–7.
27) Han W, Wang Z, Nattel S. A comparison of transient outward currents in canine cardiac Purkinje cells and ventricular myocytes. Am J Physiol Heart Circ Physiol. 2000; 279: H466–74.
28) Hannon GJ. RNA interference. Nature. 2002; 418(6894):244-51.
29) Hoshi T, Zagotta WN, Aldrich RW. Two types of inactivation in Shaker K+ channels: effects of alterations in the carboxy-terminal region. Neuron. 1991; 7(4): 547–56.
30) Isbrandt D, Leicher T, Waldschütz R, Zhu X, Luhmann U, Michel U, Sauter K, Pongs O. Gene structures and expression profiles of three human KCND (Kv4) potassium channels mediating A-type currents I(TO) and I(SA). Genomics 2000; 64: 144–54.
31) Isomoto S, Kondo C, Kurachi Y. Inwardly rectifying potassium channels: their molecular heterogeneity and function. Jpn J Physiol. 1997; 47(1): 11–39.
32) Kalman K, Nguyen A, Tseng-Crank J, Dukes ID, Chandy G, Hustad CM, Copeland NG, et al. Genomic organization, chromosomal localization, tissue distribution, and biophysical characterization of a novel mammalian Shaker-related voltage-gated potassium channel, Kv1.7. J Biol Chem 1998; 273: 5851–7.
33) Kerschensteiner D, Soto F, Stocker M. Fluorescence measurements reveal stoichiometry of K+ channels formed by modulatory and delayed rectifier alpha-subunits. Proc Natl Acad Sci U S A. 2005; 102(17): 6160–5.
34) Kramer JW, Post MA, Brown AM, Kirsch GE. Modulation of potassium channel gating by co-expression of Kv2.1 with regulatory Kv5.1 or Kv6.1 alpha-subunits. Am J Physiol 1998; 274: 1501–10.
35) Kuo HC, Cheng CF, Clark RB, Lin JJ, Lin JL, Hoshijima M, Nguyêñ-Trân VT, Gu Y, Ikeda Y, Chu PH, Ross J, Giles WR, Chien KR. A defect in the Kv channel-interacting protein 2 (KChIP2) gene leads to a complete loss of I(to) and confers susceptibility to ventricular tachycardia. Cell 2001; 107(6):801-13.

36) Lesage F, Lazdunski M. Molecular and functional properties of two-pore-domain potassium channels. Am J Physiol Renal Physiol. 2000; 279(5): F793–801.
37) Lundby A, Olesen SP. KCNE3 is an inhibitory subunit of the Kv4.3 potassium channel. Biochem Biophys Res Commun 2006; 346(3):958-67.
38) Lundquist AL, Manderfield LJ, Vanoye CG, Rogers CS, Donahue BS, Chang PA, Drinkwater DC, Murray KT, George AL. Expression of multiple KCNE genes in human heart may enable variable modulation of I(Ks). J Mol Cell Cardiol 2005; 38: 277–87.
39) Marbán E. Heart failure: the electrophysiologic connection. J Cardiovasc Electrophysiol. 1999; 10(10): 1425–8.
40) Mazhari R, Nuss HB, Armoundas AA, Winslow RL, Marbán E. Ectopic expression of KCNE3 accelerates cardiac repolarization and abbreviates the QT interval. J Clin Invest 2002; 109(8):1083-90.
41) McCrossan ZA, Abbott GW. The MinK-related peptides. Neuropharmacology 2004; 47: 787–821
42) McDonald TV, Yu Z, Ming Z, Palma E, Meyers MB, Wang KW, Goldstein SA, Fishman GI. A minK–HERG complex regulates the cardiac potassium current I(Kr). Nature 1997; 388: 289–92.
43) Mitcheson JS, Chen J, Lin M, Culberson C, Sanguinetti MC. A structural basis for drug-induced long QT syndrome. Proc Natl Acad Sci U S A. 2000; 97(22): 12329–33.
44) Nattel S, Yue L, Wang Z. Cardiac ultrarapid delayed rectifiers: a novel potassium current family o f functional similarity and molecular diversity. Cell Physiol Biochem. 1999; 9(4–5): 217–26.
45) Nerbonne JM, Kass RS. Molecular physiology of cardiac repolarization. Physiol Rev. 2005; 85(4): 1205–53.
46) Noda M, Shimizu S, Tanabe T, Takai T, Kayano T, Ikeda T, Takahashi H, Nakayama H, Kanaoka Y, Minamino N, et al. Primary structure of Electrophorus electricus sodium channel deduced from cDNA sequence. Nature. 1984; 312(5990):121–7.
47) Ohya S, Tanaka M, Oku T, Asai Y, Watanabe M, Giles WR, Imaizumi Y. Molecular cloning and tissue distribution of an alternatively spliced variant of an A-type K+ channel alpha-subunit, Kv4.3 in the rat. FEBS Lett 1997; 420: 47– 53.
48) Ordog B, Brutyo E, Puskas LG, Papp JG, Varro A, Szabad J, Boldogkoi Z. Gene expression profiling of human cardiac potassium and sodium channels. Int J Cardiol. 2006; 111(3): 386–93.
49) Ottschytsch N, Raes A, Van Hoorick D, Snyders DJ. Obligatory heterotetramerization of three previously uncharacterized Kv channel alpha-subunits identified in the human genome. Proc Natl Acad Sci U S A 2002; 99: 7986–91.
50) Paddison PJ, Cleary M, Silva JM, Chang K, Sheth N, Sachidanandam R, Hannon GJ. Cloning of short hairpin RNAs for gene knockdown in mammalian cells. Nat Methods 2004; 1(2):163-7.
51) Pak MD, Baker K, Covarrubias M, Butler A, Ratcliffe A, Salkoff L. mShal, a subfamily of A-type K+ channel cloned from mammalian brain. Proc Natl Acad Sci U S A 1991; 88: 4386–90.
52) Patel AJ, Lazdunski M, Honore E. Kv2.1/Kv9.3, a novel ATP-dependent delayed-rectifier K+ channel in oxygen-sensitive pulmonary artery myocytes. EMBO J 1997; 16: 6615–25.
53) Patel SP, Campbell DL. Transient outward potassium current, 'Ito', phenotypes in the mammalian left ventricle: underlying molecular, cellular and biophysical mechanisms. J Physiol 2005; 569(Pt 1):7-39.
54) Pfaffl MW, Horgan GW, Dempfle L. Relative expression software tool (REST) for group-wise comparison and statistical analysis of relative expression results in real-time PCR. Nucleic Acids Res. 2002; 30(9): e36.

55) Po S, Snyders DJ, Baker R, Tamkun MM, Bennett PB. Functional expression of an inactivating potassium channel cloned from human heart. Circ Res 1992; 71: 732–6
56) Pomeranz LE, Reynolds AE, Hengartner CJ. Molecular biology of pseudorabies virus: impact on neurovirology and veterinary medicine. Microbiol Mol Biol Rev 2005; 69(3):462-500.
57) Prorok J, Kovács PP, Kristóf AA, Nagy N, Tombácz D, Tóth JS, Ördög B, Jost N, Virág L, Papp JG, Varró A, Tóth A and Boldogkői Zs. Herpesvirus-Mediated Delivery of a Genetically Encoded Fluorescent Ca2+ Sensor to Canine Cardiomyocytes. J Biomed Biotechnol 2009; 2009:361795.
58) Radicke S, Cotella D, Graf EM, Banse U, Jost N, Varró A, Tseng GN, Ravens U, Wettwer E. Functional modulation of the transient outward current Ito by KCNE beta-subunits and regional distribution in human non-failing and failing hearts. Cardiovasc Res 2006; 71(4):695-703.
59) Ramsay G. DNA chips: state-of-the art. Nat Biotechnol. 1998; 16(1): 40–4.
60) Roden DM. Long QT syndrome: reduced repolarization reserve and the genetic link. J Intern Med. 2006; 259(1): 59–69.
61) Roden DM. Torsade de pointes. Clin Cardiol. 1993; 16(9): 683–6.
62) Sakmann B, Neher E. Patch clamp techniques for studying ionic channels in excitable membranes. Annu Rev Physiol. 1984; 46: 455–72.
63) Salinas M, Duprat F, Heurteaux C, Hugnot JP, Lazdunski M. New modulatory alpha subunits for mammalian Shab K+ channels. J Biol Chem 1997; 272: 24371–9.
64) Sands Z, Grottesi A, Sansom MS. Voltage-gated ion channels. Curr Biol. 2005; 15(2): R44–7.
65) Sanguinetti MC, Bennett PB. Antiarrhythmic drug target choices and screening. Circ Res. 2003; 93(6): 491–9.
66) Sanguinetti MC, Curran ME, Zou A, Shen J, Spector PS, Atkinson DL, Keating MT. Coassembly of K(V)LQT1 and minK (IsK) proteins to form cardiac I(Ks) potassium channel. Nature 1996; 384:80–3.
67) Schroeder BC, Waldegger S, Fehr S, Bleich M, Warth R, Greger R, Jentsch TJ. A constitutively open potassium channel formed by KCNQ1 and KCNE3. Nature 2000; 403(6766):196-9.
68) Schröter KH, Ruppersberg JP, Wunder F, Rettig J, Stocker M, Pongs O. Cloning and functional expression of a TEA-sensitive A-type potassium channel from rat brain. FEBS Lett 1991; 278: 211–6.
69) Serodio P, Vega-Saenz de Miera E, Rudy B. Cloning of a novel component of A-type K+ channels operating at subthreshold potentials with unique expression in heart and brain. J Neurophysiol 1996; 75: 2174–9.
70) Shih HT. Anatomy of the action potential in the heart. Tex Heart Inst J. 1994; 21(1): 30–41.
71) Shorofsky SR, Balke CW. Calcium currents and arrhythmias: insights from molecular biology. Am J Med. 2001; 110(2): 127–40.
72) Stegmeier F, Hu G, Rickles RJ, Hannon GJ, Elledge SJ. A lentiviral microRNA-based system for single-copy polymerase II-regulated RNA interference in mammalian cells. Proc Natl Acad Sci U S A. 2005; 102(37):13212-7.
73) Svensson EC, Marshall DJ, Woodard K, Lin H, Jiang F, Chu L, Leiden JM. Efficient and stable transduction of cardiomyocytes after intramyocardial injection or intracoronary perfusion with recombinant adeno-associated virus vectors. Circulation 1999; 99(2):201-5.
74) Szentadrassy N, Banyasz T, Biro T, Szabo G, Toth BI, Magyar J, Lazar J, Varro A, Kovacs L, Nanasi PP. Apico-basal inhomogeneity in distribution of ion channels in canine and human ventricular myocardium. Cardiovasc Res 2005; 65: 851–60.

75) Varro A, Baláti B, Iost N, Takács J, Virág L, Lathrop DA, Csaba L, Tálosi L, Papp JG. The role of the delayed rectifier component IKs in dog ventricular muscle and Purkinje fibre repolarization. J Physiol. 2000; 1:67-81.
76) Varró A, Biliczki P, Iost N, Virág L, Hála O, Kovács P, Mátyus P, Papp JG. Theoretical possibilities for the development of novel antiarrhythmic drugs. Curr Med Chem. 2004; 11(1): 1–11.
77) Wang WK, Chen MY, Chuang CY, Jeang KT, Huang LM. Molecular biology of human immunodeficiency virus type 1. J Microbiol Immunol Infect 2000; 33(3):131-40.
78) Wang Z, Feng J, Shi H, Pond A, Nerbonne JM, Nattel S. Potential molecular basis of different physiological properties of the transient outward K+ current in rabbit and human atrial myocytes. Circ Res 1999; 84: 551–61.
79) Weiser M, Vega-Saenz de Miera E, Kentros C, Moreno H, Franzen L, Hillman D, Baker H, Rudy B. Differential expression of Shaw-related K+ channels in the rat central nervous system. J Neurosci 1994; 14: 949–72.
80) Wiznerowicz M, Trono D. Harnessing HIV for therapy, basic research and biotechnology. Trends Biotechnol 2005; 23(1):42-7.
81) Yang N, George AL, Horn R. Molecular basis of charge movement in voltage-gated sodium channels. Neuron 1996; 16(1): 113–22.
82) Yue L, Feng J, Li GR, Nattel S. Transient outward and delayed rectifier currents in canine atrium: properties and role of isolation methods. Am J Physiol 1996; 270:H2157-68.
83) Zhuo ML, Huang Y, Liu DP, Liang CC. KATP channel: relation with cell metabolism and role in the cardiovascular system. Int J Biochem Cell Biol. 2005; 37(4): 751–64.

Acknowledgements

The fundamental part of the project that kept me busy during the past few years was formulated in a scientific cooperation program between the Department of Biology and the Department of Pharmacology and Pharmacotherapy of the University of Szeged. I wish to thank the ingenious efforts of Professor András Varró, Professor János Szabad and of Professor Zsolt Boldogkői for organizing both the scientific and the administrative frames of the project. I am also thankful for their advices. I am also very grateful to Dr Stanley Nattel, Director of the Electrophysiology Research Group of the Montreal Heart Institute, for providing the inspiring environment and support for the completion of the RNAi experiments. I extend my appreciation to the co-workers and fellow Ph.D. students in the two Departments of the University of Szeged, most especially to Endre Brutyó and János Prorok, who participated tremendously in the experimental work. I am also grateful to the colleagues in Professor Nattel's lab, particularly to Ling Xiao, who so kindly sacrificed a part of her patch-clamp time.

Support for my Ph.D. work came from scientific cooperation programs organized by Professor András Varró and Professor János Szabad: (1) A szívritmuszavarokhoz társuló hirtelen halál farmakológiai prevenciója (OM-00324/2002). (2) Az RNSi technika alkalmazása a hirtelen halált okozó szívaritmia molekuláris alapjainak felderítésében (ETT 1280-9/2003-1018 EKU); (3) A hirtelen szívhalál megelőzésének új útjai: molekuláris biológiai, genetikai és farmakológiai vizsgálata (BIO 19541945). (4) Graduate Student Program of the University of Szeged.

I.

ELSEVIER

International Journal of Cardiology 111 (2006) 386 – 393

International Journal of Cardiology

www.elsevier.com/locate/ijcard

Gene expression profiling of human cardiac potassium and sodium channels

Balázs Ördög [a], Endre Brutyó [a], László G. Puskás [b], Julius G. Papp [c], András Varró [c], János Szabad [a], Zsolt Boldogkői [a,*]

[a] *Department of Biology, Faculty of Medicine, University of Szeged, Somogyi B. 4. H-6720, Szeged, Hungary*
[b] *Laboratory of Functional Genomics, Biological Research Center, Hungarian Academy of Sciences, Szeged, Hungary*
[c] *Department of Pharmacology and Pharmacotherapy, Faculty of Medicine, University of Szeged, Szeged, Hungary*

Received 8 July 2005; received in revised form 26 July 2005; accepted 30 July 2005
Available online 27 October 2005

Abstract

Background: The native cardiac ion currents and the action potential itself are the results of the concerted action of several different ion channels. The electrophysiological properties of cardiac cells are determined by the composition of ion channels and by their absolute abundance and proportional ratio.
Methods: Our aim in this study was to compare the gene expression level of a representative panel of cardiac ion channels with each other and to compare the same channels in the atrium and ventricle of the human heart using quantitative real-time PCR analysis.
Results: We obtained a significant difference in the gene expression levels in 21 of 35 channels between atrium and ventricle of healthy human hearts. Further, we found that the expression levels of Kv1.5 and Kv2.1 transcripts in the ventricle were very high, and that mRNAs for Kv1.7 and Kv3.4 are highly abundant in both the atrium and ventricle, which might indicate a functional role of these ion channel subunits in the formation of action potential in the human ventricle and both in the atrium and ventricle, respectively.
Conclusions: This is the first report on the expression of several ion channel subunits, such as Kv1.7, Kv3.3 or Kv3.4 in human cardiomyocytes. The expression levels of these genes are comparable with that of well known ion channel subunits. Therefore, it is reasonable to assume, that these ion channel subunits may contribute to native currents in the human myocardium.
© 2005 Elsevier Ireland Ltd. All rights reserved.

Keywords: Human heart; Potassium channel; Real time PCR; Sodium channel

1. Introduction

Transmembrane ion currents and electrogenic ion pumps determine and influence the cardiac action potential in different parts and regions of the heart. Transmembrane ion currents flow through distinct ion channels which are formed from α and β protein subunits [1,2]. Determination of the expression levels of ion channel subunit-encoding mRNAs is crucially important for understanding of their electrophysiological function in the cardiac tissue. There is accumulating evidence that transmembrane ion currents are determined by ion channels composed of various protein subunits, however, a survey of the specific function of a particular ion channel subunit in native myocytes is very difficult if not impossible. Ion channel subunits have been found to exhibit altered kinetical and pharmacological properties when heterologously expressed in mammalian cell lines or in *Xenopus* oocytes as compared to native muscle cells. Furthermore, native currents generally cannot be reproduced by co-expression studies. It is important to note that in several acquired and inherited cardiac diseases the properties and densities of these transmembrane ion-currents were shown to be altered [3,4]. Therefore, there is considerable interest in defining the molecular correlates of

* Corresponding author. Tel.: +36 62 545595; fax: +36 62 545131.
E-mail address: boldog@sb4.szote.u-szeged.hu (Z. Boldogkői).

0167-5273/$ - see front matter © 2005 Elsevier Ireland Ltd. All rights reserved.
doi:10.1016/j.ijcard.2005.07.063

cardiac ion-channels and their expression in general. Since the majority of the corresponding results originate from experimental animals, mostly from rodents, detailed information in the human heart has particular significance. To comply with this need, in this study we provide evidence for the expression of a large number of ion channel mRNAs in the healthy human ventricular and atrial tissues.

2. Materials and methods

2.1. Tissue samples

Tissue samples (approximately 100–150 mg for each sample) were isolated from 19 undiseased donor hearts. The hearts were isolated from organ donor patients (see online supplement for details: doi:10.1016/j.ijcard.2005.07.063) through pulmonary and aortic valve transplantation surgery. Before explantation of the hearts, the patients did not receive any medication. Before preparation, the hearts were perfused with cardioplegic solution and were kept cool (4–6 °C) for 6–8 h. Cross sections of the ventricle and atrial walls were excised and frozen in liquid nitrogen. The protocol conforms to the principles outlined in the Declaration of World Medical Association proclaimed in Helsinki (Cardiovascular Research 1997; 35:2–4) and was approved by the Ethical Review Board of University of Szeged (No. 51–57/1997 OEj.).

2.2. RNA preparation

Total RNA samples were purified from fresh or frozen tissues as described by Gauthier et al. [5]. Briefly, tissue (100 mg) was placed into a 2 ml microfuge tube containing 1 ml guanidine thiocyanate solution (4 M guanidine thiocyanate; 25 mM sodium citrate pH 7.0; 0.5% (w/v) *N*-lauroylsarcosine; and 0.1 M 2-mercaptoethanol) and homogenized using a handheld disperser (T8 Ultra-Turrax, IKA-Werke GmbH and Co. KG). The homogenate was placed on ice and 0.1 ml 2 M sodium acetate (pH 4.0), 1 ml of Tris–HCl buffer (pH 8.0)-saturated phenol (pH 6.7) and 0.2 ml chloroform : isoamyl alcohol (24 : 1) were sequentially added, followed by vortexing after each addition. Following incubation on ice for 15 min, the mixture was centrifuged at 10,000 $\times g$ for 10 min. The upper aqueous phase was transferred to a microfuge tube and RNA was precipitated by adding two volume of ice cold ethanol. Precipitated RNA was pelleted by centrifugation at 10,000 $\times g$ for 10 min, and then washed with 70% ethanol. After washing, the pellet was dried and resuspended in 50 μl RNase-free water. RNA samples were further purified, using Nucleospin RNA II kit (Macherey-Nagel GmbH and Co. KG), as recommended by the manufacturer. The protocol contains a DNAse I digestion step for eliminating the potential genomic DNA contamination. The concentration of total RNA samples was determined by UV-photometry.

2.3. Real-time quantitative RT-PCR

The cDNA molecules were synthesized from mRNA templates by reverse transcription (RT), using Superscript II RNase H^- Reverse Transcriptase (Invitrogen), according to the manufacturer's instructions. Each RT reaction mixture contained 5 μg total RNA, 200 U reverse transcriptase and 100 pmol $dT_{(15)}$ oligonucleotide at a final volume of 20 μl. Each RT reaction was diluted 40 times to a final volume of 800 μl. Ten microliters of the diluted RT products (corresponding to 56.25 ng total RNA) were used for each real-time RT-PCR assay.

Each RNA sample was tested for the presence of genomic DNA contamination by running no-RT control reactions. RNA samples with no detectable DNA contamination were used for real time RT-PCR reactions.

Gene-specific primers were designed using the Primer Express software (Applied Biosystems) according to the software guidelines. Primer specificity was verified using the "Search for Short, Nearly Exact Matches" program on NCBI BLAST server. In the case of those genes whose splice variants have already been described, primers were designed in the invariable regions of mRNA variants. For primer sequences, see online supplement (doi:10.1016/j.ijcard.2005.07.063). All primers were purchased from Avidin Ltd. (Szeged, Hungary).

SYBR-Green PCR assays were performed on a Rotor-Gene 3000 (Corbett Research) real-time PCR platform. For each 20 μl reaction, 9 μl cDNA solution, 10 μl ABsolute QPCR SYBR Green Mix (ABgene), 0.5 μl forward primer (10 μM) and 0.5 μl reverse primer (10 μM) were mixed together. PCR parameters were as follows; 95 °C, 10 min for heat activation of DNA polymerase mix, followed by 94 °C, 25 s (denaturation); 61 °C, 25 s (annealing); 72 °C, 15 s (synthesis) for 50 cycles. After each run a melting point analysis was performed by measuring fluorescence intensity in a temperature interval ranging from 55 to 93 °C. Those samples that showed melting characteristics considerably deviated from the average were excluded from analysis. To assess primer dimer formation, blank controls, containing water as template were used for every primer pairs in each experiment.

2.4. Evaluation of data

In a typical experiment, we examined the expression levels of 8 ion channel subunit-encoding genes, as well as β-actin as an internal control using 7 cDNA samples for each gene at the same time. We calculated the relative copy numbers of ion channel subunit-encoding mRNAs by normalizing each cDNA to β-actin, using the "Comparative Quantitation" module of the Rotor-Gene software (version 6.0, Corbett Research).

To determine the ratio of β-actin expression level in the left ventricle and atrium of the human heart, we measured the absolute amount of β-actin by using a standard curve

obtained from a dilution series of a synthesized β-actin amplicon. We found that β-actin was 1.7-times more abundant in the left ventricle than in the left atrium. Hence, for a reliable comparison of gene expression levels in the ventricle with those in the atrium, we corrected the data obtained in the atrium by dividing the mean of the relative copy number of each mRNA by 1.7 (online supplement, doi:10.1016/j.ijcard.2005.07.063).

Statistical analyses were performed using Student's *t*-test and significance was set as $P<0.05$.

3. Results and discussion

3.1. Voltage gated K^+-channel α-subunits

3.1.1. I_{to}-related α-subunits: Kv1.4 (KCNA4), Kv1.7 (KCNA7), Kv3.3 (KCNC3), Kv3.4 (KCNC4), Kv4.1 (KCND1), Kv4.3 (KCND3)

The typical spike-and-dome configuration of the epicardial action potential is mediated by the transient outward current (I_{to}). We investigated the expression levels of six putative I_{to}-related K^+-channel α-subunits, Kv1.4 [6], Kv1.7 [7], Kv3.3 [8], Kv3.4 [9], Kv4.1 [10] and Kv4.3 [11]. These channels were found to produce currents with fast activation and rapid inactivation kinetics in heterologous expression systems and therefore, it is reasonable to assume that they could contribute to human I_{to}. In another report, Kv1.4 was not detectable in human heart by Western blot analysis [12]. Further, antisense oligonucleotides targeted against the Kv1.4 transcripts were reported to have no effect on human atrial I_{to} [12]. In contrast, others have recently shown that Kv1.4 is expressed in the ventricle of the human heart [13]. Kv3.3 and Kv3.4 transcripts have not been detected in rat heart [14]. However, there is no data in literature on their expression in the human heart. Kv4.1 and Kv4.3 coding mRNAs have already been shown to be expressed in human heart [15]. We detected all of the examined I_{to}-related transcripts in our tissue samples. The comparative expression levels of these genes are as follows; ventricle: Kv1.7>Kv4.3>Kv3.4>*Kv1.4>*Kv4.1>*Kv3.3[1]; atrium: Kv1.7>Kv4.3>Kv3.4>Kv4.1>Kv1.4>*Kv3.3[1] (Fig. 1a). Kv3.3 and Kv4.1 transcripts are at least 10 times more abundant in the atrium compared to the ventricle, while the expression levels of Kv1.4, Kv1.7, Kv3.4 and Kv4.3 are similar in the two regions of the heart. Surprisingly, we found that the expression levels of Kv1.7 and Kv3.4 were high and fell into the same range as that of Kv4.3 both in the ventricle and the atrium. The physiological significance of this finding is not clear, but one might assume that in the human ventricle I_{to} is flown through Kv1.7, Kv3.4 and Kv4.3 channels. Furthermore, data might indicate that Kv4.1 channels could also have an important role in the atrium. If this hypothesis were true, it would alter our view about I_{to} pharmacology, which is largely based on data obtained on Kv4.3 channels.

3.1.2. I_{Kur}-related channel proteins: Kv1.2 (KCNA2), Kv1.5 (KCNA5), Kv2.1 (KCNB1), Kv3.1 (KCNC1)

I_{Kur} is a substantial current in atrial cells, but appears to be absent in the ventricle. To date, four pore-forming α-subunits have been identified, which produce currents with kinetic properties and pharmacological profile resembling to that of I_{Kur}, Kv1.2, Kv1.5, Kv2.1, Kv3.1 [16]. Kv1.5 is thought to be the major contributor to I_{Kur} in human heart [17]. The expression pattern of these genes is Kv1.5>*Kv2.1>*Kv1.2>Kv3.1[1]; and Kv2.1>Kv1.5>*Kv1.2>Kv3.1[1] in the atrium and ventricle, respectively (Fig. 1b). As we expected, the Kv1.5 transcripts are much more (approximately 30-fold) abundant in the atrium than in the ventricle, which confirms earlier reports that Kv1.5 is responsible for I_{Kur} in the human atrium [17]. Kv3.1 was found to be approximately 5-fold more abundant in the atrium than in the ventricle, while Kv1.2 and Kv2.1 show similar expression levels in the two regions of the heart. Interestingly, the expression levels of Kv1.5- and Kv2.1-coding mRNAs in the ventricle are relatively high, which raises a possible functional role of these subunits in the human ventricle. However, further investigation is needed to establish the precise physiological role of Kv1.5 and Kv2.1 subunits in the generation of I_{Kur} in the human ventricle.

3.1.3. An I_{Kr}-related α-subunit: HERG (KCNH2)

I_{Kr} is the rapidly activating component of I_K, the major outward current involved in the repolarization in heart muscle cells [18]. HERG is thought to be the main pore-forming subunit responsible for I_{Kr}; however, when expressed in heterologous expression systems it produces a current that has somewhat slower activation and deactivation kinetics than the native I_{Kr} [18]. There is strong evidence, that HERG associates with MiRP1 and minK regulatory β-subunits to form I_{Kr} channels in the heart [19,20]. Furthermore, it is likely that HERG function is affected by other members of the KCNE gene family [21]. HERG mRNA is one of the most abundant α-subunit-coding transcripts both in the ventricle and atrium, and it is expressed at approximately the same level in the two regions (Fig. 1c). According to our data, the expression levels of potential interacting partners of HERG channel subunit are significantly lower than that of HERG, which might indicate that HERG is associated with various regulatory β-subunits in native I_{Kr} channels.

3.1.4. An I_{Ks}-related channel: KvLQT1 (KCNQ1)

I_{Ks}, the slowly activating component of I_K [18] is thought to be generated by heteromeric channel complexes formed by KvLQT1 and minK [22]. Furthermore, it has been recently demonstrated, that I_{Ks} can be modulated by various members of KCNE gene family [23]. Similarly to

[1] Asterisk (*) indicates significant differences at $P<0.05$.

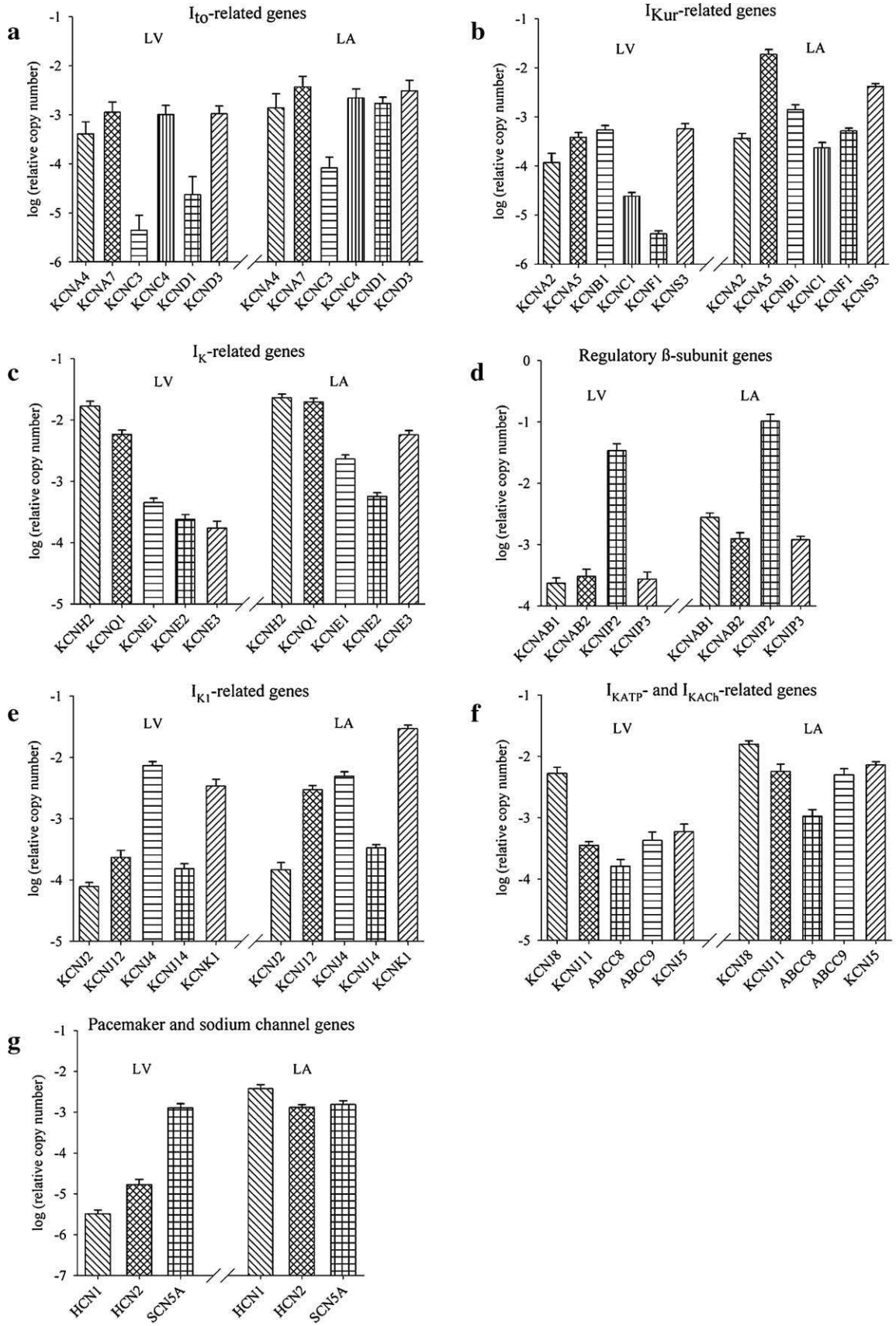

Fig. 1. Relative expression levels of different ion channel subunit genes in the human heart as determined by real-time quantitative RT-PCR. The mRNA levels were quantified in tissue samples collected from the left ventricle (LV) and left atrium (LA). The data were normalized to the expression level of cytoplasmic β-actin and are presented as mean ± standard error.

HERG channel, KvLQT1 was found to be expressed at a higher level than its possible interacting partners, both in the ventricle and atrium (Fig. 1c). Comparing the abundance of pore-forming subunits of the two I_K components we found that HERG mRNA was somewhat more abundant than KvLQT1 transcripts ($P<0.05$) in the ventricle, while in the atrium the two genes were expressed at approximately the same level ($P<0.05$).

3.1.5. Voltage gated K^+-channel regulatory ("silent") α-subunits: Kv5.1 (KCNF1), Kv9.3 (KCNS3)

The members of Kv5–Kv11 subfamilies are electrically silent in homotetrameric configuration; however, they show all structural characteristics of voltage gated K^+-channels [24]. Both studied silent subunits are thought to alter kinetic parameters of current produced by Kv2.1 [25,26,27]. Kv9.3 message was found to be much more abundant than that of Kv5.1 in both the ventricle (approximately 100 times more abundant) and the atrium (almost 10 times more abundant). In addition, Kv9.3 expression level is slightly higher than that of its interacting partner Kv2.1 (Fig. 1b).

3.2. Auxiliary subunits of voltage gated K^+-channels

3.2.1. Kvβ subunits: Kvβ1 (KCNA1B), Kvβ2 (KCNA2B)

Kvβ subunits are cytoplasmic proteins and mainly interact with the members of Kv1 subfamily of voltage-gated K^+-channels. Co-assembly with β-subunits can alter the time and voltage-dependence of the current produced by the channel complex and can affect subcellular trafficking of α-subunits [28]. Primer pairs used for the amplification of Kvβ1 and Kvβ2 mRNAs were designed to recognize all known splice variants of these genes (3 for Kvβ1 and 2 for Kvβ2). We found that in the atrium, Kvβ1 was more abundant than Kvβ2 ($P<0.05$), while in the ventricle there was no significant difference between the expression levels of the two genes (Fig. 1d).

3.2.2. minK-related peptides: minK (KCNE1), MiRP1 (KCNE2), MiRP2 (KCNE3)

The products of *KCNE* gene family are membrane proteins (termed mink-related peptides; MiRPs) with one transmembrane domain promiscuously interacting with Kv, KCNQ and ERG channels in heterologous expression systems [29]. To date, five members of the *KCNE* gene family have been described [23]. We investigated the expression levels of three members of *KCNE* gene family and in the atrium we found the following expression pattern; *KCNE1*>**KCNE3*>* *KCNE2*[1] (Fig. 1c), which confirms the results reported by Lundquist et al. [23]. Nevertheless, in contrast to the data obtained by these authors, we did not detect significant differences in the abundance of these transcripts in the ventricle. It has been previously shown, that co-assembly of MiRP2 with KvLQT1–minK channels results in I_{Ks} with faster activation kinetics [23]. Based on this observation one may speculate, that different expression ratios of these auxiliary subunits may result in different I_{Ks} in atria than in the ventricle, which thus could account for the different action potential configuration in the two regions of the heart.

3.2.3. KChIP channel subunit: KChIP2 (KCNIP2), KChIP3 (KCNIP3)

Proteins encoded by the *KCNIP* gene family are cytoplasmic Ca^{2+} binding proteins interacting with Kv4 channels (K^+-channel interacting proteins; KChIPs) both in heterologous systems and in vivo [30,31]. In the heart, KChIP2 is assumed to be responsible for the transmural gradient of I_{to} in human, but not in rat [32]. Until now, 18 KChIP2 transcript variants have been described in various species [33]. Primers for PCR amplification of *KCNIP2* cDNAs were designed to recognize all of the eight described human isoforms of this gene. KChIP2 shows the first and the third highest expression level among all of the mRNAs we examined in ventricle and atrium, respectively (Fig. 1d). The high abundance of KChIP2 isoforms may indicate a more diverse physiological role, than it is currently believed.

3.3. Inward rectifier K^+-channel α-subunits

3.3.1. Kir2.1 (KCNJ2), Kir2.2 (KCNJ12), Kir2.3 (KCNJ4), Kir2.4 (KCNJ14)

Inward rectifier channels produce I_{K1} current, which plays a critical role in maintaining resting membrane potential and contributes to the terminal repolarization in heart muscle cells [34]. Heteromerization of Kir2 subunits was described in *Xenopus laevis* oocytes [35], in rabbit heart muscle cells [36] and was suggested to take place in human cardiomyocytes [37]. We analyzed the four known Kir2 subunits contributing to I_{K1}. Primer pairs designed for Kir2.3 and Kir2.4 recognize the two transcript variants found in GenBank of both genes. We obtained the following expression pattern both in the ventricle (Kir2.3>* Kir2.2> Kir2.4>Kir2.1)[1] and atrium (Kir2.3>Kir2.2>* Kir2.4>* Kir2.1)[1] (Fig. 1e). With the exception of Kir2.2, which is almost 8-fold more abundant in the atrium than in the ventricle, all genes show similar expression level in the two regions of the heart. Notably, the primer pair used for the quantification of Kir2.2 transcripts amplifies the same product from the normal and the negative regulator subunit Kir2.2v [38]. It seems to be reasonable to assume, that the higher Kir2.2–Kir2.2v abundance in the atrium might explain the smaller macroscopic I_{K1} conductance in atrial muscle cells.

3.4. An $I_{K,ACh}$-related channel subunit

3.4.1. Kir3.4 (KCNJ5)

$I_{K,ACh}$ is produced by the G-protein-regulated inwardly rectifying K^+ channels (GIRK). GIRK channels are hetero-tetramers of Kir3.1–3.4 subunits [39]; however Kir3.4 homo-tetramers were also detected in bovine atrium [40]. A

lower abundance of Kir3.4 was described in rat ventricle compared to rat atrium by [41]. We measured a similar distribution of the *KCNJ5* transcripts in the human heart (Fig. 1f).

3.5. I_{KATP}-related channel subunits

3.5.1. Kir6.1 (KCNJ8), Kir6.2 (KCNJ11)

Kir6.1 and Kir6.2 are the pore-forming subunits of K_{ATP}-channels [42]. Kir6.1 was shown to be ubiquitously expressed in rat tissues [43], while Kir6.2 expression was described in pancreas, heart, skeletal muscle and brain [44]. Studies on Kir6.1 knock-out mice showed that this subunit could not contribute to the formation of the sarcolemmal K_{ATP}-channels in cardiomyocytes, but it plays a critical role in regulating vascular tone [42]. We observed a high expression level of both K_{ATP}-channel subunits (Fig. 1f). The relative high Kir6.1 expression might indicate that our tissue homogenates possibly contain vascular smooth muscle-derived elements.

3.6. Auxiliary subunits of ATP-sensitive K^+-channels

3.6.1. SUR1 (ABCC8), SUR2 (ABCC9)

Sulfonylurea receptors determine the electrophysiological and pharmacological properties of nucleotide sensitive K^+-channel complexes. Several alternatively spliced SUR isoforms were recently described in guinea pig [45] and human [46,47]. SUR1/Kir6.2 complexes form K_{ATP}-channels found in pancreatic β-cells, SUR2A/Kir6.2 form the cardiac type, SUR2B/Kir6.2 form the smooth muscle type, while SUR2B/Kir6.1 complexes form the vascular smooth muscle type K_{ATP}-channels [42]. For quantifying SUR2 expression, we selected primers to recognize all of the three human SUR2 variants found in GenBank (SUR2A, SUR2B and SUR2A-delta-14). SUR2 message is expressed at a higher level in both the atrium and ventricle; however, SUR1 which is involved in formation of the pancreatic type K_{ATP}-channel complex, has also been found to be abundant in both regions (Fig. 1f).

3.7. A "leaky" K^+-channel subunit

3.7.1. TWIK1 (KCNK1)

TWIK1 is a member of the two-pore-domain forming K^+-channel family. It produces constitutive background current and almost ubiquitously expressed in all human tissues, except skeletal muscle, thymus and peripheral blood leukocytes [48]. In another study, a ten-fold higher expression level was described in the ventricle, compared to the atrium [49]. On the contrary, our data shows a 5-fold higher expression level in the atrium (Fig. 1e). Comparing the abundance of *KCNK1* transcripts to other inwardly rectifying subunits generating I_{K1} current (Kir2.1, Kir2.2, Kir2.3, Kir2.4), we found the *KCNK1* mRNAs to be the most abundant in the atrium and it was the second most abundant in the ventricle.

3.8. Pacemaker channel subunits (I_f)

3.8.1. HCN1 (HCN1), HCN2 (HCN2)

We analyzed the expression level of HCN1 and HCN2 out of the four known hyperpolarization-activated pacemaker current producing cation channel subunits (HCN1 through HCN4; [50]). As expected, both gene transcripts are far more abundant in the atrium, than in the ventricle. In the ventricle HCN2 is expressed at a higher level than HCN1, while in the atrium mRNA for HCN1 is more abundant (Fig. 1g). Therefore, the expression level of these genes in the human atrium resembles more to that of rabbits [51], than to that of mice [52].

3.9. The cardiac Na^+ channel

3.9.1. Nav1.5 (SCN5A)

Mutations in the cardiac Na^+-channel gene *SCN5A* are responsible for multiple ventricular arrhythmias including Brugada syndrome, congenital long QT syndrome and isolated conduction disease [53]. *SCN5A* is strongly expressed both in ventricle and atrium, and we found no significant difference between the expression levels of the gene in the two regions of heart (Fig. 1g).

4. Conclusion

In summary, we conclude, that the known pore-forming and auxiliary K^+-channel subunits detected earlier in other mammalian cardiac preparations are also expressed in human atrial and ventricular muscles. Differences in the expression levels of α- and β-subunits and their respective ratios to each other may account for the species- and tissue-specific configuration of the commonly investigated trans-membrane currents, such as I_{to}, I_{Kr}, I_{Ks} and I_{Kur}. In addition, differences in the contribution of these channel proteins to native currents may result in variations in drug sensitivity among species and heart regions. These problems explain the difficulties in the extrapolation of the results of animal experiments to man. Further investigations using molecular and electrophysiological approaches are needed to reveal the molecular basis of ionic currents in different species and heart regions.

It should be noted, that due to the sampling method used in this study, our tissue homogenates might be contaminated by vascular smooth muscle-derived elements. However, it is reasonable to presume, that this could exert an important distorting effect on the data of weakly expressed genes. Therefore, these data require careful interpretation and further confirmation.

Acknowledgements

This work was funded by grants from National Research and Development Programs (NKFP 1A/0011) to A. Varró,

the Hungarian Ministry of Education (Bio-37 KPI), the Hungarian Ministry of Health (ETT 43907/2003), the National Fund for Scientific Research to Z. Boldogkői (OTKA T049171), and National Fund for Scientific Research to A. Varró (OTKA T048698).

Appendix A. Supplementary data

Supplementary data associated with this article can be found, in the online version, at doi:10.1016/j.ijcard.2005.07.063.

References

[1] Nerbonne JM. Molecular basis of functional voltage-gated K^+ channel diversity in the mammalian myocardium. J Physiol 2000; 525:285–98.
[2] Pourrier M, Schram G, Nattel S. Properties, expression and potential roles of cardiac K^+ channel accessory subunits: MinK, MiRPs, KChIP, and KChAP. J Membr Biol 2003;194:141–52.
[3] Kaab S, Dixon J, Duc J, et al. Molecular basis of transient outward potassium current downregulation in human heart failure: a decrease in Kv4.3 mRNA correlates with a reduction in current density. Circulation 1998;98:1383–93.
[4] Priori SG, Napolitano C. Genetics of cardiac arrhythmias and sudden cardiac death. Ann N Y Acad Sci 2004;1015:96–110.
[5] Gauthier ER, Madison SD, Michel RN. Rapid RNA isolation without the use of commercial kits: application to small tissue samples. Pflugers Arch 1997;433:664–8.
[6] Po S, Snyders DJ, Baker R, Tamkun MM, Bennett P. Functional expression of an inactivating potassium channel cloned from human heart. Circ Res 1992;71:732–6.
[7] Kalman K, Nguyen A, Tseng-Crank J, et al. Genomic organization, chromosomal localization, tissue distribution, and biophysical characterization of a novel mammalian Shaker-related voltage-gated potassium channel, Kv1.7. J Biol Chem 1998;273:5851–7.
[8] Weiser M, Vega-Saenz de Miera E, Kentros C, et al. Differential expression of Shaw-related K^+ channels in the rat central nervous system. J Neurosci 1994;14:949–72.
[9] Schroter KH, Ruppersberg JP, Wunder F, Rettig J, Stocker M, Pongs O. Cloning and functional expression of a TEA-sensitive A-type potassium channel from rat brain. FEBS Lett 1991;278:211–6.
[10] Pak MD, Baker K, Covarrubias M, Butler A, Ratcliffe A, Salkoff L. mShal, a subfamily of A-type K^+ channel cloned from mammalian brain. Proc Natl Acad Sci U S A 1991;88:4386–90.
[11] Serodio P, Vega-Saenz de Miera E, Rudy B. Cloning of a novel component of A-type K^+ channels operating at subthreshold potentials with unique expression in heart and brain. J Neurophysiol 1996;75:2174–9.
[12] Wang Z, Feng J, Shi H, Pond A, Nerbonne JM, Nattel S. Potential molecular basis of different physiological properties of the transient outward K^+ current in rabbit and human atrial myocytes. Circ Res 1999;84:551–61.
[13] Szentadrassy N, Banyasz T, Biro T, et al. Apico-basal inhomogeneity in distribution of ion channels in canine and human ventricular myocardium. Cardiovasc Res 2005;65:851–60.
[14] Ohya S, Tanaka M, Oku T, et al. Molecular cloning and tissue distribution of an alternatively spliced variant of an A-type K^+ channel alpha-subunit, Kv4.3 in the rat. FEBS Lett 1997;420:47–53.
[15] Isbrandt D, Leicher T, Waldschutz R, et al. Gene structures and expression profiles of three human KCND (Kv4) potassium channels mediating A-type currents I(TO) and I(SA). Genomics 2000;64: 144–54.
[16] Nattel S, Yue L, Wang Z. Cardiac ultrarapid delayed rectifiers: a novel potassium current family of functional similarity and molecular diversity. Cell Physiol Biochem 1999;9:217–26.
[17] Feng J, Wible B, Li GR, Wang Z, Nattel S. Antisense oligodeoxynucleotides directed against Kv1.5 mRNA specifically inhibit ultrarapid delayed rectifier K^+ current in cultured adult human atrial myocytes. Circ Res 1997;80:572–9.
[18] Sanguinetti MC, Jurkiewicz NK. Two components of cardiac delayed rectifier K^+ current. Differential sensitivity to block by class III antiarrhythmic agents. J Gen Physiol 1990;96:195–215.
[19] Abbott GW, Sesti F, Splawski I, et al. MiRP1 forms IKr potassium channels with HERG and is associated with cardiac arrhythmia. Cell 1999;97:175–87.
[20] McDonald TV, Yu Z, Ming Z, et al. A minK–HERG complex regulates the cardiac potassium current I(Kr). Nature 1997;388: 289–92.
[21] Anantharam A, Lewis A, Panaghie G, et al. RNA interference reveals that endogenous *Xenopus* MinK-related peptides govern mammalian K^+ channel function in oocyte expression studies. J Biol Chem 2003;278:11739–45.
[22] Sanguinetti MC, Curran ME, Zou A, et al. Coassembly of K(V)LQT1 and minK (IsK) proteins to form cardiac I(Ks) potassium channel. Nature 1996;384:80–3.
[23] Lundquist AL, Manderfield LJ, Vanoye CG, et al. Expression of multiple KCNE genes in human heart may enable variable modulation of I(Ks). J Mol Cell Cardiol 2005;38:277–87.
[24] Ottschytsch N, Raes A, Van Hoorick D, Snyders DJ. Obligatory heterotetramerization of three previously uncharacterized Kv channel alpha-subunits identified in the human genome. Proc Natl Acad Sci U S A 2002;99:7986–91.
[25] Kramer JW, Post MA, Brown AM, Kirsch GE. Modulation of potassium channel gating by co-expression of Kv2.1 with regulatory Kv5.1 or Kv6.1 alpha-subunits. Am J Physiol 1998;274: 1501–10.
[26] Patel AJ, Lazdunski M, Honore E. Kv2.1/Kv9.3, a novel ATP-dependent delayed-rectifier K^+ channel in oxygen-sensitive pulmonary artery myocytes. EMBO J 1997;16:6615–25.
[27] Salinas M, Duprat F, Heurteaux C, Hugnot JP, Lazdunski M. New modulatory alpha subunits for mammalian Shab K^+ channels. J Biol Chem 1997;272:24371–9.
[28] Pongs O, Leicher T, Berger M, et al. Functional and molecular aspects of voltage-gated K^+ channel beta subunits. Ann N Y Acad Sci 1999;868:344–55.
[29] McCrossan ZA, Abbott GW. The MinK-related peptides. Neuropharmacology 2004;47:787–821.
[30] An WF, Bowlby MR, Betty M, et al. Modulation of A-type potassium channels by a family of calcium sensors. Nature 2000;403:553–6.
[31] Rhodes KJ, Carroll KI, Sung MA, et al. KChIPs and Kv4 alpha subunits as integral components of A-type potassium channels in mammalian brain. J Neurosci 2004;24:7903–15.
[32] Rosati B, Pan Z, Lypen S, et al. Regulation of KChIP2 potassium channel beta subunit gene expression underlies the gradient of transient outward current in canine and human ventricle. J Physiol 2001;533:119–25.
[33] Pourrier M, Schram G, Nattel S. Properties, expression and potential roles of cardiac K^+ channel accessory subunits: MinK, MiRPs, KChIP, and KChAP. J Membr Biol 2003;194:141–52.
[34] Lopatin AN, Nichols CG. Inward rectifiers in the heart: an update on I(K1). J Mol Cell Cardiol 2001;33:625–38.
[35] Schram G, Melnyk P, Pourrier M, Wang Z, Nattel S. Kir2.4 and Kir2.1 K(+) channel subunits co-assemble: a potential new contributor to inward rectifier current heterogeneity. J Physiol 2002;544: 337–49.
[36] Zobel C, Cho HC, Nguyen TT, et al. Molecular dissection of the inward rectifier potassium current (IK1) in rabbit cardiomyocytes: evidence for heteromeric co-assembly of Kir2.1 and Kir2.2. J Physiol 2003;550:365–72.

[37] Schram G, Pourrier M, Wang Z, White M, Nattel S. Barium block of Kir2 and human cardiac inward rectifier currents: evidence for subunit-heteromeric contribution to native currents. Cardiovasc Res 2003;59:328–38.
[38] Namba N, Inagaki N, Gonoi T, Seino Y, Seino S. Kir2.2v: a possible negative regulator of the inwardly rectifying K^+ channel Kir2.2. FEBS Lett 1996;386:211–4.
[39] Nichols CG, Lopatin AN. Inward rectifier potassium channels. Annu Rev Physiol 1997;59:171–91.
[40] Corey S, Clapham DE. Identification of native atrial G-protein-regulated inwardly rectifying K^+(GIRK4) channel homomultimers. J Biol Chem 1998;273:27499–504.
[41] Dobrzynski H, Marples DD, Musa H, et al. Distribution of the muscarinic K^+ channel proteins Kir3.1 and Kir3.4 in the ventricle, atrium, and sinoatrial node of heart. J Histochem Cytochem 2001;49:1221–34.
[42] Seino S. Physiology and pathophysiology of K(ATP) channels in the pancreas and cardiovascular system: a review. J Diabetes its Complicat 2003;17:2–5.
[43] Inagaki N, Tsuura Y, Namba N, et al. Cloning and functional characterization of a novel ATP-sensitive potassium channel ubiquitously expressed in rat tissues, including pancreatic islets, pituitary, skeletal muscle, and heart. J Biol Chem 1995;270:5691–4.
[44] Inagaki N, Gonoi T, Clement JP, et al. Reconstitution of IKATP: an inward rectifier subunit plus the sulfonylurea receptor. Science 1995;270:1166–70.
[45] Hambrock A, Preisig-Muller R, Russ U, et al. Four novel splice variants of sulfonylurea receptor 1. Am J Physiol Cell Physiol 2002;283:587–98.
[46] Davis-Taber R, Choi W, Feng J, et al. Molecular characterization of human SUR2-containing K(ATP) channels. Gene 2000;256:261–70.
[47] Scott VE, Davis-Taber RA, Silvia C, et al. Characterization of human urinary bladder KATP channels containing SUR2B splice variants expressed in L-cells. Eur J Pharmacol 2004;483:195–205.
[48] Lesage F, Lazdunski M. Molecular and functional properties of two-pore-domain potassium channels. Am J Physiol Renal Physiol 2000;279:793–801.
[49] Wang Z, Yue L, White M, Pelletier G, Nattel S. Differential distribution of inward rectifier potassium channel transcripts in human atrium versus ventricle. Circulation 1998;98:2422–8.
[50] Ludwig A, Zong X, Hofmann F, Biel M. Structure and function of cardiac pacemaker channels. Cell Physiol Biochem 1999;9:179–86.
[51] Shi W, Wymore R, Yu H, et al. Distribution and prevalence of hyperpolarization-activated cation channel (HCN) mRNA expression in cardiac tissues. Circ Res 1999;85:1–6.
[52] Moosmang S, Stieber J, Zong X, Biel M, Hofmann F, Ludwig A. Cellular expression and functional characterization of four hyperpolarization-activated pacemaker channels in cardiac and neuronal tissues. Eur J Biochem 2001;268:1646–52.
[53] Viswanathan PC, Balser JR. Inherited sodium channelopathies: a continuum of channel dysfunction. Trends Cardiovasc Med 2004;14:28–35.

II.

Hindawi Publishing Corporation
Journal of Biomedicine and Biotechnology
Volume 2009, Article ID 361795, 12 pages
doi:10.1155/2009/361795

Research Article

Herpesvirus-Mediated Delivery of a Genetically Encoded Fluorescent Ca^{2+} Sensor to Canine Cardiomyocytes

János Prorok,[1] Péter P. Kovács,[1] Attila A. Kristóf,[2] Norbert Nagy,[1] Dóra Tombácz,[3] Judit S. Tóth,[3] Balázs Ördög,[3] Norbert Jost,[2] László Virág,[1] Julius G. Papp,[1,2] András Varró,[1] András Tóth,[1] and Zsolt Boldogkői[3]

[1] *Department of Pharmacology and Pharmacotherapy, Faculty of Medicine, University of Szeged, H-6720 Szeged, Hungary*
[2] *Division of Cardiovascular Pharmacology, Hungarian Academy of Sciences, H-6720 Szeged, Hungary*
[3] *Department of Medical Biology, Faculty of Medicine, University of Szeged, H-6720 Szeged, Hungary*

Correspondence should be addressed to Zsolt Boldogkői, boldogkoi@yahoo.com

Received 27 February 2009; Accepted 4 May 2009

Recommended by Mohamed Boutjdir

We report the development and application of a pseudorabies virus-based system for delivery of troponeon, a fluorescent Ca^{2+} sensor to adult canine cardiomyocytes. The efficacy of transduction was assessed by calculating the ratio of fluorescently labelled and nonlabelled cells in cell culture. Interaction of the virus vector with electrophysiological properties of cardiomyocytes was evaluated by the analysis of transient outward current (I_{to}), kinetics of the intracellular Ca^{2+} transients, and cell shortening. Functionality of transferred troponeon was verified by FRET analysis. We demonstrated that the transfer efficiency of troponeon to cultured adult cardiac myocytes was virtually 100%. We showed that even after four days neither the amplitude nor the kinetics of the I_{to} current was significantly changed and no major shifts occurred in parameters of $[Ca^{2+}]_i$ transients. Furthermore, we demonstrated that infection of cardiomyocytes with the virus did not affect the morphology, viability, and physiological attributes of cells.

Copyright © 2009 János Prorok et al. This is an open access article distributed under the Creative Commons Attribution License, which permits unrestricted use, distribution, and reproduction in any medium, provided the original work is properly cited.

1. Introduction

The past decade has witnessed an explosive progress of virus-based gene delivery technologies. The reason for this is that, albeit traditional approaches, such as calcium phosphate precipitation, electroporation, or liposome-mediated gene transfer perform excellently in immortalized cells of various origins, they mostly fail in primary cultured cells and under in vivo conditions. Viruses had millions of years to evolve several means for effective infection of cells that can be employed by utilizing viruses as vectors for delivering exogenous genes to the desired cells. Virus-mediated gene transfer methods have also become powerful and widely used experimental tools in cardiovascular research. The most important prerequisites for successful in vitro gene transfer into adult cardiomyocytes include high quality of primary cell culture and an effective transfer vector with limited cytotoxicity and other side effects. However, adult cardiomyocytes are difficult to transduce using methods that work well in other systems because cardiac cells do not divide, have a relatively short lifetime in culture, and are highly sensitive to toxic effects. Gene transfer methods used in cardiovascular research can be divided into two groups: physicochemical and viral vector-based systems. Nonviral methods involve cationic liposome/plasmid DNA complexes, incubation with naked DNA, and calcium phosphate precipitation [1, 2]. All of these methods suffer from severe limitations such as cytotoxicity, very low transfection efficiency especially in vivo applications, and short-term expression of transduced genes due to intracellular degradation of foreign DNA. The above limitations urged the application of more efficient virus vector-based approaches for gene delivery to the cardiovascular system. The following viral systems have been applied in molecular cardiology: adenovirus vectors (Ads), adeno-associated viruses (AAVs), retroviruses (RV) like lentivirus (HIV-1), and herpes simplex virus (HSV-1)-derived vectors [1, 2]. Currently, Ads and AAVs are the most frequently used tools for delivering genes into the

cells of the cardiovascular system, both in vivo and in vitro [3, 4]. While Ads-based vectors allow relatively highly efficient delivery of transgenes to cardiac cells, this system provides only transient expression of transferred genes since the virus does not integrate into the host genome [5]. The application of Ads have further limitations including strong immune responses by the host organism, limited space for transgene integration, and during adaptation may have moderately difficult quality control. An additional problem with Ads systems is related to the infection efficiency. The coxsackie adenovirus receptor (CAR) is a key determinant for the attachment and cellular uptake of adenoviruses [6]. However, CAR expression is maximal in neonates and gets reduced rapidly after birth in several organs such as heart, muscle, and brain resulting in lower penetration rate of adenovirus vectors [7].

Recombinant AAV vectors are able to effectively transduce foreign genes to a variety of cell types including both dividing and postmitotic cells in both in vitro and in vivo experimental systems [8]. The AAV-based systems have a number of favourable attributes, such as lack of parental agent pathogenicity and vector-related cytotoxicity, minimal immunogenicity, and the capacity for stable long-term transgene expression. The main disadvantages of AVV vector-based approaches include the difficulty of producing high-titer virus stocks of consistent purity and bioactivity, and the limited packaging capacity of a maximum 4.8 kb insert-size [9]. Lentivirus-based gene transfer has been reported in a wide variety of cell types, including cardiomyocytes [10]. Current lentiviral vectors are capable of transducing mitotically quiescent cells, particularly within the cardiovascular system. The strengths of this system include the ability of long-term stable transgene expression, an increased packaging capacity compared with AAV, and the other commonly used integrating vector [11]. The disadvantages of lentivirus-based gene delivery systems are the relative low level of transgene expression and the limited transgene carrying capacity of the virus.

Pseudorabies virus (PRV), a causative agent of Aujeszky's disease of swine, is an alpha-herpesvirus belonging to family of Herpesviridae. Several previous reports have been successful in construction of PRVs for delivering foreign genes to neurons [12]. PRV is especially an important tool for labelling neural circuits [13], which was combined with delivery of activity markers to labelled neurons [14].

In this study, we have developed a method for short-term culture of isolated myocytes that retains their morphological as well as physiological integrity and a pseudorabies virus (PRV)-based system for delivery of foreign genes to adult cardiac muscle cells. Troponeon (TN-L15) [15], an FRET-based activity marker was selected as a model transgene system. Troponeon is a genetically-encoded fluorescent Ca^{2+} sensor that is suitable for the imaging of cellular activity in neurons, muscle, and cardiac cells. Pseudorabies virus was modified to disable to replicate on postmitotic cells but retaining its capacity for high titer multiplication on dividing cultured epithelial cells. The strengths of the presented system is a very high gene transfer efficiency, low toxic effect, the capacity for relative long-term transgene expression, and the delivery of large or multiple transgenes. The suitability of PRV-based gene delivery technique was evaluated in several ways. We performed simultaneous measurements in non-infected control and infected myocytes following isolation and infection. Retained functionality of the sarcolemmal ion channels was tested by measuring a characteristic multi-channel current I_{to}. Intactness of the excitation-contraction coupling (ECC) machinery and contractile function was demonstrated by monitoring intracellular calcium transients and cell shortening. Finally, undisturbed functioning of the transmitted gene was verified by FRET monitoring of the calcium transient currents.

2. Materials and Methods

2.1. Cells and Viruses. The wild type Kaplan strain [16] of pseudorabies virus (PRV) was used as parent strain for the generation of recombinant viruses used in this study. Viruses were propagated on subconfluent monolayer of porcine kidney (PK-15) cells. Cells were grown in DMEM supplemented with 5% fetal calf serum at 37°C with 5% CO_2. The stocks of PRV were prepared as follows: PK-15 cells were infected with PRV at a multiplicity of 1 p.f.u/cell, harvested after 24 hours, followed by freezing and thawing three times. The cells were then centrifuged and the pellet discarded. The supernatant fluid was stored in 400 μL aliquots at −80°C.

2.2. Reporter Genes. Tn-15 (troponeon), an FRET-based fluorescent calcium sensor [15], was used as an activity marker in our experiments. The troponeon gene was placed under the control of the major immediate early promoter of human cytomegalovirus (pCMV), which provided a high level of gene expression. The marker gene expression cassette also contained simian virus 40 (SV40)-derived sequences including polyadenylation signal and transcription termination sequences. In addition, a lacZ gene equipped with the above regulatory sequences was also used as a reporter gene for the identification of mutant viruses.

2.3. Construction of Targeting Vectors. In our system, a typical targeting plasmid contains a marker gene expression cassette flanked by subcloned viral DNA sequences, which serves as homologous DNA regions for the insertion of marker genes via homologous recombination. The DNA sequences used for mutagenesis and as insertion sites for reporter genes are listed on Figure 1.

2.3.1. Ribonucleotide Reductase (RR) Gene. The details of the construction of RR gene targeting vector was described elsewhere [17]. Briefly, a 5-kbp *Sal*I-F fragment of PRV DNA containing both subunits of RR gene was isolated and cloned to pRL494, a palindrome-containing positive selection vector [18]. This plasmid was cut with *Sca*I and *Mlu*I restriction endonucleases generating a 1805-bp deletion, which included a 1789-bp DNA fragment from the 3′ end of large (RR1) and a 7-bp DNA sequence from the 5′ end of small subunit (RR2) of ribonucleotide reductase gene. Subsequently, free DNA ends were filled up by Klenow

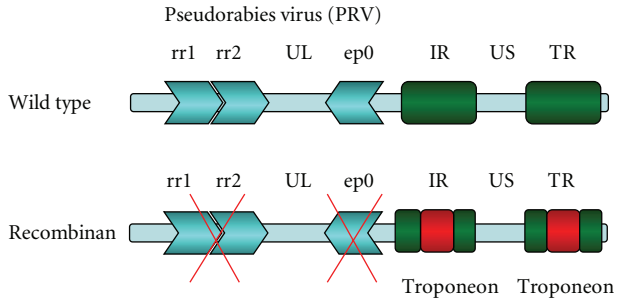

Figure 1: This panel shows a part of recombinant herpesvirus genome. To adapt for applicability as virus vector we deleted the two ribonucleotide reductase (rr) and the early protein (ep0) genes from the virus genome by homologue recombination. The rr1 and rr2 genes are in charge for production of raw material of viral DNA. The recombinant virus is not able to productively infect postmitotic cells without rr genes, while ep0 gene is responsible for virus reactivation from latency. Troponeon calcium sensor gene was inserted into the antisense promoter region in two copies.

enzyme followed by attaching an *Eco*RI linker to the blunt DNA ends. As a final step, a lacZ gene expression cassette bracketed by *Eco*RI sites was subcloned to the *Eco*RI site of this plasmid.

2.3.2. Early Protein 0 (EP0) Gene. Generation of EP0 gene targeting vector was described previously [19]. Briefly, the 9.4-kb *Kpn*I-F DNA fragment containing the EP0 gene was subcloned into pRL425; followed by cleaving with *Bam*HI restriction endonuclease, which resulted in the deletion of a 1390-bp sequence, including almost the entire EP0 gene. Free DNA ends were converted to *Eco*RI sites via linker insertion and then religated. The same lacZ gene expression cassette as above was subcloned to the *Eco*RI site of this plasmid.

2.3.3. Putative Antisense Promoter (ASP) Region. The 4.9-kb *Bam*HI-8′ PRV DNA fragment was isolated and subcloned to pRL525 cloning vector [18, 20]. The *Dra*I site located in the putative TATAA box of ASP was used for the insertion of *Eco*RI thereby destroying its potential function. The fluorescent marker gene expression cassettes (GFP, troponeon) were inserted to the *Eco*RI site of this plasmid.

2.4. Generation and Isolation of Recombinant Viruses. Recombinant viruses were generated by means of homologous recombination between parent PRV genomes and targeting plasmids containing reporter genes bracketed by virus sequences. Viral DNA was transfected to actively growing PK-15 cells along with the appropriate targeting plasmid using lipid-mediated gene delivery (Lipofectamine 2000 Reagent, Invitrogen). Viral DNA for the transfection was prepared from virions purified from the medium of infected cells showing total cytopathic effects by isopycnic centrifugation on a discontinuous gradient, as described previously [12]. The lacZ gene-expressing viruses were screened based on their blue plaque appearance in the presence of 5-bromo-4-chloro-3-indolyl-*b*-D-galactopyranoside (X-Gal), the chromogenic substrate of β-galactosidase. Blue plaques were picked and plaque purified to complete homogeneity. Plaques formed by recombinant viruses carrying the fluorescent markers were detected visually on the basis of their fluorescence. Recombinant viruses were isolated by 6–15 cycles of plaque purification procedure using a fluorescence microscope (Olympus IX-71).

2.5. Isolation of Adult Canine Cardiomyocytes. All experiments were conducted in compliance with the *Guide for the Care and Use of Laboratory Animals* (USA NIH publication No. 85-23, revised 1985). The protocols were approved by the review board of the Committee on Animal Research (CAR) of the Albert Szent-Györgyi Medical University. The modified protocol for cell isolation was based on established procedures described earlier in detail [21].

Canine ventricular myocytes were enzymatically dissociated as follows. A portion of the left ventricular wall containing an arterial branch large enough to cannulate was perfused in a modified Langendorff apparatus with solutions in the following sequence:

(1) normal Tyrode's solution (10 minutes), (2) Ca^{2+}-free Tyrode solution (10 minutes), and (3) Ca^{2+}-free Tyrode solution containing collagenase (type I, 0.66 mg/mL) and bovine serum albumin (fraction V, fatty acid free, 2 mg/mL) (15 minutes). Protease (type XIV, 0.12 mg/mL) was added to the final perfusate while and another 15–30 minutes of digestion was allowed. Cells were stored in KB solution. The composition of solutions were (in mM): (a) *normal Tyrode's solution*—NaCl 135, KCl 4.7, KH_2PO_4 1.2, $MgSO_4$ 1.2, HEPES 10, $NaHCO_3$ 4.4, glucose 10, and $CaCl_2$ 1.0 (pH 7.2 adjusted with NaOH); (b) *Ca^{2+}-free Tyrode solution*—NaCl 135, KCl 4.7, KH_2PO_4 1.2, $MgSO_4$ 1.2, HEPES 10, $NaHCO_3$ 4.4, Glucose 10, and taurine 20 (pH 7.2 adjusted with NaOH); (c) *KB solution*—KOH 90, L-glutamic acid 70, taurine 15, KCl 30, KH_2PO_4 10, $MgCl_2$ 0.5, HEPES 10, glucose 11, and EGTA 0.5 (pH 7.3 adjusted with KOH). All chemicals used in this method were purchased from Sigma Chemical Co.

2.6. Culture and Infection of Myocytes. The entire culture procedure was performed in a class II flow hood. The freshly isolated myocytes were centrifuged five times for 1 minute at 50 g in sterile 10% PBS. The supernatant was replaced first by 500 μM then by 1 mM Ca^{2+} containing PBS solution. The mild centrifugation steps removed the majority of bacterial cells, most nonmyocytes and nonfunctioning myocytes. Precipitated cells were resuspended in culture medium and plated on laminin coated (1 $\mu g/cm^2$) sterile cover glass at densities of up to 10^3 rod-shaped cells cm^{-2}. Cells were left 4 hours to attach to the plate and after this time period non attached cells were removed. Following the first medium change, subsequent medium changes were carried out every day. Culture medium consisted of serum-free medium 199 (M199) supplemented with 25 mM $NaHCO_3$, 5 mM ceratine, 2 mM L-carnitine, 5 mM taurine, 100 units/mL insulin (CCTI supplemented medium) and

50 μg/mL gentamycin. All chemicals used in this procedure were purchased from Sigma. Cells were maintained at 37°C under sterile conditions in an incubator ventilated with 5% CO_2 and 95% air. After 4 hours, plate attached cells were infected. Freshly isolated canine cardiomyocytes were first washed with PBS, followed by low-speed centrifugation and resuspension in culture medium. Subsequently, after a 4-hour incubation at 37°C in a CO_2 incubator, cells were infected with various titers of recombinant viruses for 12 hours then washed and the culture medium was changed. Infected cells were used for analysis at various time points.

2.7. Evaluation of Infection Efficacy and Morphological Changes in Cultured Cardiomyocytes. Cell shape and morphology are closely linked with some aspects of cell function such as excitation-contraction coupling. Therefore, monitoring these properties may give indications of physiological changes that are occurring. Morphological changes of cells were observed by light microscope on a daily basis parallel with physiological measurements. Troponeon-positive cells were examined by fluorescence microscopy from one to three days following isolation at standard titer of viruses. Infection efficacy was determined separately for infected cells by manual cell counting using a fluorescent microscope (Olympus IX-71).

2.8. Evaluation of the Physiological State of the Virus-Infected Cells

2.8.1. Evaluation of the Electrophysiological State of the Cells by $\mathbf{I_{to}}$ *Analysis.* I_{to} currents were measured at 37°C using the whole-cell configuration of the patch-clamp technique. Measurements were performed daily starting with day 0, when only freshly isolated noninfected myocytes were investigated. In the following days control and infected cells were studied separately by placing cover glasses with the attached cells in the recording chamber mounted on the stage of an inverted microscope equipped with epifluorescence assembly (Olympus IX50, Tokyo, Japan). Only rod-shaped cells with clear cross-striations and relatively strong GFP signal were used. HEPES-buffered Tyrode's solution containing (in mM): NaCl 144, NaH_2PO_4 0.33, KCl 4.0, $CaCl_2$ 1.8, $MgCl_2$ 0.53, glucose 5.5, and HEPES 5.0 at pH of 7.4 (by NaOH) served as normal superfusate. Cell capacitance (199.3 ± 13.7 pF, $n = 69$) was determined by applying a 10 mV hyperpolarizing pulse from a holding potential of −10 mV. Cell capacity was calculated as the integral of the capacitive transient divided by the amplitude of the voltage step. Patch-clamp micropipettes were fabricated from borosilicate glass capillaries (Clark, Reading, UK) using a P-97 Flaming/Brown micropipette puller (Sutter Co, USA). These electrodes had resistances between 1.5 and 2.5 Mohms when filled with pipette solution containing (in mM): K-aspartate 100, KCl 45, K_2ATP 3, $MgCl_2$ 1, EGTA 10, and HEPES 5. The pH of this solution was adjusted to 7.2 by KOH. Nisoldipine (1 μM) (obtained as a gift from the Bayer AG, Leverkusen, Germany) was used in the external solution to eliminate inward Ca^{2+} current (I_{Ca}). Membrane currents were recorded with Axopatch-200B patch-clamp amplifiers (Axon Instruments, USA). After establishing a high (1–10 Gohm) resistance seal by gentle suction, the cell membrane beneath the tip of the electrode was disrupted by suction or by application of 1.5 V electrical pulses for 1–5 milliseconds. The series resistance was typically 4–8 Mohm before compensation (50–80%, depending on the voltage protocols). Experiments where the series resistance was high, or substantially increased during measurement, were discarded. Membrane currents were digitized using a 333 kHz analogue-to-digital converter (Digidata 1200, Axon Instruments) under software control (pClamp 8.0, Axon Instruments). Analyses were performed using pClamp 8.0 (Axon Instruments) software after low-pass filtering at 1 kHz. All patch-clamp data were collected at 37°C.

2.8.2. Evaluation of Cell Function by Monitoring $[Ca^{2+}]_i$ *Transient and Cell Shortening.* 24–72 hours following viral infection cultured myocytes were loaded by incubation for 20 minutes with the acetoxymethyl ester (AM) form of a single wavelength calcium-sensitive fluorescent dye (Fluo-4, Molecular Probes Inc. 1–2 μM from a stock of 1 mM in DMSO + 20% pluronic acid) at room temperature. The technique for calcium transient detection was based on established procedures described earlier [22]. After this incubation period the cover glass with attached cultured myocytes was mounted in a low volume imaging chamber (RC47FSLP, Warner Instruments, USA) and placed on the stage of an inverted fluorescent microscope (IX71, Olympus, Japan). The cells were superfused with normal Tyrode solution at 37°C (1 mL/min). Myocytes were stimulated at a constant frequency of 1 Hz through a pair of platinum electrodes by an electronic stimulator. The dye was excited at 480 nm, fluorescence emission was recorded at 535 nm (Chroma, USA). Optical signals were recorded by a photon counting photomultiplier module (H7828, Hamamatsu, Japan), and sampled at 1 kHz. Measurements were performed and data were analyzed using the Isosys software (Experimetria Ltd, Hungary). Cell shortening from both ends was determined by a video edge detection system (VED-105, Crescent Electronics, USA). All experiments were performed at 37°C, using an automatic temperature controller (TC-344B, Warner Instruments, USA).

2.8.3. Evaluation of the Functionality of the Transferred Gene by FRET Measurement. For testing the functionality of the transferred gene, following the incubation period the cover glass with the attached primary cultured cardiomyocytes was mounted in a low volume imaging chamber (RC47FSLP, Warner Instruments, USA) on the stage of an Olympus IX71 inverted microscope outfitted with a 75 W Xe arc lamp for epi- and a 100 W tungsten-halogen lamp for transillumination. The myocytes in the chamber were superfused with normal Tyrode solution (1 mL/min) and stimulated at a constant frequency of 1 Hz by an electronic stimulator (Experimetria) through a pair of platinum electrodes. All measurements were performed at

37°C, by using an automatic temperature controller (TC-344B, Warner Instruments, USA). The optical signals were typically monitored 20–36 hours after infection in selected myocytes expressing the genetically encoded FRET-based sensor troponeon (csTnC-L15). Cells with medium-high level of fluorescence were selected for measurement. Though often troponeon fluorescence is already visible 16 hours following infection, optical signals were found to be optimal for recording after 24 hours.

Fluorescent optical signals were monitored by a dual channel photon counting system. An Olympus filter cube containing a CFP excitation filter (436/20 x) and a CFP dichroic mirror (455DCLP) but no emission filter was inserted into the light path of the microscope. A connector box for dual emission fluorescence with two interchangeable dichroic mirror holders and three detector ports (P226/0II/011, Cairn Research Ltd, UK) equipped with two photons counting photomultiplier modules (H7828, Hamamatsu, Japan) was attached to the left side port of the microscope. The fluorescent signal from the microscope was splitted by a YFP dichroic mirror (515LP). A second dichroic mirror (565DCLP) was used to separate the longer wavelength (FRET) fluorescence from the red filtered (> 580 nm) transillumination light used for visual observation of the cell by a video camera mounted on the 3rd back port of the connector box. The splitted fluorescence components were band pass filtered (480/30 m and 535/30 m for CFP and citrine, resp.), integrated with 1 milliseconds time resolution by two photons to voltage converter units (Ionoptics, US) and collected for data processing. All interference filters and dichroic mirrors used are avaiable in filter sets 31036V2 and 41028 from Chroma Technology Corporation (US).

Changes in $[Ca^{2+}]_i$ levels were characterized by the ratio of the emitted fluorescence intensities obtained at 480 and 535 nm wavelengths, ($F_{FRET\_CITRINE}$ 535/ F_{CFP} 480) following optical signal correction steps for photobleaching and nonspecific background fluorescence. Photobleaching leads to a steady decrease in the FRET ratio over time, because citrine is less photostable than CFP. To correct for bleaching, we multiplied the intensity of the CITRINE channel by a correction factor calculated from the intensity shift between two time points. For background correction we subtracted from the optical signals the nonspecific background fluorescence determined at both wavelengths by moving off the cell from the light path: $F_{RATIO\_corr} = (F - F_0)_{CITRINE} / (F - F_0)_{CFP}$. The background-corrected fluorescence ratio versus time curve can be considered as a representation of the intracellular Ca^{2+} transients Figure 7.

2.9. Data Analysis. All patch-clamp results and optical measurements were compared using Student's *t*-tests for paired and unpaired data and expressed as mean ± SEM values. Statistical significance of differences obtained between control and virus infected preparations was evaluated with Student's *t*-test for paired or unpaired data, as relevant. Differences were considered significant when $P < .05$.

Table 1: This table shows the survival of noninfected and virally infected cells from day 0 to day 5. It can be seen that virally infected cells exhibit slightly better survival than noninfected cells, for which the reason remains to be ascertained.

		Day 0	Day 1	Day 2	Day 3	Day 4	Day 5
Control	Average (%):	100	60,0	44,9	4,3	2,8	2,2
	Standard error:		6,0	8,4	0,5	0,3	0,3
Virus infected	Average (%):	100	85,5	69,2	12,8	3,1	1,3
	Standard error:		4,7	9,3	3,7	1,5	0,6

3. Results

3.1. Morphological Changes of Cultured Cardiomyocytes. Using the described method for isolation of adult dog left ventricular myocytes, we routinely obtained a high yield (more than 80%) and high (more than 80%) percentage of rod-shaped myocytes that were suitable not only for acute functional studies but, more importantly, for short-term culture and gene transfer. Figure 2(a) shows a transillumination image of freshly isolated and 1-day-old cultured cardiomyocytes from the left ventricle. To establish optimal surviving conditions several culture conditions were tested based on microscopic evaluation of changes in cellular morphology during the four days of culture. Cultured cells were used 1–3 days after isolation. During this period, visible small-scale changes in cell shape and cross-striation could be observed. Figure 2(b) shows representative photographs of canine myocytes over time in culture. Features typical of acutely isolated (Day 0) cells were the rod shape with rectangular stepped ends and clear cross-striations. After 1 day (Day 1) in culture, the cells were still rod-shaped with clear cross-striations; however, the ends of the cells started to become slightly rounded in appearance. After 3 days (Day 3) in culture, cells remained rod-shaped and cross-striated, and the main change was that cell ends became progressively more rounded (see Table 1 for cell survivals).

3.2. Efficacy of Virus Infection in Cultured Cardiomyocytes. Survival rates were found to be dependent on the isolation procedure, density of the attached myocytes, and the applied virus titer. Intriguingly, a higher total number of viable cells were observed on the laminin-coated surfaces after plating in CCTI supplemented medium. As respective panels of Figures 2 and 3 (upper panel) show, even after three days, the cell culture contained a substantial number of good quality cells both in the control and virus-infected groups. Surprisingly, a moderately but consistently higher cell survival rate was found in virus-infected groups as compared to noninfected groups (not shown). The infection efficiency was found to be 100%, that is 24 hours postinfection every surviving cells emitted fluorescent signals provided that high dose of virus was used for the infection (Figure 3 bottom panel).

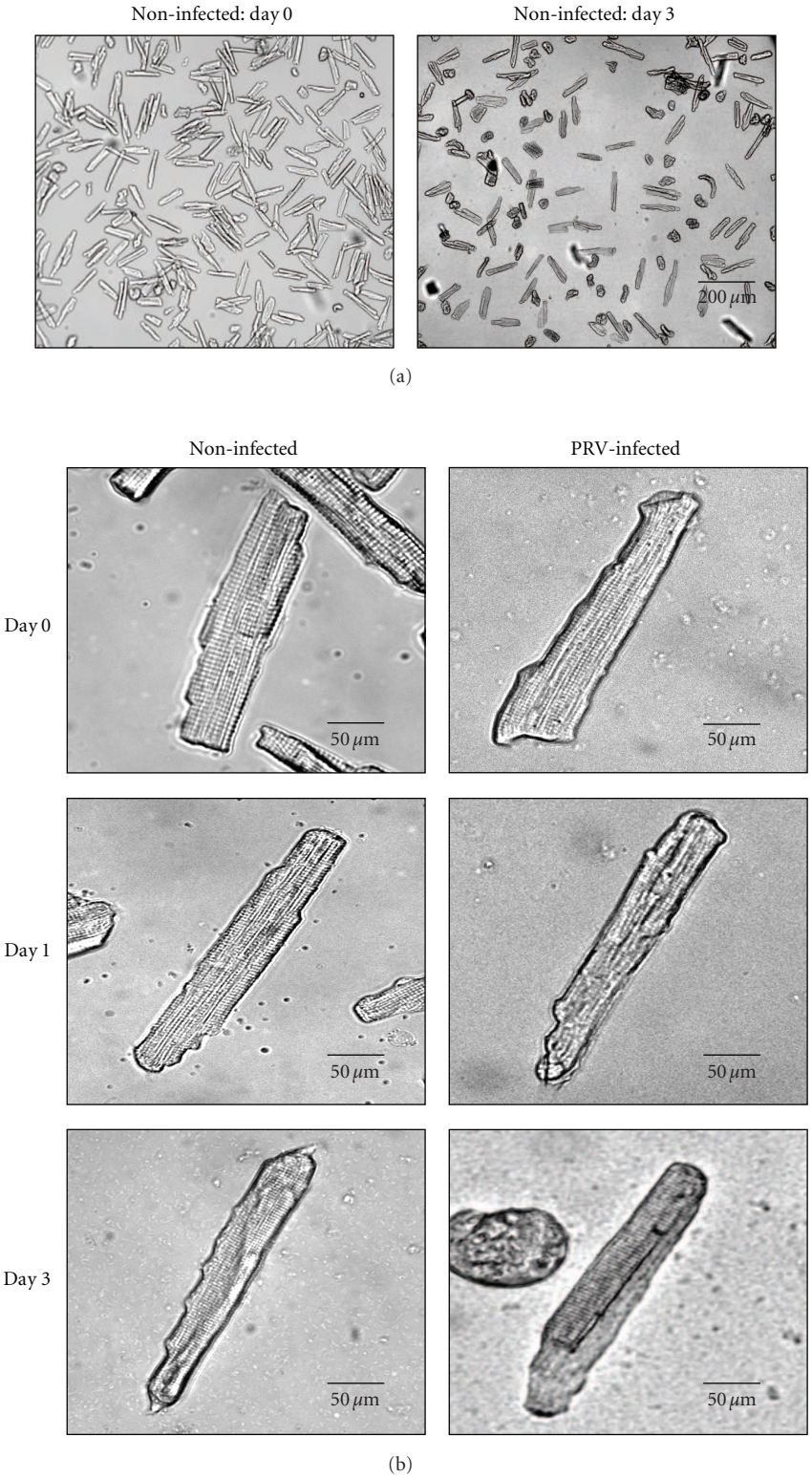

FIGURE 2: Representative low- and high-magnification transillumination of adult dog myocytes after isolation (day 0) and 1–3 days of culture (day 1, day 3). (a) shows the yield of the myocytes before and one day after culturing and infection. The high-magnification transillumination (b) shows the morphology of adult dog myocytes after isolation (day 0) and 1–3 day of culture (day 1, day 3) and the morphological changes of living cells, versus the culturing time from noninfected (right) and the virus-infected groups (left). After one day plated myocytes more than 80% displayed a rod-shaped morphology and healthy cross-striation. After 3 days (day 3) in culture, cells remained rod-shaped and partially cross-striated, and the main change was that cell ends became progressively more rounded.

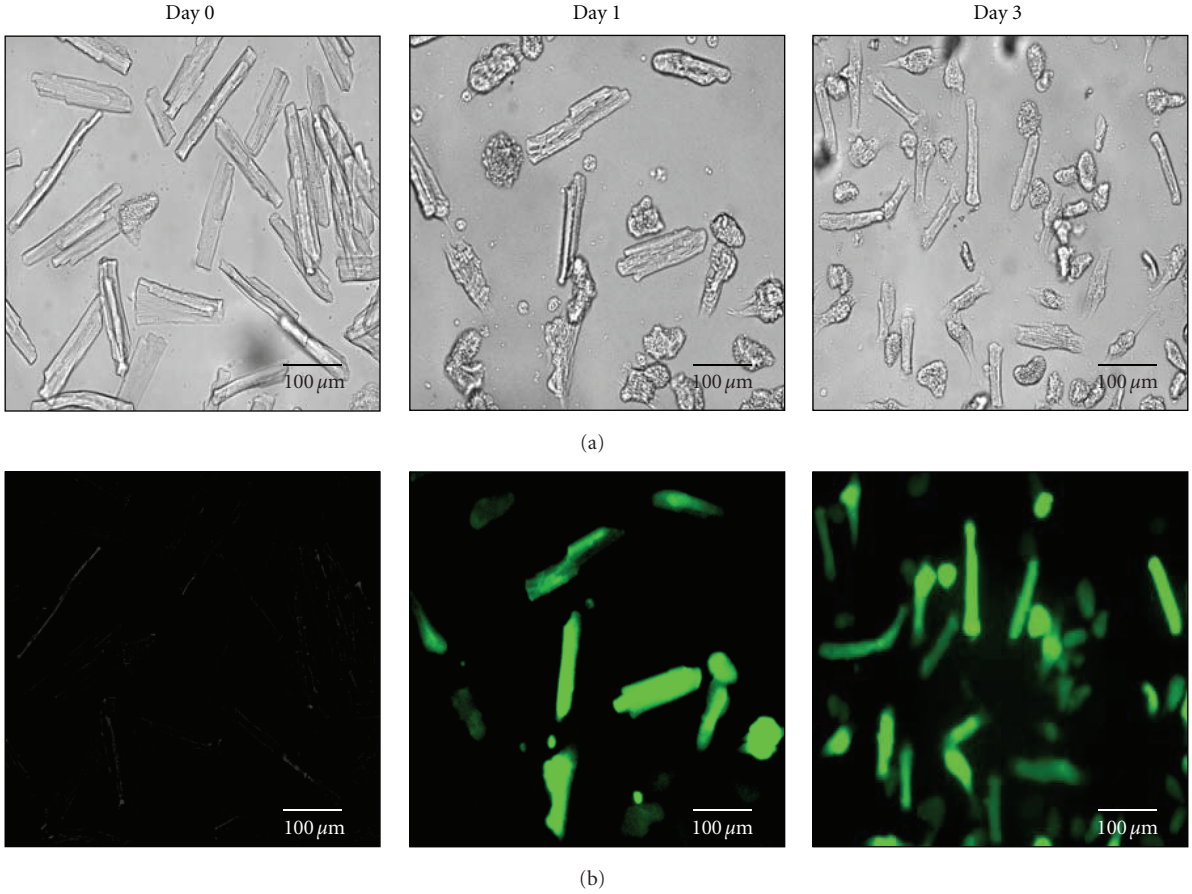

Figure 3: (a) Representative light and (b) fluorescent microscopic images of cell culture, before and after 1 day and 3 days of virus infection. Expression of recombinant pseudorabies-viral troponeon transgenes appeared on high level in cultured adult dog ventricular myocytes. The isolation of adult dog left ventricular myocytes yielded more than 80% living cells. After three days the troponeon expression and the physiological features of survival myocytes was appropriate for the physiological studies.

3.3. Whole-Cell Patch-Clamp Recordings. The whole-cell configuration of the patch-clamp technique was used to record the transient outward I_{to} current. I_{to} was chosen as a physiological assay because it is a large current that can be measured relatively easily in isolated canine ventricular myocytes. The current was activated by 300 milliseconds long depolarizing voltage pulses from the holding potential of −90 mV to test potentials ranging from 0 to +60 mV with a pulse frequency of 0.33 Hz. The amplitude of I_{to} was measured as the difference between the peak and the sustained current at the end of the voltage pulse. Figure 4(a) shows typical recordings of I_{to} measured after one (Day 1) and three days (Day 3) of culture either in control (top panels) or virus-infected cells (bottom). Figure 4(b) summarizes all I_{to} measurements performed after 0–4 days of culture in both groups. As the corresponding panels of Figure 4 show, the amplitude of the I_{to} was reduced by less than 10% in virus-infected myocytes (VM) compared to control noninfected cells (CM) even after 4 elapsed days. Moreover current amplitude was somewhat larger in PRV-infected cells compared to that of observed in control cells. Mean I_{to} density (Figure 4(b)) was similar for CM and VM cells after 1 day. The I_{to} current density in VM changed in four days from 19.6 ± 1.4 to 24.6 ± 2.6 pA/pF (n = 10–12), which corresponds well with that observed in CM (from 19.3 ± 2.1 to 17.1 ± 1.5 pA/pF, n = 8–10). Although mean I_{to} density of several-day-old (2, 3, 4) cultured myocytes was significantly larger in VM than CM. The I_{to} kinetics (activation and inactivation properties) was also not significantly altered by the virus infection.

3.4. Parameters of Intracellular Ca^{2+} Transients and Contractility. Cultured myocytes were stimulated at a constant frequency of 1 Hz through a pair of platinum electrodes. Similarly to I_{to} measurements, the steady-state $[Ca^{2+}]_i$ transient and contractile function were measured and compared on a daily basis both in the infected and control cell populations. Original recordings of $[Ca^{2+}]_i$ transients and cell shortening before and after virus infection are presented in Figure 5. The calcium transient kinetics were significantly distorted in culture, but were also not significantly altered by the virus-infection. As Figure 6 summarizes, we found no statistically significant differences in either the amplitude of

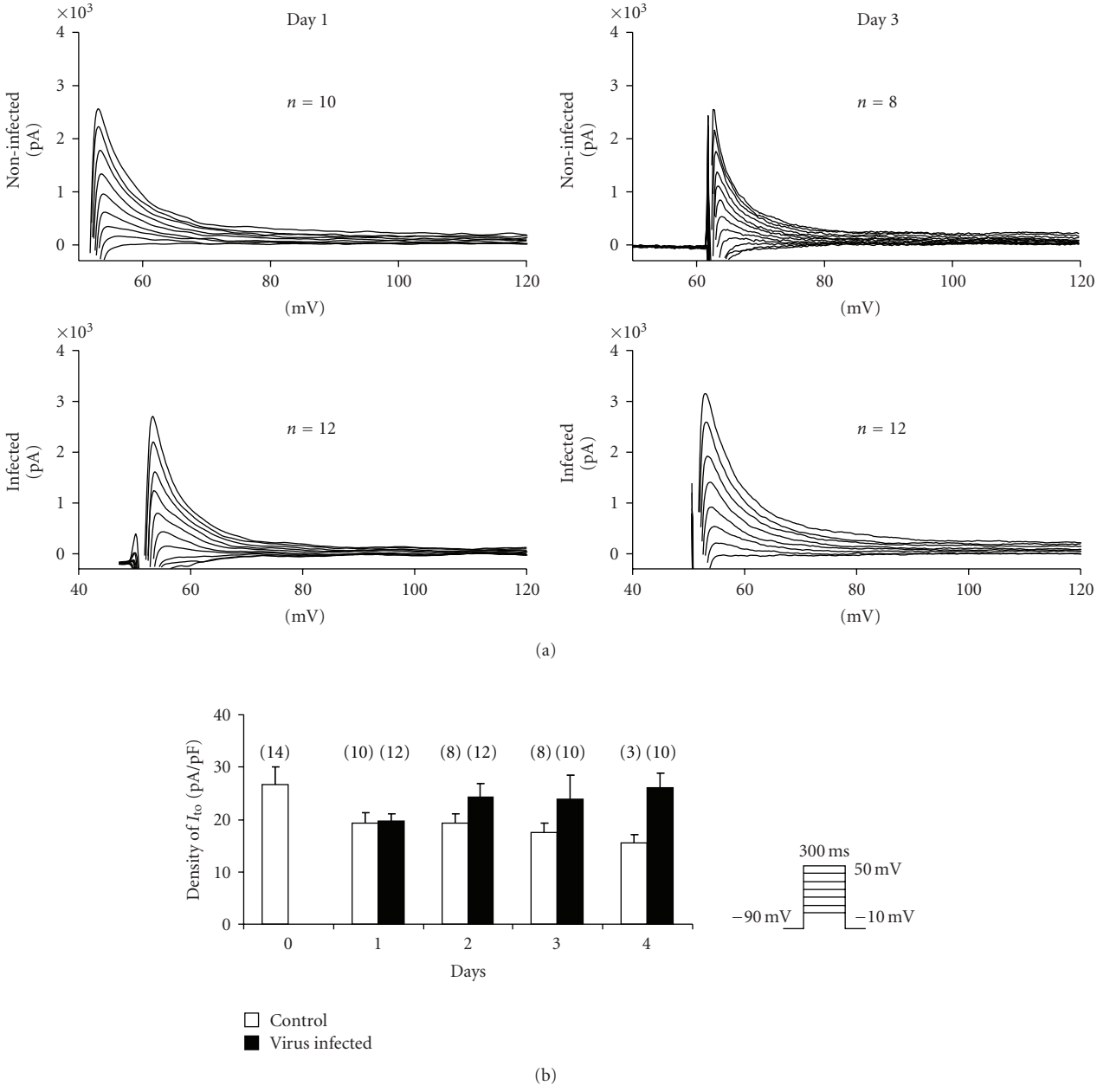

FIGURE 4: (a) Transient outward K current (I_{to}) recordings from control and from virus-infected myocytes after (a) 1 and (b) 3 days of culture. Inset shows applied voltage protocol. (b) shows the I_{to} current densities from control and from virus-infected myocytes after 1 to 4 days long culture. Data represent means ± SEM, and *n* represents the number of experiments.

calcium transient (A) or diastolic calcium level (B) between the studied groups. Moreover, transient decay time (C) in noninfected control myocytes was significantly larger than in the virus infected group after two and three days in culture. Conversely in virus-infected group's decay time was similar to freshly isolated cells. The cell-shortening measurements (D) represent a significant decline in noninfected cell culture after 1 and 3 days. Data indicate no significant changes in these parameters.

3.5. Functionality of FRET-Based Calcium Sensor. Freshly isolated ventricular myocytes were infected with the virus following 4 hours plating and fluorescence could already be detected within 16 hours. The functionality of the transferred gene was verified by monitoring $[Ca^{2+}]_i$. Figure 7 shows two typical fluorescence signal emissions measured in troponenon-expressed cells obtained at 485 nm and 535 nm excitation (upper panel). The lower panel shows the ratio of the citrine and CFP emitted signals representing the changes of the $[Ca^{2+}]_i$ levels in the studied cells. This measurement

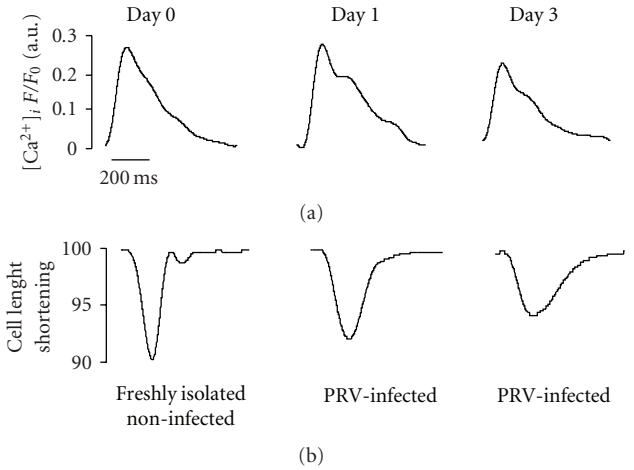

FIGURE 5: Original Ca^{2+} transients and cell contraction recording in cardiomyocytes cultured for 1 and 3 days. The top panel shows the intracellular Ca^{2+} concentration as Ca^{2+} transient fluorescent signal (F535 nm), and bottom panel shows the changes in cell length.

clearly shows that virally-encoded troponenon retained its ability of indicating $[Ca^{2+}]_i$ levels in cardiomyocytes.

4. Discussion

Recent advances of transgenesis and gene targeting technologies have heralded a new era of cellular physiology to study molecular function using genetically engineered animal models and genetically encoding vector-based gene transfer systems. Practically, the mouse is the only mammalian species in which transgenic technology efficiently works. Several transgenic and gene-targeted models have been generated for the overexpression [23, 24], and genetic ablation of key proteins [25, 26] governing cardiac structure and function.

However, the mouse is not an ideal species for modelling human disease like heart failure, myocardial infarction, and arrhythmia studies, because the mouse heart has distinctly different action potential waveform due to its different underlying ionic current structure [27, 28]. Transducing foreign genes to cardiac cells of living animals is a feasible technique in several animal models; however, performing electrophysiological measurements in vivo is not easy therefore in vitro electrophysiological techniques are usually used in cultured cells for this purpose. Similar experiments were performed in a recently published work using cultured human atrial myocytes [29] and myocytes isolated from rat, a species from which producing long-term cell culture is much easier.

Gene transfer to cardiac myocytes has been traditionally carried out in neonatal cells. However, these cells undergo differentiation, and as a result, this model is inappropriate for certain experiments since differentiating cells have different currents than that of from adult cells. Therefore, in vitro transducing of isolated cardiac myocytes can be a useful alternative for investigations of cardiovascular cell physiology and diseases.

The structural changes during culturing ventricular myocytes were studied and as well [30, 31]. These changes are associated with culturing procedures associated effects, which may change a number of physiological properties of cells in culture. Therefore, some possible alterations in the Ca^{2+} handling and sarcolemmal ionic currents may have been diminished in cultured cells.

Another potential application of our viral gene transfer strategy is to introduce siRNA for silencing pore or auxiliary ionic channel subunits underlying transmembrane ionic currents. In this study we opted for canine model, since the dog unlike the mouse and rat is known to have action potential and ionic current characteristics similar to human [32]. We have chosen the transient outward current for testing the possible effects of viral infection because I_{to} is a relatively large current and present in all cells. Also it can be relatively easily measured. The I_{to} gene structure is rather complex. The I_{to} current in canine myocytes resembles human myocytes and has a large conducting pore forming unit Kv4.3 connected with several auxiliary subunits such as KChIP2, KCNE2, and DPPX [33]. In the present work, we measured the effect of the viral infection on I_{to} and we found that the virus did not affect either the density or kinetics of I_{to} current (Figure 4).

Since their introduction more than twenty years ago of Ca^{2+}-sensitive fluorescent dyes have been used to evaluate intracellular free calcium concentration ($[Ca^{2+}]_i$) [34], enabling investigators to gain unprecedented insights into the mechanisms of cell signalling. The dynamics of changing Ca^{2+} concentrations at cellular level and well-defined subcellular spaces in excitable cells, during the course of membrane depolarization can now be understood in the context of disease processes such as cardiac arrhythmias and heart failure. Although many details of excitation-contraction coupling were described previously, novel quantitative fluorescence techniques have significantly improved our understanding of major cell regulatory pathways.

Fluorescent dyes commonly used for Ca^{2+} imaging are based on bis(2-aminophenoxy)ethane tetraacetic acid (BAPTA) structure and subsequently on bis(2-aminoethyl ether) tetraacetic acid (EGTA) backbone conjugated to a fluorescent moiety. Fura-2, indo-1, and fluo-4 are the most widely used fluorescent dyes for monitoring intracellular $[Ca^{2+}]$; in their acetoxymethyl ester form they can relatively easily be loaded into cells, are relatively photostable, and are well suited for reliable detection of changes in Ca^{2+} concentration under physiological conditions [35]. These Ca^{2+} indicators with low molecular weight have some important advantages as great dynamic range, increased sensitivity, high fluorescent intensity, and rapid response kinetics, but also have some limitations, being not targetable and subcellular localization of dye cannot be controlled [36]. Recently developed genetically encoded Ca^{2+} indicators (GECIs) are defined as optical Ca^{2+} sensors produced by the expression of specific genes. These proteins contain a light-emitting fluorescent protein unit and a Ca^{2+}-responsive unit. Troponeon, a typical member of the GECI family is

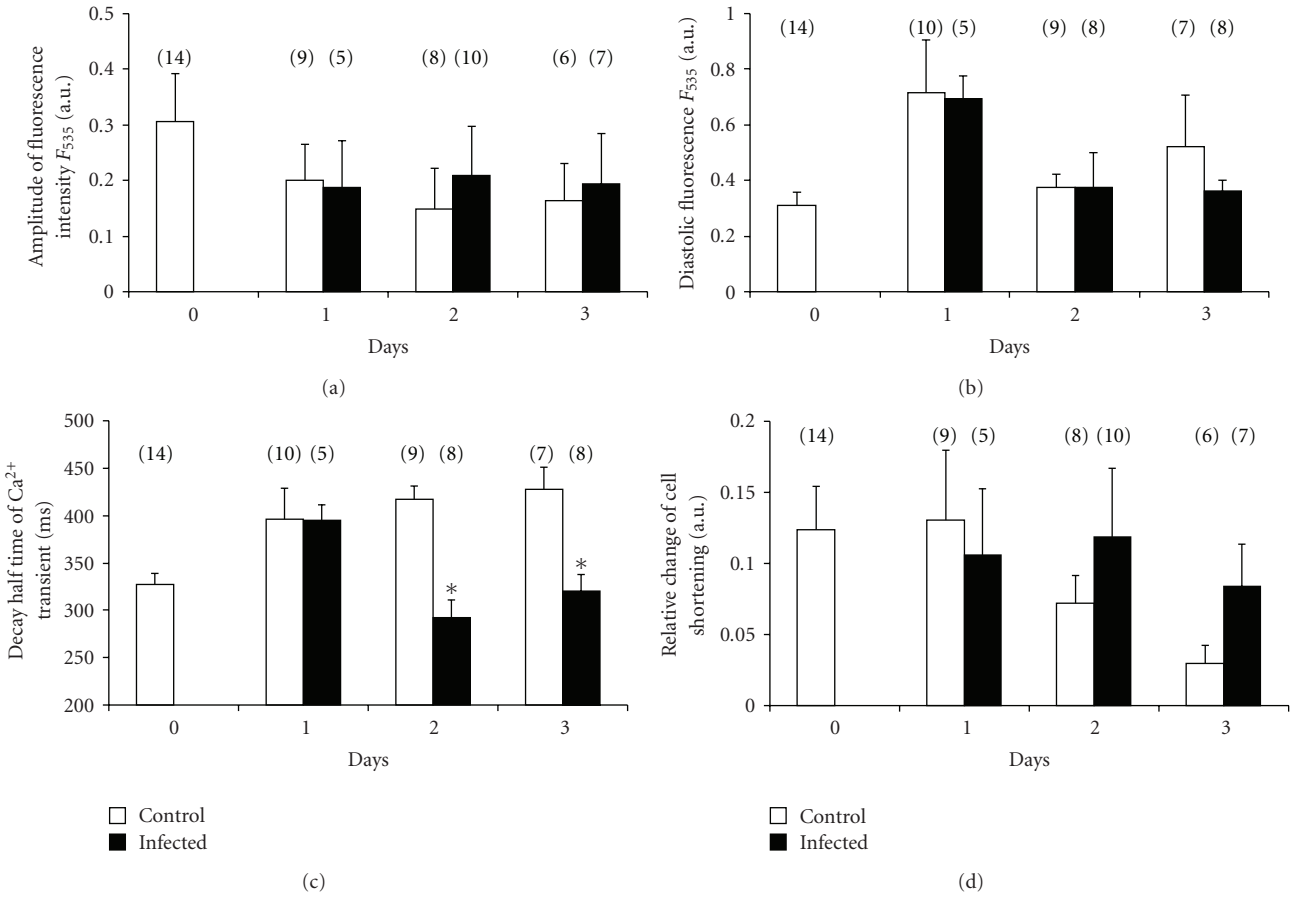

Figure 6: This figure shows several parameters of intracellular free calcium transient such as (a) amplitude of calcium transients, (b) diastolic calcium levels, (c) changes of calcium transient decay constant, and (d) cell-shortening measurements from recordings from control and from virus infected myocytes after 1 to 3 days long culture. Bars represent means ± SEM, and n represents the number of experiments.

composed of a calcium-binding domain carrying a variant of troponin C protein and a pair of mutant green fluorescent proteins (CFP and Citrine) engineered for fluorescence resonance energy transfer (FRET) [15]. A significant difficulty in using these new Ca^{2+} sensors is their low efficiency of transfection into several cell types, cardiomyocytes included. On the other hand, the strengths of GECIs include the following: localization can be controlled by a custom signal sequence; it can be genetically fused to a protein of interest. GECIs can be maintained within cells over days to weeks and expression level/concentration of GECIs can be well controlled by incorporating a promoter [37].

At present, in spite of permanent improvements, techniques for introducing foreign genes to cultured adult cardiomyocytes suffer from substantial limitations, such as relatively low infection efficacy and/or cell surviving rate for the integration of transgenes be delivered [38, 39]. In addition, a number of studies demonstrated that vector associated cytotoxic effects directly affect a number of (electro) physiological properties of the cells [1].

In this study, we demonstrated that pseudorabies virus vectors can effectively penetrate cultured dog cardiomyocytes and that the transferred foreign gene (troponeon) could be detected already at 16 hours following infection and until at least four days postinfection. Furthermore, we showed that infected cardiomyocytes tolerated the presence of PRV

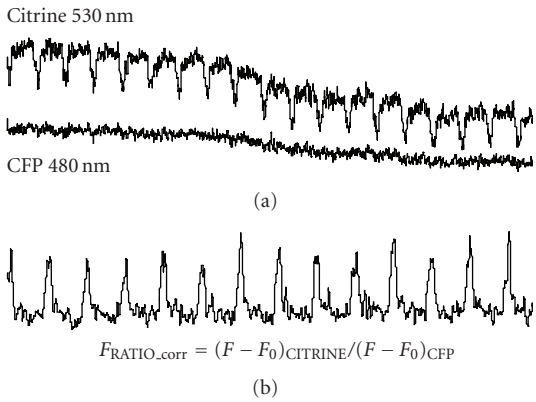

Figure 7: (a) Original recordings from cells expressed troponeon at the excitation wavelength of (a) 485 and 535 nm and (b) the characterized calcium transient by ratio of the fluorescence intensity (FCFP 485 / FCITRINE 535) from one day after infection.

vector since their electrophysiological properties were not fundamentally changed by the virus. The survival of the cells suitable for electrophysiological studies even after 4 days was high enough, proving that the virus entered the cells did not cause any observable substantial cytotoxic effects; moreover the cells displayed unaltered electrophysiological properties. This was analyzed by (1) measuring the properties of a specific transmembrane ionic current, the transient outward current (I_{to}), which is known to be ubiquitously present in all ventricular myocytes; (2) analyzing the intracellular Ca^{2+} transient by FRET. In these measurements we found that I_{to} was present in all cells even after 72 hours of viral infection, and neither the density nor the kinetics was different than that of observed in control cells (Figure 4). On the other hand we found that the kinetics of the intracellular Ca^{2+} transient was not significantly different between infected and noninfected cells (Figures 5 and 6). Specifically, we found that infected adult dog myocytes had a lower rate of physiological degradation than that of the noninfected control cell culture in every parameter. One possible explanation for this unexpected result is that delayed apoptosis was induced by the virus infection probably by inactivating the caspase system [40]. Recent studies have suggested that the latency-associated transcript (LAT) region of herpes simplex virus type 1 (HSV-1) is effective at blocking virus-induced apoptosis in vitro in various cell types [41, 42]. Alternatively, since antiapoptotic effects depend on intracellular Ca^{2+} level [43], it is possible that Ca^{2+} level was decreased by binding a portion of Ca^{2+} to troponeon therefore the lower Ca^{2+} level inhibited cell death. However, the verification of this effect needs further investigation.

5. Conclusions

We have developed a PRV-based vector for delivery of genetically encoded activity sensors to cultured canine cardiomyocytes. This system has several advantageous features: the virus enters to cells without destroying the intact physiological properties of the cells for a prolonged period; the virus does not change the measured physiological properties. We tested the survival rate, physiological changes on ionic current, contractile function, and Ca^{2+} signalling under effect of virus-mediated gene transfer in cultured adult canine cardiomyocytes. Our results show that novel herpesvirus-based vectors can transduce genes efficiently into nondividing cardiac myocytes. Future studies are required to evaluate, whether PRV will be effective for in vivo infection for physiological research or gene therapeutic application.

Acknowledgments

This work was supported by Grants from the Hungarian Scientific Research Fund (OTKA NI-61902, F-67879, K-68911 to A. Varró and by: T049171 to Z. Boldogkői), Human Frontiers Science Program Young Investigator Grant to Z.B.; Hungarian Ministry of Health (T-353/2006, T-483/2006 and T-542/2006), the National Office for Research and Technology—Ányos Jedlik Programme TECH_08_A1_CARDIO08), European Community (EU FP6 Grant LSHM-CT-2005-018833, EUGeneHeart; EU FP6 Grant LSHM-CT-2006-018676, NORMACOR; EU FP7 Grant ICT-2008-224381, preDiCT) and by the Hungarian Academy of Sciences, and GVOP. The authors would like to thank Dr. Oliver Griesbeck (Max Planck Institute of Neurobiology, Martinsried, Germany) for providing TN-L15.

References

[1] L. G. Melo, A. S. Pachori, D. Kong, et al., "Gene and cell-based therapies for heart disease," *The FASEB Journal*, vol. 18, no. 6, pp. 648–663, 2004.

[2] H. Ly, Y. Kawase, R. Yoneyama, and R. J. Hajjar, "Gene therapy in the treatment of heart failure," *Physiology*, vol. 22, no. 2, pp. 81–96, 2007.

[3] R. J. Guzman, P. Lemarchand, R. G. Crystal, S. E. Epstein, and T. Finkel, "Efficient gene transfer into myocardium by direct injection of adenovirus vectors," *Circulation Research*, vol. 73, no. 6, pp. 1202–1207, 1993.

[4] J. K. Donahue, K. Kikkawa, D. C. Johns, E. Marban, and J. H. Lawrence, "Ultrarapid, highly efficient viral gene transfer to the heart," *Proceedings of the National Academy of Sciences of the United States of America*, vol. 94, no. 9, pp. 4664–4668, 1997.

[5] A. H. Schulick, K. D. Newman, R. Virmani, and D. A. Dichek, "In vivo gene transfer into injured carotid arteries: optimization and evaluation of acute toxicity," *Circulation*, vol. 91, no. 9, pp. 2407–2414, 1995.

[6] W. Poller, H. Fechner, M. Noutsias, C. Tschoepe, and H.-P. Schultheiss, "Highly variable expression of virus receptors in the human cardiovascular system: implications for cardiotropic viral infections and gene therapy," *Zeitschrift fur Kardiologie*, vol. 91, no. 12, pp. 978–991, 2002.

[7] J. Nalbantoglu, G. Pari, G. Karpati, and P. C. Holland, "Expression of the primary coxsackie and adenovirus receptor is downregulated during skeletal muscle maturation and limits the efficacy of adenovirus-mediated gene delivery to muscle cells," *Human Gene Therapy*, vol. 10, no. 6, pp. 1009–1019, 1999.

[8] Y. Maeda, U. Ikeda, M. Shimpo, et al., "Efficient gene transfer into cardiac myocytes using adeno associated virus (AAV) vectors," *Journal of Molecular and Cellular Cardiology*, vol. 30, no. 7, pp. 1341–1348, 1998.

[9] L. Du, M. Kido, D. V. Lee, et al., "Differential myocardial gene delivery by recombinant serotype-specific adeno-associated viral vectors," *Molecular Therapy*, vol. 10, no. 3, pp. 604–608, 2004.

[10] T. Sakoda, N. Kasahara, Y. Hamamori, and L. Kedes, "A high-titer lentiviral production system mediates efficient transduction of differentiated cells including beating cardiac myocytes," *Journal of Molecular and Cellular Cardiology*, vol. 31, no. 11, pp. 2037–2047, 1999.

[11] J. Zhao, G. J. Pettigrew, J. Thomas, et al., "Lentiviral vectors for delivery of genes into neonatal and adult ventricular cardiac myocytes in vitro and in vivo," *Basic Research in Cardiology*, vol. 97, no. 5, pp. 348–358, 2002.

[12] Z. Boldogkői, A. Szabó, G. Vrbová, and A. Nógrádi, "Pseudorabies virus-based gene delivery to rat embryonic spinal

cord grafts," *Human Gene Therapy*, vol. 13, no. 6, pp. 719–729, 2002.

[13] Z. Boldogkői, A. Sík, Á. Dénes, et al., "Novel tracing paradigms—genetically engineered herpesviruses as tools for mapping functional circuits within the CNS: present status and future prospects," *Progress in Neurobiology*, vol. 72, no. 6, pp. 417–445, 2004.

[14] Z. Boldogkői, K. Balint, G. B. Awatramani, et al., "Genetically timed, activity-sensor and rainbow transsynaptic viral tools," *Nature Methods*, vol. 6, no. 2, pp. 127–130, 2009.

[15] N. Heim and O. Griesbeck, "Genetically encoded indicators of cellular calcium dynamics based on troponin C and green fluorescent protein," *Journal of Biological Chemistry*, vol. 279, no. 14, pp. 14280–14286, 2004.

[16] A. S. Kaplan and A. E. Vatter, "A comparison of herpes simplex and pseudorabies viruses," *Virology*, vol. 7, no. 4, pp. 394–407, 1959.

[17] Z. Boldogkői, A. Braun, J. Antal, and I. Fodor, "A restriction cleavage and transfection system for introducing foreign DNA sequences into the genome of a herpesvirus," *Research in Virology*, vol. 149, no. 2, pp. 87–97, 1998.

[18] J. Elhai and C. P. Wolk, "A versatile class of positive-selection vectors based on the nonviabilty of palindrome-containing plasmids that allows cloning into long polylinkers," *Gene*, vol. 68, no. 1, pp. 119–138, 1988.

[19] Z. Boldogkői, A. Braun, and I. Fodor, "Replication and virulence of early protein 0 and long latency transcript deficient mutants of the Aujeszky's disease (pseudorabies) virus," *Microbes and Infection*, vol. 2, no. 11, pp. 1321–1328, 2000.

[20] Z. Boldogkői, F. Erdélyi, and I. Fodor, "A putative latency promoter/enhancer (P(LAT2)) region of pseudorabies virus contains a virulence determinant," *Journal of General Virology*, vol. 81, no. 2, pp. 415–420, 2000.

[21] A. Varró, B. Baláti, N. Iost, et al., "The role of the delayed rectifier component IKs in dog ventricular muscle and Purkinje fibre repolarization," *Journal of Physiology*, vol. 523, no. 1, pp. 67–81, 2000.

[22] P. Birinyi, A. Tóth, I. Jóna, et al., "The $Na^+/Ca2^+$ exchange blocker SEA0400 fails to enhance cytosolic $Ca2^+$ transient and contractility in canine ventricular cardiomyocytes," *Cardiovascular Research*, vol. 78, no. 3, pp. 476–484, 2008.

[23] S. Adachi-Akahane, L. Lu, Z. Li, J. S. Frank, K. D. Philipson, and M. Morad, "Calcium signaling in transgenic mice overexpressing cardiac Na^+-$Ca2^+$ exchanger," *Journal of General Physiology*, vol. 109, no. 6, pp. 717–729, 1997.

[24] N. Chossat, F. Griscelli, P. Jourdon, et al., "Adenoviral SERCA1a gene transfer to adult rat ventricular myocytes induces physiological changes in calcium handling," *Cardiovascular Research*, vol. 49, no. 2, pp. 288–297, 2001.

[25] L. Pohlmann, I. Kröger, N. Vignier, et al., "Cardiac myosin-binding protein C is required for complete relaxation in intact myocytes," *Circulation Research*, vol. 101, no. 9, pp. 928–938, 2007.

[26] A. Rinne, C. Littwitz, M.-C. Kienitz, et al., "Gene silencing in adult rat cardiac myocytes in vitro by adenovirus-mediated RNA interference," *Journal of Muscle Research and Cell Motility*, vol. 27, no. 5–7, pp. 413–421, 2006.

[27] H. Xu, W. Guo, and J. M. Nerbonne, "Four kinetically distinct depolarization-activated K+ currents in adult mouse ventricular myocytes," *Journal of General Physiology*, vol. 113, no. 5, pp. 661–677, 1999.

[28] H. M. Himmel, E. Wettwer, Q. Li, and U. Ravens, "Four different components contribute to outward current in rat ventricular myocytes," *American Journal of Physiology*, vol. 277, no. 1, pp. H107–H118, 1999.

[29] X. Liu, J. Yang, F. Shang, et al., "Silencing GIRK4 expression in human atrial myocytes by adenovirus-delivered small hairpin RNA," *Molecular Biology Reports*, pp. 1–8, 2008.

[30] P. Lipp, J. Hüser, L. Pott, and E. Niggli, "Spatially non-uniform $Ca2^+$ signals induced by the reduction of transverse tubules in citrate-loaded guinea-pig ventricular myocytes in culture," *Journal of Physiology*, vol. 497, no. 3, pp. 589–597, 1996.

[31] C. Viero, U. Kraushaar, S. Ruppenthal, L. Kaestner, and P. Lipp, "A primary culture system for sustained expression of a calcium sensor in preserved adult rat ventricular myocytes," *Cell Calcium*, vol. 43, no. 1, pp. 59–71, 2008.

[32] N. Jost, L. Virág, M. Bitay, et al., "Restricting excessive cardiac action potential and QT prolongation: a vital role for IKs in human ventricular muscle," *Circulation*, vol. 112, no. 10, pp. 1392–1399, 2005.

[33] S. Radicke, D. Cotella, E. M. Graf, et al., "Functional modulation of the transient outward current Ito by KCNE β-subunits and regional distribution in human non-failing and failing hearts," *Cardiovascular Research*, vol. 71, no. 4, pp. 695–703, 2006.

[34] G. Grynkiewicz, M. Poenie, and R. Y. Tsien, "A new generation of $Ca2^+$ indicators with greatly improved fluorescence properties," *Journal of Biological Chemistry*, vol. 260, no. 6, pp. 3440–3450, 1985.

[35] H. J. Knot, I. Laher, E. A. Sobie, et al., "Twenty years of calcium imaging: cell physiology to dye for," *Molecular Interventions*, vol. 5, no. 2, pp. 112–127, 2005.

[36] A. E. Palmer and R. Y. Tsien, "Measuring calcium signaling using genetically targetable fluorescent indicators," *Nature Protocols*, vol. 1, no. 3, pp. 1057–1065, 2006.

[37] J. E. McCombs and A. E. Palmer, "Measuring calcium dynamics in living cells with genetically encodable calcium indicators," *Methods*, vol. 46, no. 3, pp. 152–159, 2008.

[38] C. Communal, F. Huq, D. Lebeche, C. Mestel, J. K. Gwathmey, and R. J. Hajjar, "Decreased efficiency of adenovirus-mediated gene transfer in aging cardiomyocytes," *Circulation*, vol. 107, no. 8, pp. 1170–1175, 2003.

[39] Z. Li, R. V. Sharma, D. Duan, and R. L. Davisson, "Adenovirus-mediated gene transfer to adult mouse cardiomyocytes is selectively influenced by culture medium," *Journal of Gene Medicine*, vol. 5, no. 9, pp. 765–772, 2003.

[40] C. Communal, M. Sumandea, P. de Tombe, J. Narula, R. J. Solaro, and R. J. Hajjar, "Functional consequences of caspase activation in cardiac myocytes," *Proceedings of the National Academy of Sciences of the United States of America*, vol. 99, no. 9, pp. 6252–6256, 2002.

[41] M. Ahmed, M. Lock, C. G. Miller, and N. W. Fraser, "Regions of the herpes simplex virus type 1 latency-associated transcript that protect cells from apoptosis in vitro and protect neuronal cells in vivo," *Journal of Virology*, vol. 76, no. 2, pp. 717–729, 2002.

[42] M. Inman, G.-C. Perng, G. Henderson, et al., "Region of herpes simplex virus type 1 latency-associated transcript sufficient for wild-type spontaneous reactivation promotes cell survival in tissue culture," *Journal of Virology*, vol. 75, no. 8, pp. 3636–3646, 2001.

[43] X. Chen, X. Zhang, H. Kubo, et al., "$Ca2^+$ influx-induced sarcoplasmic reticulum $Ca2^+$ overload causes mitochondrial-dependent apoptosis in ventricular myocytes," *Circulation Research*, vol. 97, no. 10, pp. 1009–1017, 2005.

III.

Szívdobbanások és ioncsatornák

Ördög Balázs és Szabad János

Szegedi Tudomány Egyetem, Általános Orvostudományi Kar, Orvosi Biológia Intézet
6720 Szeged, Somogyi B. u. 4.

Tel: (62) 545-109
Fax: (62) 545-131
E-vél: ordog@sb4.szote.u-szeged.hu

Szívünk dobbanása létünk nélkülözhetetlen feltétele. A szív legnagyobb részét az a szívizomszövet alkotja, amely terheltségünktől, lelkiállapotunktól függően percenként átlagosan 65-ször, egy ember életében csaknem egy milliárdszor húzódik össze. Vajon mi teszi képessé szívünket arra, hogy életünk során fáradhatatlanul végezze munkáját? Miért nem rándul sohasem görcsbe a szívizom? Hogyan képes kielégíteni pillanatnyi szükségleteinket akkor is, amikor alszunk, és akkor is, ha a százméteres síkfutás döntőjében küzdünk a győzelemért? Szívünket azok az ioncsatornák teszik különlegessé, amelyek a szívizomsejtek sejthártyájában vannak. A dolgozat a szívizom ioncsatornáinak varázslatos világába ad bepillantást. Ha megismerjük az ioncsatornák funkcióját, talán megérthetjük a sérült funkció olyan következményeit, mint a szívritmuszavar vagy a hirtelen szívhalál.

Ionáramok, nyugalmi és akciós potenciál

Olvasóink tudják, hogy minden sejtet sejthártya burkol. A sejthártyának két alapvető szerkezeti eleme van. Az egyik az a kettős foszfolipid réteg, amely bár alig 4 nanométer „vastag", kiváló szigetelő, elválasztja a sejt belsejét a külvilágtól. A másikat a fehérje molekulák olyan típusai alkotják, amelyek jellegzetes kapcsolatot teremtenek a sejt belseje és környezete között. A fehérjék is többfélék. Közéjük tartoznak az ioncsatornák, amelyeken - amikor nyitva vannak - ionok áramlanak át, és az ionpumpák is, amelyek az ATP-ben tárolt energia felhasználásával ionokat pumpálnak át a sejthártya túlsó oldalára (1. ábra).

Az is ismert, hogy a sejthártya két oldala között potenciálkülönbség van (az ún. nyugalmi, vagy membránpotenciál), amely oka lényegében az, hogy a sejthártya két oldalán eltérő az ionok koncentrációja (1. ábra). A koncentrációkülönbséget a fent említett pumpák teremtik meg. A potenciálkülönbséget az okozza, hogy a sejthártyában olyan K^+ ioncsatornák is vannak, az ún. állandó K^+ ioncsatornák, amelyek mindig nyitva vannak, és rajtuk a koncentrációkülönbségnek megfelelően K^+ ionok szivárognak ki a sejtből. A távozó K^+ ionok negatív töltéseket hagynak maguk mögött (amelyek a fehérjék töltései), ami miatt a sejthártya belső felszíne a külsőhöz képest egyre negatívabbá válik. Egy idő után azonban annyira negatív lesz a sejt belseje a külsejéhez képest, hogy az vonzza a pozitív töltésű K^+ ionokat, és végeredményben –80mV érték körül egy dinamikus egyensúly alakul ki. Az egyensúlyi helyzetre jellemző membránpotenciált nevezik nyugalmi potenciálnak.

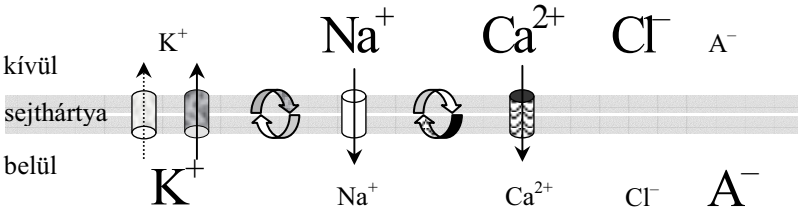

1. ábra. A különféle kationok és anionok eloszlása a sejthártya két oldalán nyugalmi állapotban. Az ábra feltünteti azokat a fontosabb ioncsatorna és ionpumpa típusokat, amelyeknek fontos szerepe van a membránpotenciál kialakulásában és fenntartásában. Az A^- jel a fehérjék negatív töltését szimbolizálja. Az ionkoncentráció különbségeket az eltérő betűméret érzékelteti. Az állandó K^+ csatornákat szaggatott, a feszültségszabályozott ioncsatorna féleségeket folytonos nyíl jelöli. A nyilak iránya azt mutatja, hogy milyen irányban áramlanak át az ionok az ioncsatornákon, ha azok nyitottak. A ⟲ jelek egy-egy Na^+/K^+, illetve Na^+/Ca^{2+} pumpát szimbolizálnak.

Nyugalmi helyzetben a sejt belseje tehát negatív töltésű a külsejéhez képest. Ha „utasítás” érkezik a sejthez, a membránpotenciál a sejthártya egy adott pontján előbb hirtelen lecsökken, és polaritása a legtöbb esetben át is fordul: a sejthártya belső felszíne lesz pozitív a külsejéhez képest. Aztán rövidesen helyreáll az eredeti állapot (2. ábra). (A membránpotenciál csökken, hisz’ nulla membránpotenciál értéknél nincs potenciálkülönbség a sejthártya két oldala között. Bármely, a nullától eltérő pozitív vagy negatív érték esetén mérhető potenciálkülönbség.) A membránpotenciál-változás alapja az, hogy az „utasítás” hatására előbb nyílnak, majd csukódnak a Na^+ illetve a K^+ ioncsatornák. Mialatt az ioncsatornák nyitva vannak, rajtuk Na^+ illetve K^+ ionok áramlanak át, és minthogy változik az ionok koncentrációja, változik a membránpotenciál is. Az ionok specifikus ioncsatornákon áramlanak át. Úgy, hogy a csatornák érzékelik a membránpotenciál-változásokat, és annak értékétől függően nyitódnak, majd rövidesen automatikusan csukódnak. Tulajdonságuk alapján feszültségszabályozott ioncsatornáknak is nevezik őket. Fontos tudni, hogy az ioncsatornákon az ionok csak az egyik irányba áramlanak át: a nagyobb koncentrációtól a kisebb felé, diffúzióval. A K^+ csatornákon K^+ ionok áramlanak ki a sejtből, a Na^+ csatornákon pedig Na^+ ionok áramlanak be a sejtbe.

Amíg az eredeti állapot az izom, valamint az idegsejtek esetében néhány ezredmásodperc alatt áll helyre, a szívizomsejtek esetében 2-3 tizedmásodpercet vesz igénybe (2. ábra). Sőt, a szívizomsejtek nemcsak a membránpotenciál-változás időtartamában, hanem a lefutásában is különböznek az izom, illetve az idegsejtektől (2. ábra). Mi a különbség alapja? A membránpotenciál-változásokat a szívizomsejtekből ki- és az oda beáramló, elsősorban Na^+, K^+ és Ca^{2+} ionok árama okozza a szívizomsejtek funkciója, egy-egy szívdobbanás során. Mi minden történik a szívizomsejtek membránjában egyetlen összehúzódás alatt?

A nyugalomban lévő szívizomsejtek sejthártyájában a feszültség-szabályozott K^+ és Na^+ csatornák zárva vannak. A szomszédos szívizomsejtek, vagy a szív speciális ingerületvezető rendszere felől érkező „utasítás” hatására a Na^+ csatornák kinyílnak, és Na^+ ionok áramlanak be a sejtbe (I_{Na}; 2. ábra), ami következtében a membránpotenciál értéke hirtelen lecsökken, depolarizáció történik. A legtöbb szívizomsejtben vannak ún. átmeneti K^+ csatornák, melyek szintén feszültségszabályozottak. A depolarizáció hatására az átmeneti K^+ csatornák kinyílnak, és rajtuk keresztül K^+ ionok szöknek ki a sejtből (I_{to}, 2. ábra), és mivel a sejthártya belső oldalán csökken a pozitív töltések száma, a membránpotenciál értéke növekszik, gyors repolarizáció következik be. A gyors átmeneti repolarizációt az ún. plató fázis követi. A plató fázisban a membránpotenciál értéke hosszú ideig csak lassan növekszik. A tipikusan a

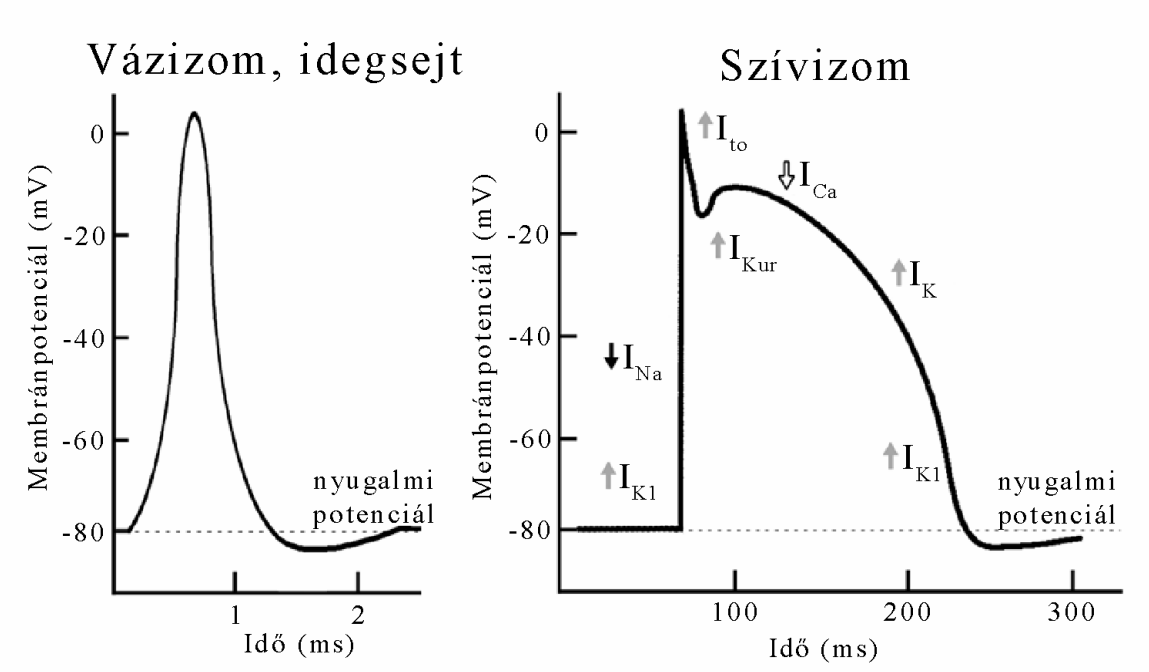

2. ábra. A membránpotenciál-változás időbeli alakulása a sejthártya egy pontján vázizom és idegsejt, valamint egy szívizomsejt esetében. Amíg a vázizom és az idegsejtek esetében a nyugalmi potenciál néhány ezredmásodperc, a szívizomsejtek esetében százszor annyi idő alatt áll helyre. A szívizomra jellemző membránpotenciál-változás bonyolult lefutása a különféle típusú ioncsatornák tevékenységének eredőjeként alakul ki. Amíg a K^+ ioncsatornák különféle típusain a sejtből kifelé (↑) folynak az ionáramok (I_{K1}, I_{to}, I_{Kur} és I_K), a Na^+ és a Ca^{2+} ioncsatornákon a sejtekbe (↓) áramlanak az ionok (I_{Na} és I_{Ca}).

szívizomsejtekre jellemző plató fázis azonban csak látszólag eseménytelen. Közben nagymennyiségű Ca^{2+} áramlik be a sejtbe a feszültségszabályozott Ca^{2+} csatornákon keresztül (I_{Ca}, 2. ábra), és K^+ ionok áramlanak ki a sejtből az ún. késleltetett K^+ csatornákon át (I_K, 2. ábra). A befelé és a kifelé irányuló ionáramok között fennálló egyensúly miatt a membránpotenciál értéke a plató fázis folyamán csak kis mértékben változik. A plató fázis akkor ér véget, amikor bár a Ca^{2+} csatornák bezáródnak, ám a késleltetett és az állandó K^+ csatornákon keresztül további K^+ ionok távoznak a sejtből (I_K és I_{K1}; 2. ábra). A folyamat nyomán a membránpotenciál értéke folyamatosan növekszik, a sejt repolarizálódik. Sőt, a repolarizációt követően a membránpotenciál egy rövid időre meg is haladja a nyugalmi potenciál értékét, amely állapotot hiperpolarizációnak nevezzük. A nyugalmi állapotra jellemző ioneloszlást végül a Na^+/Ca^{2+} illetve a Na^+/K^+ pumpák állítják helyre.

A fent bemutatott folyamat a sejthártya egy adott pontján történő eseményeket írta le. A membránpotenciál változás azonban nem marad meg a sejthártya egyetlen pontjában. A membránpotenciál-csökkés nyomán nyílnak a szomszédos feszültségszabályozott ioncsatornák, és végeredményben a membránpotenciál-csökkenés tovaterjed a sejthártya mentén. A sejthártya mentén tovaterjedő membránpotenciál-csökkenést nevezik akciós potenciálnak. A tovaterjedő akciós potenciál az az „utasítás” (ingerület), amely nyomán funkcionálnak az ioncsatornák, összehúzódnak a szívizomsejtjeink, dobog a szívünk.

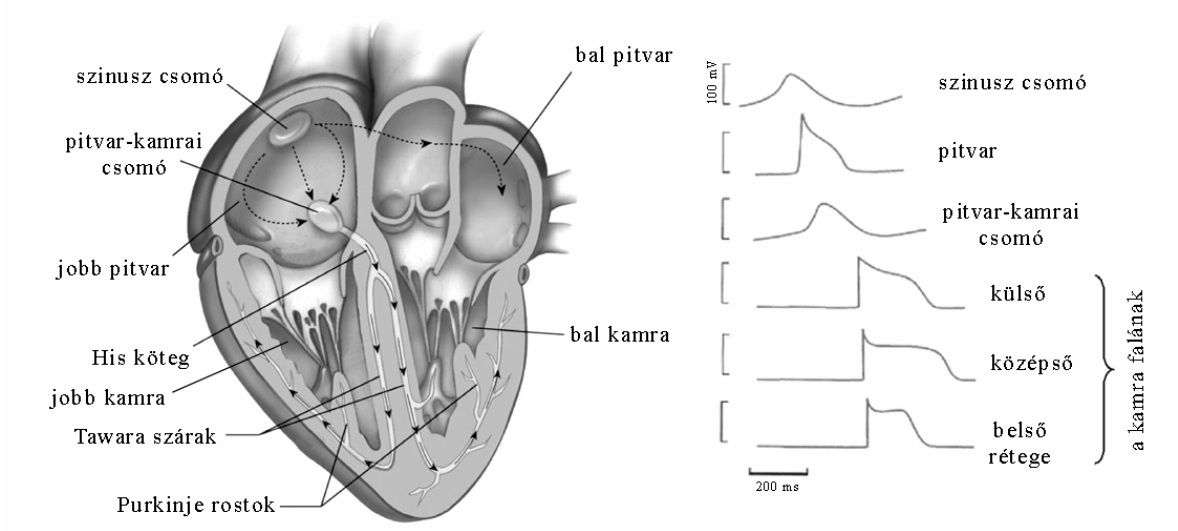

3. ábra. A szív ingerületképző és -vezető rendszere. A nyilak az ingerület terjedési irányát jelzik. Az ábra jobb oldala azt mutatja, hogy milyen az akciós potenciál lefutása a szív különböző régióiban.

A szívdobbanás

Egy vázizom rostjai a mozgatóidegek felől érkező „utasítás" hatására húzódnak össze. A szívizomnak viszont saját ingerképző és ingerületvezető rendszere van. A központ a szinusz csomó, ahol a szív az összehúzódásokhoz szükséges „utasítást" állítja elő (3. ábra). A szinusz csomóban olyan speciális szívizomsejtek vannak, amelyek időről-időre akciós potenciált hoznak létre (angolul pacemaker aktivitásnak nevezik), biztosítva a szívizom ritmusos összehúzódását, a szív dobogását. A szinusz csomótól az akciós potenciál a pitvarokra terjed át, ahol a pitvar izomsejtjeinek összehúzódását okozza. A pitvarizomzat után az akciós potenciál a szív második ingerületképző területére, a pitvar-kamrai csomóra terjed, azt hozza ingerületi állapotba (3. ábra). Itt az ingerület néhány ezredmásodpercet késik. A gondolatnyi késés teszi lehetővé, hogy az összehúzódó pitvarok a még ellazult állapotban lévő kamrákba pumpálhatják a vért. Az ingerület a pitvar-kamrai csomótól a His-kötegeken halad tovább, majd a Tawara-szárakon és a Purkinje rostokon keresztül jut el a kamrák izomzatáig, ahol a kamrafal izomsejtjeinek összehúzódását okozza.

A dobogó szívben akciós potenciálok, elektromos impulzusok képződnek, és terjednek. Az elektromos jelek a szívből kiindulva a test különböző részei felé terjednek, és a testfelszínen elhelyezett elektródákkal meg is mérhetők. Ha a testfelszínen mérhető feszültség változásait az idő függvényében ábrázoljuk jellegzetes lefutású hullám-mintázatot kapunk, az ún. elektrokardiogramot (EKG; 4. ábra).

Az EKG egyes szakaszai a szív különböző területeinek elektromos aktivitásáról nyújtanak információt. A P hullám a pitvarokon végig futó ingerület eredménye. A nagy amplitúdójú Q, R és S csúcsok által jellemzett motívum pedig a nagy számú kamrai szívizomsejt közel egyidőben történő depolarizációjának a következménye. A T hullám a kamrai izomsejtekben lejátszódó repolarizáció nyomán alakul ki. Az EKG alapján a szívizom állapotáról, a szív ingerületvezető rendszerének állapotáról lehet felvilágosítást nyerni. A QT távolság megnyúlása (az ún. hosszú QT szindróma) a repolarizációban részt vevő K^+ csatornák csökkent működését jelzi.

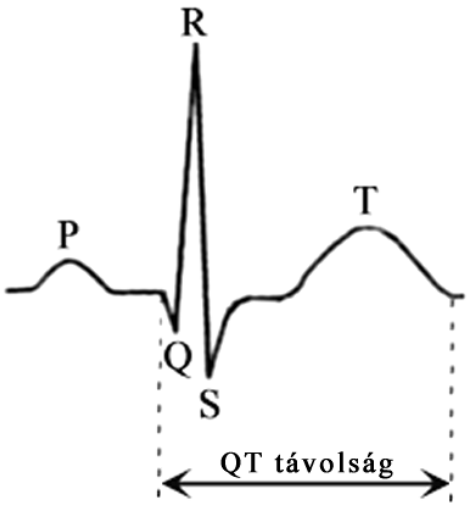

4. ábra. Elektrokardiogram: a szív elektromos aktivitásának időbeli lefutása, amint azt a jobb csuklón és a bal bokán elhelyezett elektródokkal rögzíthetjük. A P hullám a pitvar, a Q, az R és az S csúcsok, valamint a T hullám a kamra izomzatának aktivitását jellemzik. A QT távolság a szívizom ioncsatornáinak állapotát jellemző mérőszám.

A hosszú QT szindróma lehet genetikai vagy szerzett eredetű. A genetikai rendellenességet leggyakrabban olyan mutációk okozzák, amelyek a K^+ csatornákat kódoló gének valamelyikében következtek be. A csökkent aktivitású mutáns csatornákon a repolarizáció alatt a normálisnál kevesebb K^+ ion áramlik ki a sejtekből, ami miatt a repolarizáció a rendesnél csak hosszabb idő alatt történik meg. Szerzett hosszú QT szindrómát anyagcsere zavarok (mint pl. hipokalémia, hipokalcémia, anorexia nervosa), vagy hosszantartó gyógyszeres kezelés okozhat (elsősorban pszcihotróp, antiaritmiás szerek). A hosszú QT szindróma azért veszélyes, mert bár többnyire nem okoz betegséget, tüneteket, megnöveli a szívritmuszavarok kialakulásának kockázatát, az ún. hirtelen szívhalál bekövetkeztének esélyét. Hirtelen szívhalált okozhat hosszú QT szindrómás emberekben némely gyógyszer is (mint pl. az antibiotikumok egyike-másika, az antidepresszáns szerek, stb.). Azok a hatóanyagok veszélyesek, amelyek gátolják a repolarizációban részt vevő K^+ csatornák működését. A repolarizáló ioncsatornák genetikai alapú, és/vagy gyógyszeres blokkolása nagy valószínűséggel vezet a szívritmus összeomlásához, halálos kimenetelű ritmuszavarhoz.

Különbségek a szív különféle részei között

Mivel a szív különböző régióinak más és más a feladata, érthető, hogy az akciós potenciál lefutása eltérő a szív különböző területein (3. ábra). Mint azt már említettük, a szinusz és a pitvar-kamrai csomó sejtjei szabályos időközönként akciós potenciált generálnak. Különleges képességüket szokatlan ioncsatorna összetételüknek köszönhetik. Bennük speciális „pacemaker”, vagyis ritmusképző feszültségszabályozott ioncsatornák vannak. A ritmusképző csatornák különleges tulajdonsága az, hogy nem a depolariáció alatt, hanem a nyugalmi potenciálnál nagyobb értéknél nyílnak. (Amiért hiperpolarizációra aktiválódó csatornáknak is hívjuk őket.) K^+ szelektivitásuk gyenge, ami miatt nyitott állapotban a K^+ ionok mellett Na^+ ionok is átjutnak rajtuk (4 K^+ mellett 1 Na^+ ion). A szinusz csomó ritmusképző sejtjeinek további jellegzetessége, hogy nincsenek bennük állandó K^+ csatornák, melyek kialakíthatnák

és fenntarhatnák a nyugalmi potenciált. Hiányukban a ritmusképző sejtekben a nyugalmi potenciál alacsonyabb, mint egy „átlagos” szívizomsejt esetében. Az előzőek miatt a szinusz csomó ritmusképző sejtjeiben az akciós potenciál szokatlanul zajlik le. Az akciós potenciál utolsó szakaszában K^+ ionok hagyják el a sejtet, főként a késleltetett K^+ csatornákon keresztül. A távozó pozitív töltések miatt a membránpotenciál értéke folyamatosan növekszik, eléri a nyugalmi potenciál értékét, sőt meg is haladja azt, hiperpolarizáció következik be. A hiperpolarizáció hatására kinyílnak a ritmusképző csatornák és rajtuk keresztül a K^+ és Na^+ ionok - szokatlan módon - a sejtek közötti térből a sejt belseje felé áramlanak. (A hiperpolarizált sejthártya belső felszíne a nyugalmi helyzethez képest sokkal több negatív töltést hordoz, ami miatt a kationok a sejt belseje felé igyekeznek.) A ritmusképző csatornákon befelé csordogáló K^+ és Na^+ kationok miatt a sejthártya fokozatosan depolarizálódik, amely depolarizáció végeredményben egy újabb akciós potenciál kiváltásához vezet. A pacemaker sejtekben a folyamat ismétlődik, belőlük időről időre akciós potenciálok indulnak ki, biztosítva a szív ritmikus funkcióját.

A pitvari szívizomsejtekben mérhető akciós potenciál jellegzetesen rövid lefutású (3. ábra). Itt ugyanis a repolarizáló K^+ áramok erőteljesek, és rövid idő alatt képesek helyreállítani a membránpotenciál értékét a nyugalmi szintre a depolarizációt követően. A hatékony repolarizációt a pitvar specifikus ultra gyors K^+ csatornák biztosítják (I_{Kur}; 2. és 3. ábra). Az ultra gyors K^+ csatornák a késleltetett csatornák olyan változatai, melyek gyorsan reagálnak a membránpotenciál értékének csökkenésére. Társaiknál jóval korábban, közvetlenül a depolarizációt követően nyílnak. Rajtuk K^+ ionok áramlanak ki a sejtből, a sejthártyát tehát repolarizálják.

A kamrák falának különböző rétegeiben mért akciós potenciálok bár az általános sémától kevésbé markánsan térnek el, vannak köztük lényeges különbségek (3. ábra). Az akciós potenciál a kamra falának legkülső rétegében játszódik le a legrövidebb idő alatt, a belső rétegben valamivel hosszabb, és a középső rétegben tart a leghosszabb ideig. A külső és a középső rétegre erőteljes plató fázis jellemző (az ún. tüske és kupola konfiguráció), miközben a belső rétegben az akciós potenciál második fázisában a membránpotenciál folyamatosan nő. A jelenség pontos okai nem ismertek, azonban tudjuk, hogy az átmeneti K^+ áram (I_{to}, 2. ábra) a külső rétegben a legerőteljesebb, a kamra falának belső rétegei felé haladva egyre alacsonyabb intenzitású. A plató fázis meredeksége pedig két tényező kölcsönhatásától függ. Nevezetesen a beáramló Ca^{2+} és a kiáramló K^+ ionok mennyiségétől. Ha a sejtbe belépő és a sejtet elhagyó töltések mennyisége megegyezik, a membránpotenciál értéke változatlan marad.

Általánosságban elmondhatjuk, hogy a különböző feladatokat ellátó szívizomsejtekben eltérő az akciós potenciál lefutása. Az akciós potenciál alakja elsősorban attól függ, hogy az adott sejtben milyen ioncsatorna-féleségek és milyen arányban vannak jelen. Egy biztos: a szív olyan tökéletesen „megszerkesztett” része szervezetünknek, amelyben minden a helyén van. A szív funkciója végső soron a különféle ioncsatornák összehangolt funkciójának az eredménye. Minthogy az ioncsatornák fehérjék, érthető, hogy szerepüket végső soron az őket kódoló gének, illetve a gének expressziós mintázata határozza meg: mely sejtben mely gén terméke van jelen, milyen mennyiségben, és milyen aktívan.

Az akciós potenciál és a kontrakció kapcsolata

Az izom-összehúzódás közvetlen oka nem más, mint a Ca^{2+} ionok kiszabadulása izom belső Ca^{2+} raktárából (a szarkoplazmatikus retikulumból; SR) a szívizomsejt citoplazmájába (5. ábra). A Ca^{2+} felszabadulást az akciós potenciál első és második fázisában, a feszültségszabályozott Ca^{2+} csatornákon keresztül a citoplazmába áramló Ca^{2+} ionok okozzák. A jelenséget Ca^{2+} indukálta Ca^{2+} felszabadulásnak is nevezik. A szívizom sejteket, amint a

harántcsíkoltakat is, át meg átszövik a sejthártya betüremkedései, az ún. t-csövecskék (5. ábra). Bizonyos helyeken a t-csövecskék és a SR membránja egészen közel fekszenek egymáshoz. Olyannyira, hogy a t-csövecskékben levő feszültségszabályozott Ca^{2+}-csatornák és a SR membránjában levő Ca^{2+}-csatornák (az ún. rianodin receptorok) egymás közvetlen közelébe kerülnek (5. ábra). A rianodin receptor lényegében egy olyan Ca^{2+}-ot érzékelő Ca^{2+} csatorna, amely Ca^{2+} hatására nyitott konformációt vesz fel, és lehetővé teszi, hogy a SR-ból Ca^{2+} ionok áramoljanak a citoplazmába. Amikor tehát kinyílnak a t-csövecskékben levő feszültségszabályozott Ca^{2+}-csatornák, a beáramló Ca^{2+} ionok a rianodin receptor citoplazmatikus felszínéhez jutnak. Kinyílnak a rianodin receptor csatornák, a SR-ból Ca^{2+} ionok áramlanak a citoplazmába, ahol kiváltják az izomfilamentumok összehúzódását.

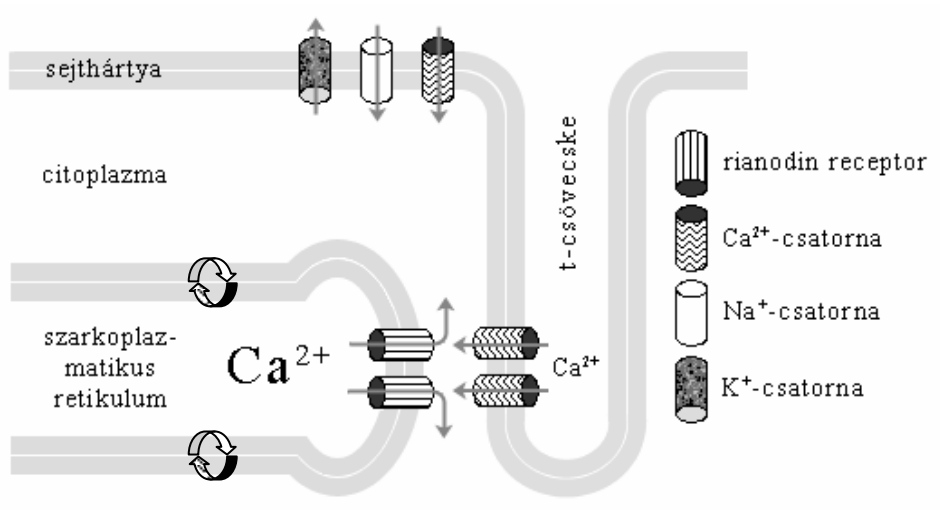

5. ábra. A különféle típusú ioncsatornák eloszlása a sejthártya, a t-csövecskék, valamint a szarkoplazmatikus retikulum (SR) membránjában. A citoplazmába kiáramló Ca^{2+} ionokat a Ca^{2+} ion pumpák (**( )**) szállítják vissza a szarkoplazmatikus retikulumba**.**

A vázizmok esetében az akciós potenciál időtartama sokkal rövidebb, mint az izom összehúzódása és elernyedése (6. ábra). Meg-megtörténik, hogy az izomhoz annak teljes elernyedése előtt újabb akciós potenciál érkezik, ami az izom ismételt összehúzódását váltja ki. Ha az akciós potenciálok elég sűrűn érkeznek, az izom összehúzódva marad. Könnyen belátható, hogy a vérkeringés megszűnéséhez, halálhoz vezetne, ha szívizomzat folyamatosan összehúzódva maradna. Szerencsére a természet gondoskodott arról, hogy a szívizomzat folyamatos összehúzódása ne történhessen meg: a szívizomzat esetében az akciós potenciál és az izom összehúzódása majdnem ugyanannyi ideig tart (7. ábra). Újabb akciós potenciál csak akkor indulhat, amikor az izom már elernyedt állapotban van, ami biztosítéka a szívizom ritmusos működésének, a vérkeringés fenntartásának, életünknek.

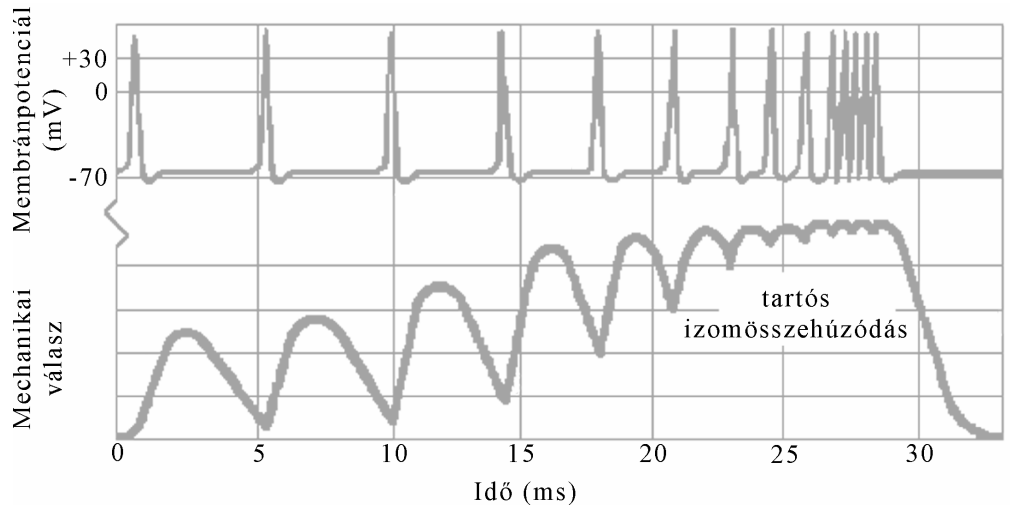

6. ábra. Akciós potenciál és az izomösszehúzódás kapcsolata vázizmokban.

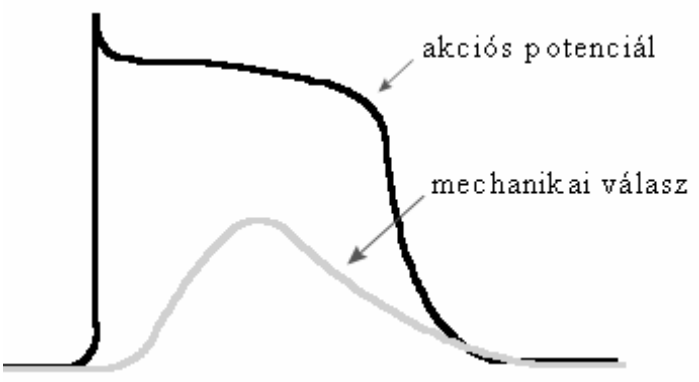

7. ábra. Akciós potenciál és kontrakció szívizomban.

Hogyan alkalmazkodik a szív testünk pillanatnyi szükségleteihez?

Szívünk legfontosabb feladata az, hogy a vér keringetésével a testünket alkotó sejtek oxigén és tápanyagellátását biztosítsa. A test szöveteinek oxigén igényéhez elsősorban a szívritmus idegi szabályozása révén alkalmazkodik szívünk. A szabályozás a két ingerületképző központ, a szinusz csomó és a pitvar-kamrai csomó működésének vegetatív idegrendszeri módosításán keresztül történik. A szimpatikus hatást közvetítő idegvégződésekben noradrenalin szabadul fel, amely úgy befolyásolja a ritmusképző csatornák működését, hogy azok 10 mV-al alacsonyabb (kevésbé negatív) membránpotenciál értéknél, vagyis a szokottnál hamarabb nyitnak ki a repolarizációt követően. És minthogy hamarabb nyílnak ki, a ritmusképző sejtekben hamarabb történik meg a depolarizáció (2. ábra), a szívritmus tehát gyorsul, a szaporábban dobogó szív elegendő oxigénnel teli friss vért pumpálhat a test különböző részeibe. A paraszimpatikus hatást a bolygóideg ideg közvetíti. Idegvégződésein acetilkolin

szabadul fel. Az acetilkolin egy többlépéses jelátviteli folyamat révén a ritmusképző sejtek eddig nem említett, olyan speciális K^+ csatornáit aktiválja, amelyek nyitódása és csukódása egy anyag kötődésétől függ. Az ilyen típusú csatornákat ligandfüggő ioncsatornáknak nevezik. Az itt említett csatornák hiperpolarizáló hatásúak, vagyis növelik a membránpotenciált. A magasabb membránpotenciál érték miatt a „pacemaker" csatornák a szokottnál valamivel később nyílnak ki, ami miatt lassul a szívritmus.

Bár a szív igyekszik alkalmazkodni testünk fizikai igénybevételéhez, szükség van egy olyan kontroll mechanizmusra, amely megakadályozza, hogy a fokozott igénybevétel visszafordíthatatlan károsodásokat okozzon a szívizomsejtekben, a szívben. A feladatot a ligand függő K^+ csatornák egy további speciális változata látja el, amelyet, minthogy „biztosíték" funkciót lát el „biztosíték" csatornának nevezhetnénk. A „biztosíték" csatornák mindaddig zárva vannak, amíg a szívizomsejtek citoplazmájában az ATP koncentrációja legalább 1 mM. Fokozott terhelés, vagy elégtelen ATP képződés nyomán előfordulhat, hogy a szívizomsejtek ATP tartalékai kimerülnek. Ha az ATP koncentráció 1 mM alá süllyed, a „biztosíték" csatornák kinyílnak és hiperpolarizálják a sejthártyát. A hiperpolarizáló hatás miatt lerövidül az akciós potenciál időtartama, és csökken a Ca^{2+} beáramlás. Összességében tehát csökken a szívizomsejtek terhelése, csökken az ATP felhasználás, javul a szívizomsejtek túlélési esélye. Sőt, az is ismert, hogy egy rövid ideig tartó oxigén hiányos állapot után a szívizom védetté válik egy újabb oxigén hiányos terheléssel szemben: csökken a ritmuszavarok kialakulásának kockázata, az infarktusban elhalt területek aránya. A szív tehát képes valamelyest alkalmazkodni a sorozatos stresszhatások okozta igénybevételhez. Valószínű, hogy az adaptációs folyamat egyik fontos komponensét a „biztosíték" csatornák adják.

Az ioncsatornák szerkezete és funkciója

Bár az ionok mozgását az idegsejtek sejthártyáján keresztül már 1952-ben leírták, az ioncsatornák létezésére csak az 1970-es évek óta vannak bizonyítékok. Az ioncsatornák molekuláris szintű tanulmányozása 1984-ben kezdődött, amikor molekulárisan klónozták az elektromos angolna Na^+ csatorna génjét. Az első K^+ csatorna gént 1987-ben ismerték meg muslicában. Legnépesebb a K^+ ioncsatorna géncsalád a jelenleg ismert csaknem 80 génnel. Az ioncsatornák szerkezetéről sok mindent kideríthetünk, ha ismerjük a kódoló gének bázissorrendjét. A bázissorrend, a genetikai kód ismeretében meghatározható, hogy milyen aminosavak és milyen sorrendben alkotják a kódolt fehérjét, az aminosavak sorrendje alapján pedig meghatározható a kódolt fehérje legvalószínűbb térbeli szerkezete.

A legtöbb K^+ csatorna négy alegységből áll (8. ábra). Az egyes alegységek azonos szerkezetűek, még ha különböző gének kódolják is őket. A legegyszerűbb K^+ csatorna egy alegységében két α-hélix van, és köztük egy olyan ún. pórus motívum, amely megszabja, hogy a csatornán milyen ion haladhat át. A „négy alegység" szabálya alól vannak kivételek. Az állandó K^+ csatornák bizonyos típusai két alegységből szerelődnek össze, alegységenként négy hélixszel, és két pórus motívummal. A kódoló DNS szekvenciák összehasonlítása alapján derült arra fény, hogy a négy hélix az ősi, két hélixet kódoló gén egy részének duplikációja révén keletkezet. A bonyolultabb, feszültségszabályozott K^+ csatornák négy alegységből szerelődnek össze. Egy alegység hat α-hélixet és egy pórus motívumot tartalmaz (8. ábra). A Ca^{2+} és a Na^+ csatornákban a négy alegység egyetlen fehérje része, ugyanannak a génnek a terméke. A feszültségszabályozott ioncsatorna alegységek alapvető fontosságú részei az α-hélixek, a sejthártyába ágyazottak, és minthogy átérik a sejthártyát, transzmembrán motívumnak is nevezik őket.

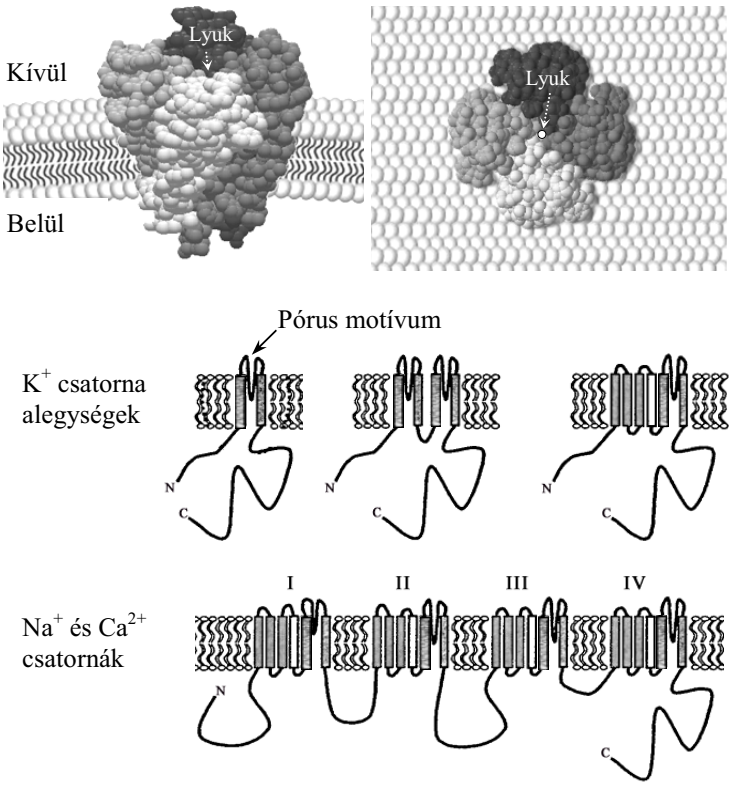

8. ábra. Az ioncsatornák szerkezete. Felül, egy K^+ ioncsatorna háromdimenziós modellje oldal- és felülnézetben. Egy csatorna négy alegységből szerelődik össze. Középen és lent, a különféle ioncsatorna féleségek alegységeinek síkban kiterített szerkezete. Amíg a különféle típusú K^+ csatornák két, vagy négy alegységből szerelődnek össze, addig a Na^+ és Ca^{2+} csatornákat egyetlen hosszú polipeptid lánc alkotja. A fehéren jelölt transzmembrán α-hélixek a feszültségszabályozott ioncsatornák feszültség érzékelői, azok az ún. kapuzó hélixek, amelyek szabályozzák a csatornák nyitódását.

A 9. ábra egy K^+ csatorna szerkezetét mutatja vázlatosan. A csatorna funkciója szempontjából legfontosabb a szűk nyaki rész, amely mindössze 1,2 nm hosszú, átmérője pedig 0,28 nm. (Egy nm = 10^{-9} m.) A csatorna átmérője szabja meg, hogy milyen ionok haladhatnak át rajta. A nyaki rész falát a pórus motívum aminosavai burkolják. Minthogy a K^+ ionok hidrát-burkát alkotó víz molekulák 0,28 nm-re vannak a K^+ ion középpontjától nyilvánvaló, hogy a járat túl szűk egy K^+ ion áthaladásához. Ne feledjük azt sem, hogy a hidrát-burok víz molekuláit csak komoly energia-befektetés árán lehet eltávolítani, és a K^+ csatornák működésük során nem fogyasztanak energiát. Mégis miként lehetséges, hogy a nyitott K^+ csatornán másodpercenként nagyjából egy millió K^+ ion halad át? És hogyan képes az ioncsatorna különbséget tenni a K^+ és Na^+ ionok között? A magyarázat az, hogy a szűk járat belső felszínén karbonil (C=O) oxigén atomok vannak. Az oxigén atomok részleges negatív töltést hordoznak, és úgy helyezkednek el, hogy a járaton áthaladó K^+ ionok hidrát-burkának víz molekulái az oxigén atomokkal lépnek kölcsönhatásba. A kölcsönhatás energetikailag kedvező környezetet teremt az ionok áthaladásához. A K^+-nál kisebb átmérőjű Na^+ ionok számára a karbonil oxigén atomok túlságosan távol helyezkednek el, amiért nem tudnak az ionnal kölcsönhatásba lépni, ami miatt a Na^+ ionok nem tudnak átjutni a K^+ csatornákon. Lényegében tehát az ioncsatorna aminosav összetétele, és az abból következő fizikai szerkezete szabályozza az ionok mozgását a csatornán, a sejtmembránon keresztül.

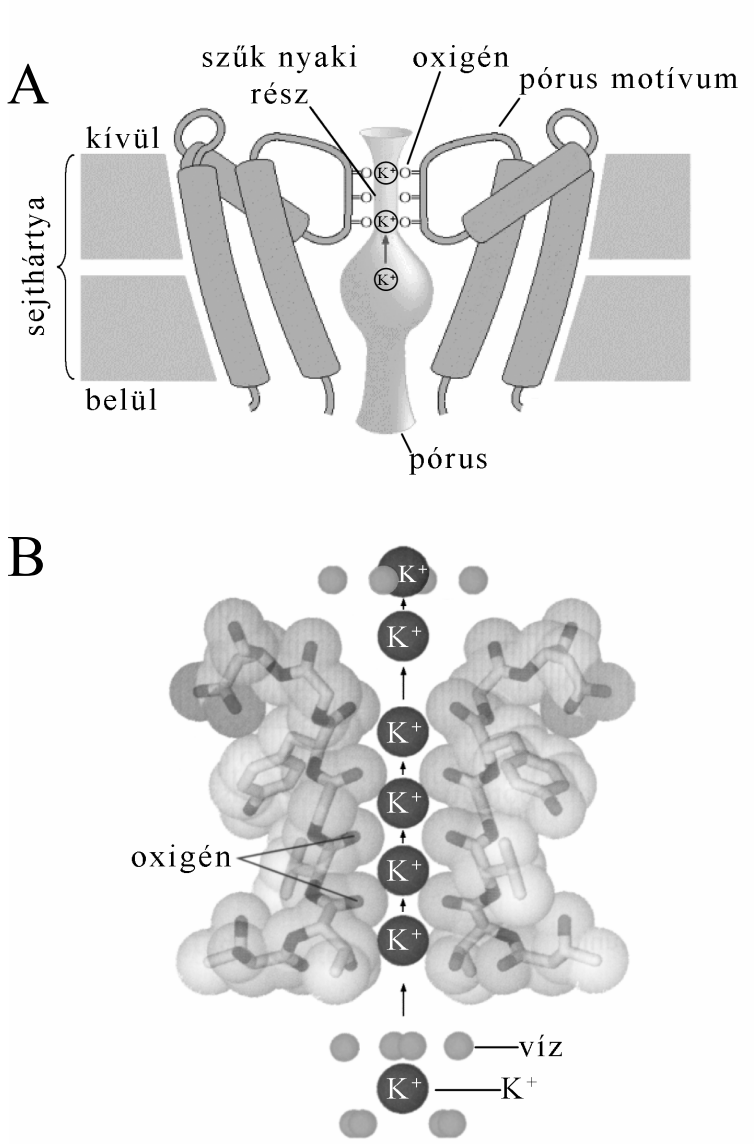

9. ábra. Egy K^+ csatorna szerkezete. A: a sejthártyába illeszkedő csatorna, közepén a szürkén jelölt űrrésszel. B: A csatorna legszűkebb, nyaki része határozza meg, hogy rajta milyen ion haladhat át.

A feszültségszabályozott ioncsatornák működése a fent leírtaknál összetettebb: a membránpotenciál pillanatnyi értékének függvényében nyílnak ki, vagy záródnak be, és csak akkor láthatják el feladatukat, ha folyamatosan figyelik a membránpotenciált, annak változásait. Az ioncsatorna „szeme” a negyedik α-hélix, az ún. feszültség érzékelő, vagy kapuzó hélix. A kapuzó hélixben minden harmadik aminosav pozitívan töltött, arginin vagy lizin (11. ábra). Az argininok és a lizinek meghatározó szerepét az mutatja, hogy minél többüket helyettesítjük más aminosavakkal (pl. alaninnal, glicinnel), annál kevésbé funkcióképesek a csatornák. A kapuzó hélix helyzetét a sejthártyában az határozza meg, hogy milyen kölcsönhatás van a sejthártya két oldalán felhalmozódott töltések, és a kapuzó hélixek töltése között (10. ábra). Depolarizáció során a kapuzó hélix a sejthártya külseje felé mozdul, és lényegében miközben megváltozik az ioncsatorna szerkezete, kinyílik, rajta ionok áramlanak át. Az átáramló ionáram erőssége már a depolarizáció alatt csökkenni kezd, mert a

csatorna inaktiválódik. A zárt, és az inaktivált állapot nem azonos. Sőt, a különféle feszültségszabályozott ioncsatornák különböző kinetikával inaktiválódnak. A két legfontosabb inaktivációs mechanizmust N- illetve C-típusúnak nevezik. Az N-típusú inaktiváció esetében az ioncsatorna fehérje N-terminálisa a pórus citoplazma felőli bejáratához kötődik, bedugaszolja a csatornát (10. ábra). C-típusú inaktivációt - nevével ellentétben - nem a fehérje C-terminálisa, hanem a szűk nyaki rész körüli fehérje részek okozzák: az ioncsatorna a fényképezőgépek blendéjéhez hasonlatos módon záródik. Az idő előrehaladtával a csatorna zárul (10. ábra), és mivel a kapuzó hélix mindaddig a sejthártya külső részében marad, amíg a nyugalmi potenciál nem áll helyre (sőt, a valóságban egy kicsit még tovább is), a csatorna egy rövidke ideig nem nyitható. A csatorna csak azután nyitható újra, miután helyreáll a nyugalmi állapotra jellemző membránpotenciál, és a kapuzó hélixek a sejthártya belső felszínére zuhannak. A kapuzó hélix jellegzetes viselkedése biztosítja az ún. refrakter szakasz létét, azt, hogy a csatorna csak valamennyi idő multán nyitható újra. A csatornák refrakter szakasza pedig azt biztosítja, hogy a depolarizációs hullám a sejthártya mentén csak egy irányba halad, visszafelé sohasem.

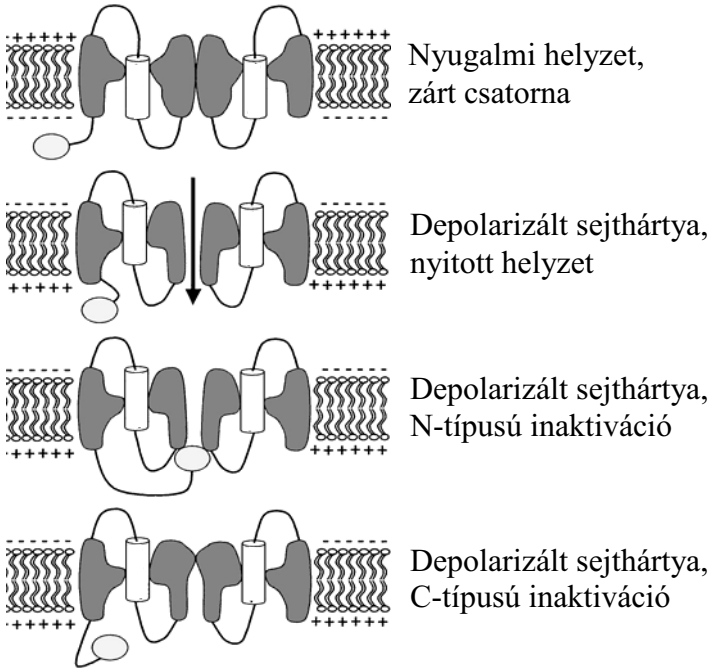

10. ábra. A kapuzó hélix működésének jellegzetes állapotai. Érdemes megfigyelni a fehéren jelölt kapuzó hélix helyzetét a sejthártyában.

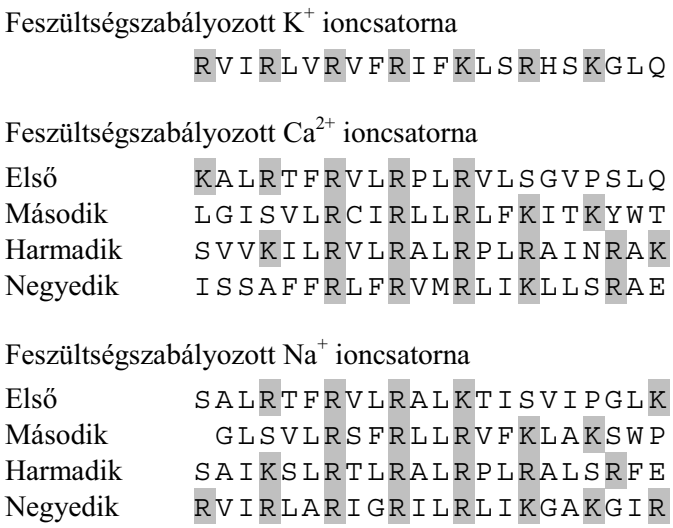

11. ábra. A kapuzó hélixeket alkotó aminosavak sorrendje a feszültségszabályozott ioncsatornákban. A pozitív töltésű arginin (R) és lizin (K) aminosavak szürkén árnyékoltak.

Az ioncsatornák eredete

A különböző fajok csatornagénjeinek nagyfokú hasonlósága közös eredetüket bizonyítja. A legegyszerűbb szerkezetű (állandó) K^+ csatornáik már a baktériumoknak is jelen vannak. Velük vannak rokonságban az eukarioták legegyszerűbb K^+ csatornái, köztük az állandó K^+ csatornák (8. ábra). Bár feszültségszabályozott K^+ csatornái vannak minden egysejtű eukariota élőlénynek, Ca^{2+} csatornák csak a fejlettebbekben (mint pl. a papucsállatkában) fordulnak elő, Na^+ csatornái pedig csak a soksejtű élőlényeknek vannak. A Ca^{2+} és a Na^+ csatornák génjei egy ősi K^+ csatorna gén ismételt duplikációja és módosulása nyomán képződtek. Nyilvánvaló, hogy az ioncsatornák génjei az evolúció során kialakult és bevált funkció megőrződéséről, variálódásáról szólnak.

2006-ban ismerjük az ioncsatornákat kódoló géneket, és sokat tudunk az ioncsatornák szerkezetéről, működéséről, ám nem eleget. A K^+ csatornák felépülhetnek azonos, de különböző alegységekből is. Nem tudjuk, hogy miként működnek, és mi a szerepük azoknak az ioncsatornáknak, amelyek különböző alegységekből szerelődnek össze. Az ioncsatornákhoz olyan járulékos fehérjék is kapcsolódnak, amelyek módosíthatják az ioncsatorna kapuzási kinetikáját, és lehetnek ismeretlen funkcióik. Napjaink kutatásainak két fő vonulata látszik. (i) Kapcsolat teremtése a DNS és az ioncsatornák funkciója között, hogy meg lehessen előzni a genetikai alapú hirtelen szívhalál eseteket. (ii) Olyan gyógyszerek tervezése, amelyek segíthetik gyógyítani azokat a betegségeket, amelyek a szív megváltozott ioncsatorna funkcióval kapcsolatosak. A két kutatási irány sikerének az alapja közös: az olyan ioncsatorna funkciók megismerése, amelyek az ép szív funkciót biztosítják, lehetővé teszik életünket.

FOGALOMGYŰJTEMÉNY

akciós potenciál: a sejthártya mentén tovaterjedő depolarizációs hullám.

állandó K^+ csatorna: olyan K^+ ioncsatorna féleség, amely mindig nyitva van, rajta K^+ ionok szivárognak ki a sejtből. Szerepe alapvető a nyugalmi potenciál kialakulásában. Vannak négy és két alegységből összeszerelődő fajtái is.

depolarizáció: folyamat, amely során a nyugalmi potenciál a kb. –80mV (sejttípustól függő) értékről 0 mV felé csökken.

elektrokardiogram (EKG): a szív elektromos aktivitás-változást az idő függvényében ábrázoló görbe. Az EKG-t a testfelszín különféle helyein elhelyezett elektródokkal mérik.

Feszültségszabályozott ioncsatorna: olyan ioncsatorna-féleségek, amelyek a membránpotenciál-változás során nyílnak, rajtuk - koncentrációkülönbségüknek megfelelő irányban - ionok áramlanak át, majd automatikusan zárulnak.

α-hélix: a fehérjék olyan csigavonalban elrendeződött szakaszai, amelyekben három aminosav alkot egy menetet. Az α-hélixeket hidrogénhíd kötések stabilizálják.

ioncsatorna: olyan fehérje féleség, amely a membránba ágyazott (transzmembrán motívumok révén), amelyen nyitott állapotban ionok áramlanak át.

ionpumpa: olyan membránba ágyazott fehérje féleség, amely az ATP-ben tárolt energia felhasználásával ionokat juttat a membrán túloldalára.

kapuzó hélix: a feszültségszabályozott ioncsatornák olyan alkotója, amely érzékeli a membránpotenciál-változást, és miközben helyzete változik a membránban, nyitja az ioncsatornát. Tehetetlensége az alapja a feszültségszabályozott ioncsatorna ún. refrakter periódusának.

membránpotenciál: a sejthártya belső és külső felszíne között nyugalomban mérhető potenciálkülönbség.

nyugalmi potenciál: a nyugalomban levő sejt sejthártyájának belső és külső felszíne között mérhető potenciálkülönbség.

pacemaker aktivitás: a szinusz csomóban levő olyan sejtek működése, amelyekből szabályos időközökben akciós potenciál generálódik, és terjed át a szomszédos sejtekre.

refrakter szakasz: a feszültségszabályozott ioncsatornák működésének olyan rövid szakasza, amely alatt az ioncsatorna nem nyitható ki.

repolarizáció: folyamat, amely során (depolarizációt követően) helyreáll a sejtre jellemző nyugalmi- vagy membránpotenciál.

rianodin receptor: a szarkoplazmatikus retikulum membránjában levő Ca^{2+}-csatornák, amelyeken aktiválódásuk után Ca^{2+} ionok áramlanak ki a szarkoplazmatikus retikulumból a citoplazmába.

ritmusképző (pacemaker) ioncsatorna: a szinusz csomó ritmusképző sejtjeinek jellegzetes K^+ ioncsatornái. A nyugalmi potenciálnál negatívabb értéknél nyílnak, rajtuk a K^+ ionok mellett Na^+ ionok is átjutnak.

szinusz csomó: a szív jobb pitvarának falában levő, pacemaker aktivitású sejteket tartalmazó, a szív ritmusos összehúzódását adó központ.

t-csövecske: a sejthártya betüremkedései az izomsejtek citoplazmájába. Rajtuk jut az akciós potenciál a sejtek belsejébe, a „jel" áttevődik a szarkoplazmatikus retikulum membránjába, hogy onnan Ca^{2+} kiszabadulása nyomán elkezdődjön az izom-összehúzódás.

transzmembrán hélix (motívum): a fehérjemolekula hélix formában elrendezett olyan szakasza, mely a membránba ékelődik, vagy átér azon. Úgy alkotja 22-25 hidrofób és semleges jellegű aminosav, hogy egy aminosav 0,15 nm-el járul hozzá a csaknem 4 nm hosszú transzmembrán motívumhoz.